Design of Platform Lift for MIT's Skywalker Gamma Project

by

Simon A. Okaine

Submitted to the
Department of Mechanical Engineering
in Partial Fulfillment of the Requirements for the Degree of
Bachelor of Science in Mechanical Engineering
at the
Massachusetts Institute of Technology

January 20, 2016
[February 2016]

Signature of Author: Signature redacted
Department of Mechanical Engineering
January 20,2016

Certified by: Signature redacted
Hermano Igo Krebs, Ph.D.
IEEE Fellow
Principal Research Scientist & Lecturer
MIT, Mechanical Engineering Dept

Adjunct Professor
University of Maryland, School of Medicine,
Dept Neurology

Visiting Professor
Osaka University, Mechanical Engineering Dept
Fujita Health University, School of Medicine
Newcastle University, Institute of Neuroscience
Thesis Supervisor

Accepted by: Signature redacted
Anette Hosoi
Professor of Mechanical Engineering
Undergraduate Officer

Design of Platform Lift for MIT's Skywalker Gamma Project

by

Simon A. Okaine

Submitted to the Department of Mechanical Engineering
on January 20,2016 in Partial Fulfillment of the
Requirements for the Degree of

Bachelor of Science in Mechanical Engineering

Abstract

The Skywalker as found in MIT's Newman lab is a device that performs Body Weight Support Treadmill Therapy a form of walking therapy for recovering stroke patients. During clinical trials conducted in the fall of 2014, it became evident that the design of the Skywalker did not fully address how patients would mount and dismount the Skywalker. The current iteration of the design requires the patients to use stairs to mount and dismount the system. Given the gait impairment of the patients using the system it is evident that an alternative must be provided for the stairs in order to make the Skywalker accessible to severe stroke patients. The following thesis explores the idea of using a leadscrew driven platform lift to solve the problem. While the solution developed during the design process is a viable option, the high material cost disqualifies the solution discussed in this thesis as a viable option for implementation in the Skywalker system. The author recommends that alternative solutions such as ramps may provide a more low-cost and effective option for mounting and dismounting the Skywalker.

Thesis Supervisor: Hermano Igo Krebs
Tile:
IEEE Fellow
Principal Research Scientist & Lecturer
MIT, Mechanical Engineering Dept

Adjunct Professor
University of Maryland, School of Medicine, Dept Neurology

Visiting Professor
Osaka University, Mechanical Engineering Dept
Fujita Health University, School of Medicine
Newcastle University, Institute of Neuroscience

Acknowledgements

I would first and foremost like to thank God for the opportunity to be able to work on this project and the experiences that I have learned from through the development of this thesis. I thank God that this experience was characterized by a combination of academic rigor and character formation.

I would also like to thank Professor Krebs for his guidance and help during this thesis project. Finally, I would like to thank my family and friends for their continual support throughout the writing of this thesis.

Contents

List of Figures

List of Tables

Chapter 1 Design Problem

The Skywalker as found in MIT's Newman lab is a device that performs Body Weight Support Treadmill Therapy a form of walking therapy for recovering stroke patients. To achieve this it uses two independently moving treadmills that allow an individual to practice the walking motion. During clinical trials conducted in the fall of 2014, it became evident that the design of the Skywalker did not fully address how patients would mount and dismount the Skywalker. Currently, patients using the Skywalker must climb a set of steps to get unto the treadmill platform. Climbing the steps can be difficult for some patients and requires assistance from a therapist or helper. Difficulty mounting the Skywalker limits the demographic of patients the Skywalker can treat. The purpose of this design thesis is to design and implement a mechanism that will allow patients to mount and dismount the Skywalker with minimal assistance from a therapist. Through the design and implementation of such a mechanism, the Skywalker will be able to expand its impact in BWSTT to a larger percentage of the population affect by stroke related gait abnormalities.

Chapter 2 Design Specification

As defined before the intent of this thesis is to design a system that will allow patients with limit mobility to mount the Skywalker which helps to improve their mobility. The system that does this must satisfy the following, structural, cost, speed, geometric, and safety specifications.

2.1 Structural Specification

The current Skywalker is able to support a weight of 450lbs with a safety factor of 1.5. Thus the, intended use of the Skywalker system is for individuals between 0-300lbs. As a result of this parameter, any supporting accessories for the Skywalker that will support the user's weight must at a minimum support the weight of 450lbs. Unlike the Body weight support system, the system that will be designed must also support the weight of the walking aids that the user needs for mobility. Thus in order to determine the structural specification for this design, we must account for the weight of a wheel chair. Depending on the type of wheel chair he weight can range from 35lbs for a manual Wheel chair to 260 lbs. for a powered wheel chair. Most manual wheel chairs however will range from 35lb-75lbs. Thus if we add the maximum weight of 300lbs and the maximum wheelchair weight of 75lbs, we find that the total weight the lifting system should hold is 570lbs. This includes a safety factor of 1.5. The combined weight of the material required to make platform and the patient and their corresponding wheel chair, cannot exceed 1000lbs. A safety factor of 2 is also applied. Thus, the design of the system must be able to withhold 2000lbs of force.

2.2 Geometric Constraints

The device that will be design falls under a classification of systems known as platform lifts. These lifts must comply with ADA, and ASME standards. According to the ADAAG 4.2.4.2 the minimum floor space for the platform is 30"x48". Additional dimensions must be added for the necessary maneuverability conditions. In addition to the ADA standards that must be satisfied, the platform lift that is designed must have the ability to lift the patient 18" to the height of the Skywalker Treadmill.

2.3 Speed

The speed specification consists of two parts. The first part deals with the amount of time needed to lift the patient to the height of 18". The maximum amount of time to travel this length is prescribed to be 12 seconds. Thus the speed requirement for this system should be no less than .91 m/min. currently, the maximum speed of lift platforms are about 5.2m/min. Thus the maximum tolerated speed will not exceed 5.2m/min.

2.4 Safety

The platform lift that is designed must also be safe according to the ASME and ADA standards. Thus, the lift must have a side walls that are 42" high. This will allow for both standing and wheelchair bound patients to see over the sides as the platform is being lifted. Moreover according to ASME 18.1, these side bars must be able to withstand 105lbs of force.

Chapter 3 Initial Designs Pursued

There were three major designs developed during the idea generation phase of this design. These concepts can be classified into two groups. There were concepts in which the body weight support of the current Skywalker gamma would move to allow for a patient to mount the system. The other class of ideas would involve having a separate platform to the current sky walker to allow for the patient to be lifted to the final height of the Skywalker.

3.1 Extended Body Weight Support Concept

The extended body weight support concept involved increasing the travel of the current body weight support. The seat attached to the leadscrew assembly would be allowed to decrease in height until the seat was directly below the patient's trunk when standing at the base of the Skywalker. Then the patient would sit on the sit and be fastened in and the seat allowed to move until the patient's feet are above the height of the Skywalker. In order to achieve such a design, the entire body weight support system would need to move back to allow the patient to either wheel or walk to the seat and be lifted to the height of the Skywalker. What this mean however, is that once the patient is on the seat and has reached the desire height, the entire body weight support structure must be accelerated back to its original position horizontally. This means that the patient would also be accelerated. This has the potential to cause the patient to fall off the body weight support system while in transit. Moreover, there would be also being a lot of automation and possible railing systems needed that would further complicate such a system. Thus for mainly the issue of safety, this concept is eliminated from the design consideration.

3.2 Car Jack Platform

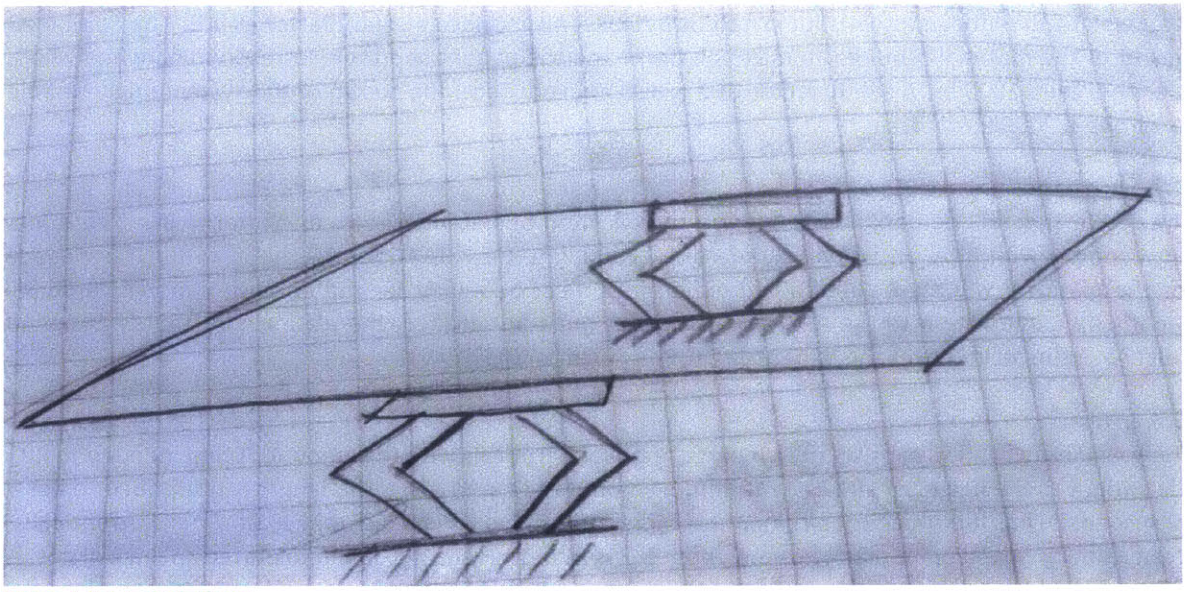

Figure 1 Car Jack Platform

This idea was initially explored because of the existence of cheap and available technology that could be used to quickly prototype a design. A typical car jack is able to support about 1.5 Tons of weight. This exceeds the amount of force needed to support the patient and the platform. Moreover, the acme leadscrews used in these designs allowed for the system to not be back drivable since there was sufficient friction in the system. While promising, there were two major draw backs to such a design. The first is that upon thorough research of the existing products on the market, no car jacks were found that would be able to lift the platform the desired 18 in to the top of the Skywalker. Moreover, the load capacities of these scissor jacks were not constant. Rather, it was dependent on the overall height of the scissor jack. Thus, in their fully collapsed position, carjacks are not capable of holding the desired load of 8909N.

3.3 Four Bar Linkage

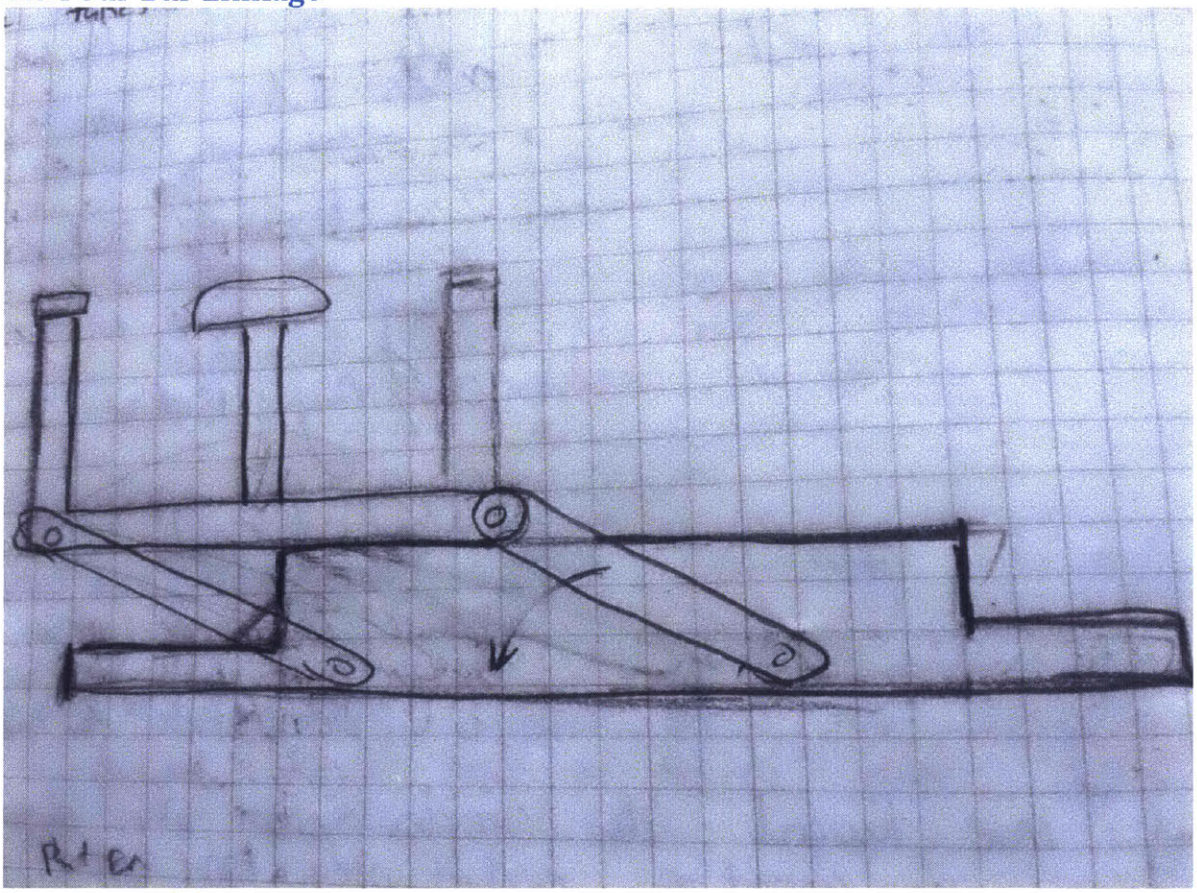

Figure 2 Four Bar linkage

The Third idea is another variation of the separate platform concept. In this concept, the platform forms one of the legs of a four bar linkage. In order to be able to rise to the height of 18" the two vertical members of the four bar linkage must be 20 in long. On of these two members would have to be driven in order to cause the platform to raise and lower to the desired position. Like the scissor jack, the four bar linkage has the same problem in that in its collapse state an infinite amount of torque is needed in order to raise a desired load. Since no motor can provide such torque having such a design proposes a potential risk of not having sufficient power to drive the system. Moreover, given the kinematics of a 4 bar linkage, the envelope of the entire platform in this case would be larger. This is because as the leg of the four bar linkage is driven; the platform will translate both vertically and horizontally. This means that

in the horizontal direction the platform will move past its 48" envelope and thus more space would be required for such a design. Thus, for these reason, the four bar linkage was also removed from consideration in this design due to the torque requirements and the power requirements.

3.4 Proposed design

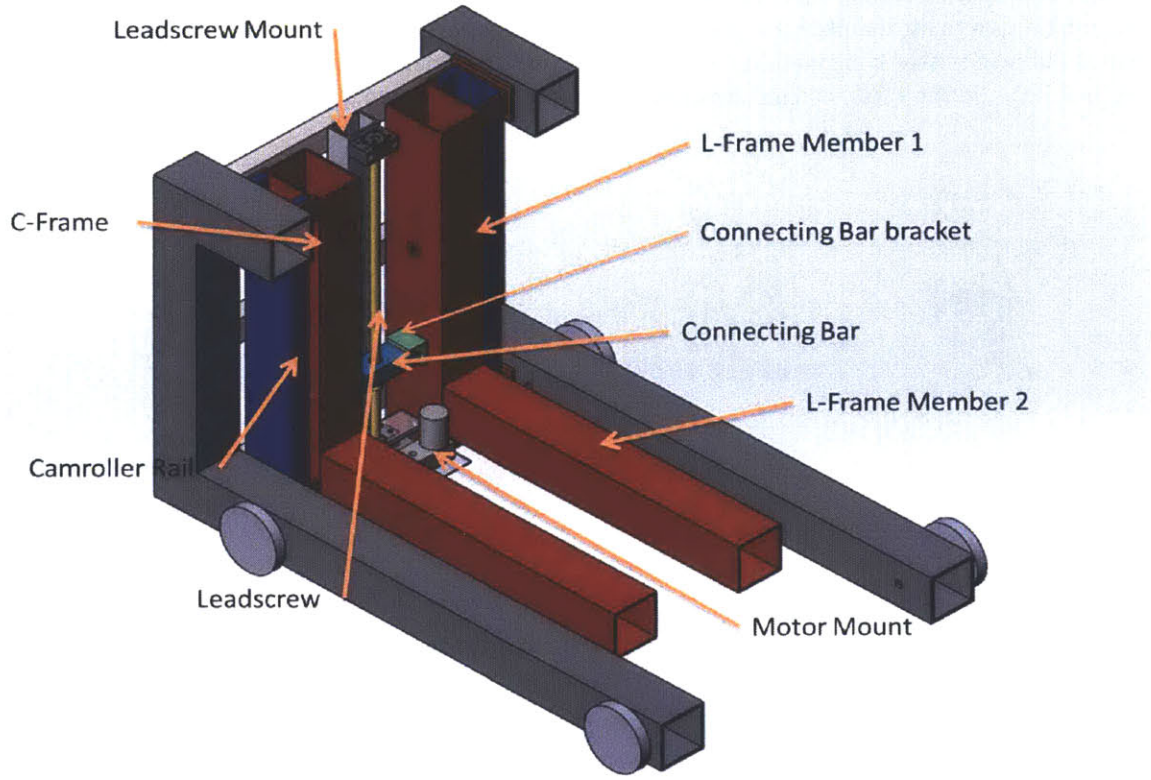

Figure 3 Proposed Lift Design: This figure excludes the platform and ramp in order to reveal the support components such as the L frame members, motor mount and connecting bar.

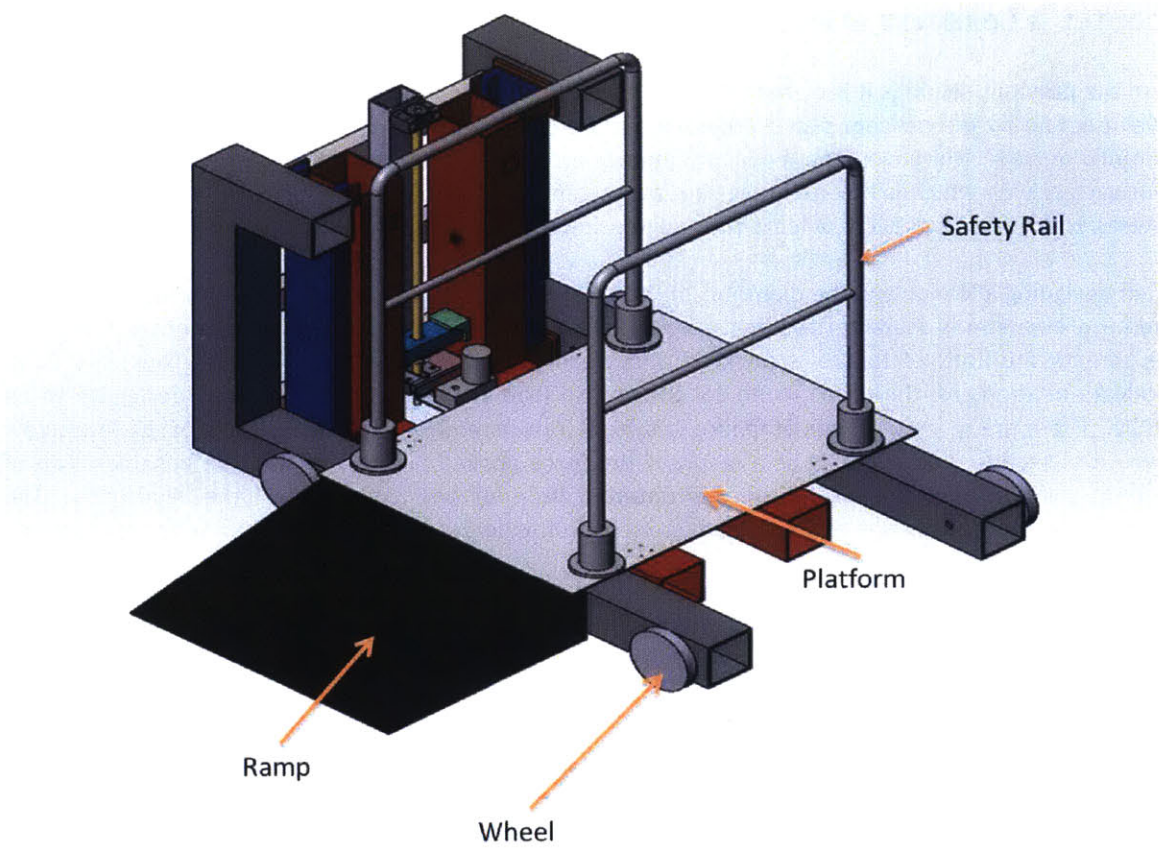

Figure 4 Overall Proposed Design. This image demonstrates the rail the safety rail, wheels and ramp. The ramp will rise 7" inches in the air to help accommodate for the design

The actuation system constitutes of a leadscrew which is driven by a geared motor. The leadscrew is fitted with a flanged bronze nut that allows for the transfer of load generated by the leadscrew and geared motor assembly to the connecting bar. This connecting bar as illustrated in figure 3 is attached to the L- frame member #1 which is attached to the cam roller. The platform is attached to the L-member # 2 using L-brackets. The platform is made of an aluminum sheet below the platform there are three inch steel tubes that are used improve the stiffness of the sheet over all. Two figures have been provided for the proposed design. Figure 3 excludes the ramp and platform in order to provide an image of the L-frame and other components of the lift. Figure 4 provides an image of the entire design all together.

Unlike the other designs this method would require the least amount of actuation. Designing a leadscrew for vertical application allows for this design to achieve the desired travel which was not available for all the car jacks found during the research of that design. Moreover, the vertical motion of the nut on the lead screw eliminates the horizontal translation that was present in the four bar linkage design. This means that this design can have smaller foot print than the design for the four bar linkage. Finally the vertical geometry of the vertical leadscrew design allow for a more constant torque once the initial static friction is overcome. Thus, given that this design is able to address the potential draw backs of the ideas listed above, this design presents itself as the most ideal of the ideas presented. The remainder of this document will discuss the selection process for each components of the overall system.

Chapter 4 Leadscrew Specification

From the previous sections it is evident that for his particular application the leadscrew among the ideas developed during the concept phase provided a more cost effect option compared to pneumatics, and hydraulic options. Moreover, the leadscrew option proposed a way to passively prevent the platform from back driving which is helpful in preventing unwanted drops of the platform. Unlike the two other systems, there is no possibility of leaks thus decreasing the possibility of catastrophic drops.

When designing a leadscrew, the diameter of the leadscrew is very important. The determination of the leadscrew diameter is characterized by the methods of failures his lead screw can experience. In his case the primary methods of failure is buckling and yielding of the cross-sectional area. Thus, the Euler buckling equations can be used. To do so, the critical load at the onset of bucking is designate to be 8909N. There are three methods of failure in a leadscrew assembly: buckling, yielding of the leadscrew at its cross-section, and shearing as a result of the force applied on the threads. The consideration of buckling and yielding are useful in the determination of the diameter of the leadscrew. The consideration of the shearing of the threads is useful in the determination of the pitch of the leadscrew.

4.1 Screw Diameter:

Using the Euler buckling equation, the diameter of the leadscrew is determined using equation 1

$$P_{cr} = \frac{\pi^2 EI}{L_e^2} \quad (1)\ [6]$$

P_{cr} is the critical load. For this design, the critical load is equivalent to the combined weight of the patient, their accompanying wheelchair and the weight of the platform with specified safety factor of 2. 'E' represents the young's modulus of the material selected for this design. 1020 steel is a typical material used to manufacture leadscrews and thus will be used in the formulation of this analysis [7]. L_e represents the effective length of the lead screw. The effective length on the leadscrew is dependent on the end constraints of the leadscrew. A table 1 provides the end constraints and the corresponding values of effective length. Please note that L denotes the distance between the supports of the proposed design.

Table 1 Values of Effective Length Based on End Constraints [6]

End Constraints	Effective Length for Actual Column Length L
Both ends pinned	L_e=L
One end Pinned, one end fixed	L_e=0.7L
One end fixed, one end free	L_e=2L
Both ends fixed	L_e=0.5L

'I' represents the moment of inertia of the cross-section. The moment of inertia is dependent on the diameter for members with circular cross-sectional area. Thus, the diameter of the leadscrew can be determined by rearranging equation 1. E, P_{cr} and L_e were determined based on design requirements and are presented in table 2.

Table 2 Design Parameters of Leadscrew

E= 210 GPa
P_{cr}=8909.1 N
L_e=.6096m

$$D_{8909N} = \left(\frac{64P_{cr}L_e^2}{\pi^3 E}\right)^{1/4} \quad (2)$$
$$D_{8909N} = 0.013m$$

While this is expressed as in equality here, it should actually be treated as an inequality since there the diameter specified would be the minimum diameter needed for the onset of buckling at the desired load. Thus, from the calculations given, the required diameter is within the range of 1/2" and 5/8". Most lead screw come in specific fractional quantities. Since the value calculated above is higher than ½" the next available diameter is the 5/8" screw.

4.2 Design for Yielding

To ensure that the leadscrew does not yield due to the compressive load, the radius is used to compute equation 3. Care should be given to ensure that the inequality is satisfied..

$$\sigma_y \geq \frac{P_{cr}}{A} \quad (3)$$
$$\sigma_y = 350\,MPa$$

Since the leadscrew has a circular cross-sectional area, the area (A) is equivalent to the area of a circle. If the yield strength of the leadscrew material is known, the corresponding diameter can be determined by manipulating equation 4.

$$r \geq \left(\frac{P_{cr}}{\sigma_y \pi}\right)^{1/2} \quad (4)$$
$$r \geq 2.846\,x10^{-3}m$$

The diameter found is much smaller than the .013m diameter need to prevent buckling. Thus, the diameter determined from the buckling equation will be used to specify the diameter of the leadscrew. The standard thread/inch used for a 5/8" leadscrew is 8 and the corresponding pitch (p) is given by equation 5. These parameters will be used as proposal for the design and modify based on the determined stresses on the threads.

$$p = \frac{1in}{thread} \quad (5)\ [7]$$
P=3.175 x 10^{-3}m

4.3 Torque Required to Raise/Lower Load

One of the important parameters that must be determined for this system is the amount of torque required to raise the desired load 18" from the ground. To determine this equation 6 is employed.

$$T_R = P_{cr} r_p \left(\frac{\cos(O_n) \sin\alpha + \mu_t \cos\alpha}{\cos(O_n) \cos\alpha + \mu_t \sin\alpha} \right) + P_{cr} r_c \mu_c \quad (6)\ [7]$$

W is the combined weight of the entire platform material and weight of the patient. The variable α is the lead angle and O is the pitch angle. The pitch angle is determined by the shape of the threads. ACME screws will be used for this application. The pitch angle of an ACME screw is 14.5°. The second term in equation 6 represents the torque generated by the friction of the thrust collar. For this application roller thrust collars will be used. Thus, the rolling friction coefficient due to the thrust collar can be neglected. r_p is the pitch radius is given by equation 7.

$r_p = \left(\frac{5in}{16} - \frac{p}{4}\right)$ [7]	(7) [7]
$r_p = 7.144 \times 10^{-3} m$	

The lead angle (α) corresponding to the specified leadscrew was computed using equation 8 and a summary of leadscrew parameters are given in table 3.

$\alpha = \tan^{-1} \frac{p}{2\pi r_p}$	(8) [7]

Table 3 Initial Leadscrew Parameters [7]

Leadscrew Parameters	Values of Leadscrew Parameters
Lead	.125 m/rotation
Lead Angle	$\alpha = 4.406\ deg$
Thread Angle	$\theta = 14.5\ deg$
	$\theta_n = \tan^{-1}(\tan O \cos\alpha)$
	$\theta_n = 14.465\ deg$
Mean Collar Radius	$r_c. = 0.254m$
Collar friction coefficient	$\mu_c = 0$
Friction Coefficient	$\mu_t = 0.34$

For this design the leadscrew will be made of steel and the nut for the leadscrew will be made of bronze. Thus, the coefficient of friction is .3 as stated in table 3. When all of these values are substituted we find that the torque required to accelerate 8909N (2000lbs) from rest is 24.763 Nm with a leadscrew with 5/8" diameter.

This is the initial amount of torque needed to accelerate the leadscrew. In this case the variable μ_t is introduced to represent the coefficient of sliding friction. μ_t is substituted for into equation 6 in order to evaluate the torque required to raise the load. Equation 6 is reproduced as equation 9 and the variables in table 3 are substituted into equation 9 to determine the torque required to raise 8909N (2000lbs).Please refer to table 3 for the parameters to substitute into equations 9. It is important to note that the coefficient of friction used in table 3 is the sliding friction for bronze on steel when dry. Thus, the torque produced would be a conservative estimate of the actual torque required torque since the intent would be to lubricate the Leadscrew.

$T_R = P_{cr} r_p \left(\frac{\cos(\theta_n) \sin\alpha + \mu_{tdynamic} \cos\alpha}{\cos(\theta_n) \cos\alpha + \mu_{tdynamic} \sin\alpha} \right) + P_{cr} r_c \mu_c$	(9) [7]
$T_R = 27.533 Nm$	

4.4 Torque Required to Lower the Load

$T_L = P_{cr} r_p \left(\frac{-\cos(\theta_n) \sin\alpha + \mu_t \cos\alpha}{\cos(\theta_n) \cos\alpha + \mu_t \sin\alpha} \right) + P_{cr} r_c \mu_c$	(10) [7]
$T_L = 17.43 Nm$	

It is important to mention that all the variables expressed in equation 10 were previously defined in table 3.

4.4.1 Self-Locking Conditions

To determine if this system is self-locking, the inequality in equation 11 is evaluated. If the inequality is true, then the system is self-locking. If it is not true, the system is over hauling and motor must continually supply pa torque to resist the platform from moving downward as a result of gravity. The parameters need to evaluate equation 11 can be found in table 3.

$\mu_t > \frac{l cos(\square)}{2\pi r_p}$	(11) [7]
$.34 > .068$	

From the results of the system, it is evident that this leadscrew application will be self-locking and thus, the motor will not have to continually provide a torque to maintain the height.

4.5 Critical Stresses

To ensure that the screw does not shear, the critical stresses of the leadscrew threads are calculated Figure 5 is provided to help illustrate the different stresses and location of stress on the leadscrew that must be considered in the critical stress analysis.

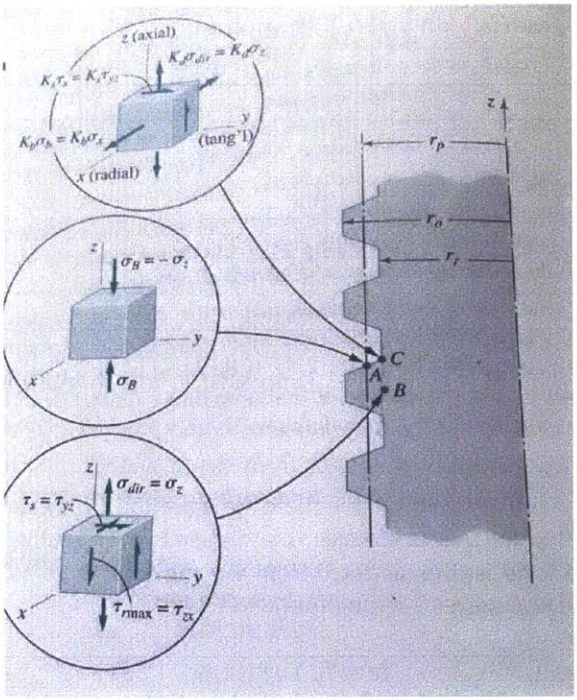

Figure 5 [1] Critical Stresses in Leadscrew this figure illustrates the different points on a screw thread and the types of stresses experienced at that point. Of the three points, points C is the most critical since it experiences the most combinations of stress and also located at a discontinuity which promotes stress concentration at that point. While point C determines the size of the threads, the stress at point A and point B help inform the calculation of stresses at point C.

From the figure 5 it is evident that the stresses at point C will experience the highest stresses, closer observation reveals that point C will experiences many of the stresses that also act on point A and B. Thus, the evaluation of the stresses at point A and B will aid the understanding of the stresses experienced at point C. To begin the bearing pressure σ_B, is evaluated in equation 13. Equation 13 provides the equation for the root radius. Table 5 provides the definition of the variables needed to evaluate equation 12 & 13.

$r_r = r_o - \frac{p}{2}$	(12) [7]
$r_r = 6.35 \times 10^{-3} m$	

$\sigma_B = \frac{P_{cr}}{\pi(r_o^2 - r_r^2)n_e}$	(13) [7]
$\sigma_B = 41.7MPa$	

Table 4 Variable Definition for Bearing Stress Calculation

Variables for Bearing Stress Calculation	
Effective number of threads in the engagement zone that carry the load	$n_e \equiv 3$
Major Thread Radius	$r_o = .0079m$
Root Radius	r_r

Pitch	p
Critical Load	P_{cr}

The allowable stress that is possible between on the screw is 2000 psi which is equivalent to 13.8 MPa. This recommendation is based on the assumption that the nut is a sleeve that is passing over the leadscrew thus acting as a bearing surface. According to the assumed limit, the current design exceeds the allowable stress thus failure would occur at point A. To redesign, the pitch can be increased to decrease the stress experienced at point A. alternatively, the outer diameter of the screw can be increased to help decrease the stress. Thus, the proposed diameter is increased to 1" since it will lead to a more significant reduction in stress the stress is then recalculated in equation 14 and its solution given. The following sections provide the calculations for the new specified dimensions of the leadscrew. Table 5 provides a list of all the necessary values need to evaluate the remainder of this section.

Variable Definitions For 1" diameter Lead Screw		
Critical Load	8909N	
Collar Radius	$r_c = .0254m$	
Effective number of threads in the engagement zone that carry the load	$n_e \equiv 3$	
Lead Angle	$\alpha = 4.406\,deg$	
Major Thread Radius	$r_o = .0127m$	
Pitch	$p = 6.35\,x\,10^{-3}m$	
Pitch Radius	$r_p = 1.1 \times 10^{-2}$	
Thread Angle	$\theta = 14.5\,deg$	
	$\theta_n = 14.465\,deg$	

$\sigma_B = \frac{P_{cr}}{\pi(r_o^2 - r_r^2)n_e}$	(14) [7]
$\sigma_B = 13.4MPa$	

4.5.1 Torque Required to Raise the Load

$T_R = P_{cr}r_p\left(\frac{\cos(\theta_n)\sin\alpha + \mu_t\cos\alpha}{\cos(\theta_n)\cos\alpha + \mu_t\sin\alpha}\right) + P_{cr}r_c\mu_c$	(15) [7]
$T_R = 45.207\,Nm$	

The torque calculated above is the initial amount of torque need to raise the load with the 1" diameter leadscrew.

4.5.2The Torque needed to lower the Load

$T_L = P_{cr}r_p\left(\frac{-\cos(O_n)\sin\alpha + \mu_{tdynamic}\cos\alpha}{\cos(O_n)\cos\alpha + \mu_{tdynamic}\sin\alpha}\right) + P_{cr}r_c\mu_c$	(16) [7]
$T_L = 24.959\,Nm$	

The values above have defined the torque necessary to raise the load as well as lower the load. Moreover, from the torque necessary to lower the load we find that this system will not be self-locking. Thus, the motor must provide constant torque to counteract the motion or a braking mechanism will be needed.

4.45.3 Self-Locking Conditions

To determine if this system is self-locking, the inequality in equation 17 is evaluated. If the inequality is true, then the system is self-locking. If it is not true, the system is over hauling and motor must continually supply pa torque to resist the platform from moving downward as a result of gravity. The parameters need to evaluate equation 17 can be found in table 3.

$\mu_t > \frac{lcos(\square)}{2\pi r_p}$	(17) [7]
$.34 > .092$	

From the results of the system, it is evident that this leadscrew application will be self-locking and thus, the motor will not have to continually provide a torque to maintain the height.

4.5.6 Critical Point B

At this point what we are most concerned with is yielding and fatigue. Moreover, at point B, the material experiences torsional shear from the load being raised, traverse shearing and direct stresses on the root diameter. We will begin by computing the torsional shear stress that the screw experiences. This would be evaluated using equation 18.

$\tau_s = \frac{2T_R r_r}{\pi r_r^4}$	(18) [7]
$\tau_s = 93.8MPa$	

Note that in the original equation it is actually a difference between the torque required to raise the load and the torque to overcome the collar friction. However, given that the collar has a rolling element, the torque needed to overcome the friction is negligible and thus, it is neglected in this calculation.
The direct stress experienced is essentially the weight that the thread must support divided by the root diameter of the lead screw. Thus the direct stress is expressed by equation 19.

$\sigma_{dir} = \frac{3P_{cr}}{\pi r_r^2}$	(19) [7]
$\sigma_{dir} = 93.8\ MPa$	

Finally there is traverse shearing that a tooth experiences. This is calculated by assuming that the tooth of the leadscrew is a cantilevered beam. The calculation for this is as followed:

$\tau_{rmax} = \frac{3P_{cr}}{2\pi r_r \left(\frac{p}{2}\right) n_e}$	(20) [7]
$\tau_{rmax} = 46.9\ MPa$	

It is assumed that the fatigue endurance limit for the 1020 steel that will be used in this case is approximately, half of the ultimate tensile strength of steel. This is however, not the expected fatigue strength that one should expect in this case. What should be expected is a fraction of these values. The

expected fatigue limit is dependent on multiple factors that further reduce the expected fatigue limit for the desired application.

The stresses at point C will govern failure. This is because there is a geometric discontinuity that would lead to stress concentration in this region. However, the formulation and the solution of the stress in region B and it will allow for solution for the stresses at point c to be calculated more efficiently.

At point c the only other stress introduced is the stress that occurs as a result of bending caused by the load being carried. The moment in this case is the product of the weight of the platform and the moment arm which is the difference between the root radius and the pitch radius. The flexure equation is used to analyze the stresses as a result of the moment experienced by the beam (thread).

$\sigma_b = \frac{12P_{cr}(r_p - r_r)}{\pi r_r n_e \left(\frac{p}{2}\right)^2}$	(21)
$\sigma_{dir} = 187.5\ MPa$	

The stress concentration factor the screw geometry is not accurately determined as for other geometries. However, in one publication, it was determined that the stress concentration for screw threads can range between 2.7 and 6.7 [7]. A value of 3 was used for all the principle direction. With this in mind, it is important to remember that the potential methods for failure at point c will be yielding and fatigue, since the leadscrew will experience cyclical loading.

To determine the allowable fatigue we must determine the fatigue stress concentration factors that will be used in this case. Given that there are two tensile loads and one torsional load, the highest value of safety expressed in the equations below in order to find the corresponding constants to use in the calculation of the stress in this case.

$K_{fb} = 0.65 \times (3 - 1) + 1 = 2.3$
$K_{fb} = K_{fd}$
$K_{fs} = 0.70 \times (3 - 1) + 1 = 2.4$

Since cyclical loading is expected the alternating and mean stress the tooth will experience are calculated. To construct the right formulation for the cyclic load we recognize that in both the lowering and the lifting of the weight exerted on the threads does not change. However, the direction of the force does at point C. Thus, the stress experience at point c should be the same in magnitude for both lifting and lowering. Thus we can calculate the alternating stress for each case. Then we can plug these stresses into the Von mises stress equation in order to determine if yielding will occur. $\sigma_{za}, \sigma_{xa}, \tau_{yza}$ refer to stresses in the principal basis.

$\sigma_{za} = K_{fb}\left(\frac{\sigma_{dir} - \sigma}{dir}\right)2 = 215.7MPa$	(22) [7]
$\sigma_{xa} = K_{fd}\left(\frac{\sigma_b - \sigma}{b}\right)2 = 431\ MPa$	(23) [7]
$\tau_{yza} = K_{fs}\left(\frac{\tau_s - \tau}{s}\right)2 = 26.9\ MPa$	(24) [7]
$\sigma_{ya} = 0\ psi$	(25)
$\tau_{xza} = 0\ psi$	(26)
$\tau_{xya} = 0\ psi$	(27)

Once the lead screw is specified, we can now approximate the power needed by the system and find the motor needed for this design. Note that k_∞ is only used when one is concerned with the infinite life of the part. If k_∞ is neglected then the main objective would be to see if at any point, the stress experienced by the tooth will exceed the yield strength of the material. If the equivalent tensile strength

is below the desired value for yielding, we find that the material will have a high cycle capabilities. However, the cycles at this present state is not satisfied

$\sigma_{eqC} = \sqrt{\frac{1}{2} \times \left[(\sigma_{xa} - \sigma_{ya})^2 + (\sigma_{ya} - \sigma_{za})^2 + (\sigma_{za} - \sigma_{xa})^2\right] + 3(\tau_{xza}{}^2 + \tau_{yza}{}^2 + \tau_{zza}{}^2)}$	(28) [7]
$\sigma_{eqC} = 376.461\, MPa$	

The proposed steel needs to be of a grade that has a yield strength that exceeds the value given. Thus, a new material must be picked as an alternative to 1020 steel. However, the new material will in general not affect the expressed calculations above.

4.6 Cost of Lead Screw:

Given the requirements for the leadscrew, price quotes from the Nook industries, Thompson Linear motion and Joyce motions were requested. In all of the cases it was assumed that the end machining and end supports for the leadscrews will be all done by the specified companies. Table 5 gives a summary of the leadscrew specifications and cost estimate.

Table 5 Cost Estimates for Leadscrew

Company Name	Nook Industries	Thompson Linear Motion	Joyce Dayton
Product Number	104-RA/BN/BK/31.30/20104/FS	SRA1004 CTL 24" BN1004 BK-BK end supports	
End Machining	Yes	Yes	Yes
End Supports (included?)	Yes	Yes	Yes
Torque required to raise the prescribed load	23.7 Nm	24.9 Nm	21.9 Nm
Maximum Dynamic Load	2.2241×10^3	8.452×10^3 N	2.2241×10^3
Total Cost of Assembly	$1176.23	$1151.86	$2107.52

From table 5, it is important to recognize that the best leadscrew assembly for this application is provided by Nook industries. Although it is more expensive than the Thompson Linear screw, it requires less torque to raise the same amount of load. A lower required torque to raise the load means that for a given motor that would be used to drive the leadscrew, less power and greater efficiency can be achieved. Moreover, the leadscrew assemblies provided by Nook industries are able to sustain a dynamic load that is 3 times the maximum load. The leadscrew provided by Thomspon linear does not meet the design specifications of holding 8909N dynamically and thus for such reasons it is no longer consider a viable product for this application.

Chapter 5 Linear Guide System

While the leadscrews provide the force and the required motion for the lift, it is not the only aspect of the linear motion system. Cam rollers and profile rails are utilized in this design. Their main purpose in this design is to first facilitate linear motion. The rails associate cam rollers and linear guides ensure that any structure attached to these guides or the roller will continue to move in the desired direction. Moreover, the cam rollers and the profile rail bearings also aid in resisting moments in the structure. The forthcoming sections will give a brief overview of both cam rollers and profile rail bearings. It will then propose which one is best used for this application.

5.1 Cam Rollers vs. Profile Rail Bearings

The Hevi-rail cam rollers provided by PBC linear have the capability of handling loads up to a total of 4.6 tons using a standard rail. The fixed/adjustable bearing allows for the ease of alignment. PBC provides the option of welding mounting flanges to the cam roller. These welded flanges attached allow for the ease of mounting a platform to the system. Since both the profile rail and the Hevi-rail have ways of attachment, easy attachment to the system is not a metric to use to rule out one option over another. One important aspect to note is that in order for the Hevi-rail system to have a similar moment capacity as the regular profile rails, the system must have two rollers separated by a fixed distance. This is best depicted in figure 6.

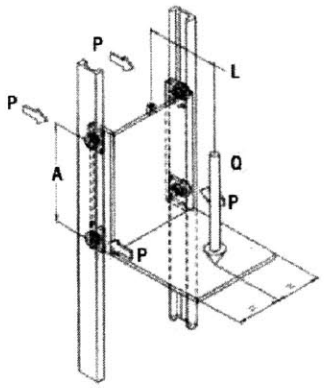

Figure 6 Image of Catilievered load provided by PBC linear This image given by PBC linear illustrates the application of the Hevi-rail system in cantilevered loading conditions. Four rollers are used: two on each side. This configuration as mentioned before, allows the Hevi-rail solution to counteract the moments generated by the cantilevered load.
[2].

Unlike Cam rollers that require 2 cam rollers on each rail in order to counter act a moment, Profile rail bearing can support moments with the use of only one bearing block. All three companies presented in table 7 provide profile guide rails. However, upon technical recommendation from the individuals at PCB Hevi-Rail was the technology consider from PCB and not their profile rail guide product line. For the current design as seen in this discussion, cam rollers will be utilized. Since the potential of misalignment loads are less forgiving in profile rails vs. cam rollers. The prices for the profile guide rails from Thompson linear and Nook industries are provided in table 7. The selection of the linear guides from Thompson linear and Joyce Dayton was determined from the moment calculations in the Frame and Structures section of this document.

5.2 Selection of Cam roller

The selection of the appropriate roller in such a configuration is motivated by the maximum amount of force that the each roller will experience in this situation. Q represents the load applied to the system. The distance L is the distance from the applied load to the suspension point. The variable P is the suspension point or, the location of the cam rollers. The variable A, is the distance between two bearings on the same rail. For this application Q, L and A are specified in table 6.

Table 6 Variable Definition for Camroller Analysis

Variable	Value
Applied Load(maximum including a safety factor of 2)	Q= 8909N
Distance to the Suspension Point	L= 914.4mm
Bearing Distance	A= 609.6 mm

Equation 23 can be used to determine the radial loads that a cam roller will experience in order to resist the moments generated by the cantilevered load. The values of the variables used in equation 23 can be found in table 6.

$F_{max,radial} = \frac{Q * L}{2 * A}$	(29) [2]
$F_{max,radial} = 6682N$	

After evaluating equation 23, it was determined that the maximum radial loads that will be experienced using cam rollers as demonstrated in figure 6 would be 6682 N. It is important to note however that this is only a preliminary result. Further structural analysis revealed that the deflection that the L-frame will experience will further load the cam rollers. Thus, the cam rollers that must be used for this application is HVB-062. This cam roller has the capability of withstanding 33.9kN of radial force. This is sufficient to support the moments generated by the cantilevered load in this application. In addition to selecting this roller, a welded flange is added to it. This takes away from possible machining time that would be necessary to fabricate an attachment device for the entire rail system.

5.3 Fixed vs. Adjustable Eccentric Bearing:

While discussing the Hevi-Rail system, it is important to introduce the Adjustable Eccentric Bearing feature that is available for the Hevi-Rail cam rollers offered by PBC linear. The eccentric bearing allows the ability to preload the rollers for the application of axial forces on the system. In this application, the system will utilize the radial force capability of the cam roller. Thus the fixed bearing option can be utilized as opposed to the adjustable bearing option.

5.4 Linear Guide System Cost

When selecting a linear guide system, there are two major elements that often dictate the cost: the cost of the cam roller or profile rail bearing, and the cost of the associated rail. The rails for this system are a

total of 1016 mm long each. Table 7 outlines the cost of different compares the cost of cam rollers, and profile rail bearings.

Table 7 Cost of Linear Guide System

Solution Type	Cam Roller	Profile Guide Rails	Profile Guide Rails
Company Name	PBC Linear	Thompson Linear	Nook Industries
Product Numbers	HVB-062/HVP4 (Roller with welded flanges) HVR-5 X 1016 mm (Rail)	511H45B0 (Profile Rail Guide) 521H45A+610 (Profile Rail)	NHRC45FLS1ZCVCN-610L-43-43S (a complete profile guide rail assembly.)
Cost of Rails	$168 x2	$286.70 x2	
Cost of Guides/ Rollers	$224.23x 4	$304.11 x2	
Total Cost	$1233	$1181.62	$851.02

Chapter 6 Motor Specification

Based on the selection the leadscrew in section 4.6, the accompanying motor must be will be able to provide the necessary torque of 23.7 Nm to lift the platform. While the evaluation of the leadscrew provides the torque requirement, the speed and the power requirements are yet to be determined. Given that the pitch of the leadscrew is 6.35mm, it is evident that in order to raise the platform .4572m in the desired 12s, the motor must have an angular velocity of 360 RPM. With the speed now specified for this system, it is possible to select a motor for this application. Table 8 provides a summary of the prices and motor specifications of various proposed motors.

Table 8 Comparison of Selected Motors

	NEMA 56 Dual Base	DC-Geared Motors	TENV	Ampflow motors
Power Requirement	1 hp	1/4	1/6	1.0
Voltage Requirement	24VDC	90 VDC	12 VDC	24 VDC
Output Torque	3.95 Nm(35-in-lbs)	17.51Nm(155in-lbs)	1.35Nm (12 in-lbs)	86.4Nm (770in-lbs)
Output RMP	1800	83	700	680
Gear Reduction	4:1	n/a	12:1	n/a
Supplier	McMaster	McMaster	Grainger	Ampflow
Price	$598.95	$520.71	$331.00	$289

Upon research it was determined that the amp flow geared motor is desirable for its price, and torque and speed capabilities. Moreover, this motor already comes with the gear reduction necessary to generate the required loads to drive the lead screw. Thus, the selection of the Amp Flow motor removes the need for the designer to create a gear reduction. I

6.1Gear Stress Analysis:

In order to allow for power transmission from the motor to the leadscrew, it was propose that mating of gears should be used. To properly choose the gear size for this application, the stresses on the gears must be analyzed to ensure that they do not yield while under load. In order to perform the stress analysis a pitch must be proposed. This pitch is used to determine of the diameter of the gear. Moreover, using the formulation of the gear tooth as a cantilevered beam, the stress on each individual gear tooth can be approximated.

6.1.1Gear Radius Calculation

To begin the stress analysis of the gear, the diametric pitch is determined to be 12 for its initial assumption. Using the equation 24 described below, we are able to determine what the radius of gear 1, and gear 2, respectively. In order for meshing between gears to be possible, the gears must have the same pitch. Thus, both gear 1 and gear 2 have the same pitch. Table 9 provides the definition of the variables need to evaluate equation 30 for both gear one and gear two. In addition, table 9 provided the values of the radius of gear 1 and gear 2 as a result of evaluating equation 30.

$r = \frac{N_1}{2P_d}$	(30) [8]

Table 9 Variable Definitions and Results for Gear Radius Calculation

Number of Teeth for Gear 1	$N_1 = 12$
Number of Teeth for Gear 2	$N_2 = 12$
Pitch Diameter	$P_d = 12\ in^{-1}$
Radius of Gear 1	$r_1 = 0.5\ in$
Radius of Gear 2	$r_2 = 0.5\ in$

6.1.2 Face width Calculation

The face width which is necessary in calculating the stresses is bounded between $9/P_d$ and $14/P_d$. For this design, a midrange value is chosen. However, these calculations will change once the parts have been determined and purchased. Thus, for the preliminary estimates, b (face width) will be $11.5/P_d$. The face width is calculated in equation 31.

$b = \frac{11.5}{P_d}$	(31) [8]
$b = 0.958\ in$	

The value for the face width determined in equation 31 is the minimum face width for the specified pitch. One should recognize however that the face width evaluated here is only an estimate. The final face width of the gears selected will be determined by the gears selected in this design.

6.1.3 Gear Tooth Stress

The flexure equation expressed in equation 31 is used to evaluate the bending stresses that the gears will experience. Equation 32 provides a modified version of the flexure equation for gear teeth.

$\sigma_b = \frac{6M}{I}$	(32) [8]

$\sigma_{gb1} = \frac{6F_{t1}P_d}{bY_{12}}$	(33) [8]

The variable Y in equation 33 is the Lewis form factor that is determined empirically and is dependent on the number of teeth a gear has. The Lewis form factor for various form factors has been tabulated. For this application, the Lewis Form factor is .245. In order to determine the tangential force (F_{t1}) the torque the motor would supply must be utilized. The torque generated by the motor and the gear radius are substituted into equation 34 in order to find the tangential force. Table 10 gives a summary of the calculated values for equations 33 and 34.

$F_{t1} = \frac{T_R}{16r_1}$	(34)

Table 10 Gear Tooth Bending Stress Parameters

Gear Tooth Bending Stress	$\sigma_{gb1} = 35.61\ MPa$
Lewis Form Factor	$Y_{12} = .245$
Tangential Force	$F_{t1} = 74.919N$

Given these requirements for the gears it was originally proposed that the McMaster 20° Pressure angle spur gear with a pitch of 12 and 21 teeth and a face width of 1" is sufficient for the application. The cost of each individual gear on McMaster Carr is $33.45. Thus the total cost of the gearing for this system is $66.90.

6.2 Chain Drive

With the current design, the distance between the motor shaft and the leadscrew would require the use of large gears which would increase the cost of the system. As a result a chain drive design is employed in the place of the standard gear mates. Typically a chain in particular a roller chain will fail as a result of fatigue. This is due to the fact that the tensile forces on the chain fluctuate between high loads on the tight side and low loads on the slack side. While fatigue is the dominating mode of failure in a chain drive design, which the operating speeds of the chain drive also affects the types of fatigue experienced. At low speeds, link plate fatigue dominates the system. When the operating speed is high, bushing fatigue will dominate the failure of the system [9].

In order to select the appropriate chains, empirical equations have been developed. These empirical equations provide the horse power limits that the system must not exceed in order to prevent the different forms of failure mentioned above.

Equation 35 demonstrates the horsepower limit that a system must satisfy in order to prevent link plate fatigue. Equation 36 describes the horse power limit in order to prevent bushing fatigue. Finally equation 30 represents the horse power limit in order to prevent excessive wear or galling. Equations 35, 36, and 37 correspond to equations 17-21, 17-22, and 17-23 respectively in Mechanical Design of Machine Elements and Machines book written by Collins, Busby and Staab.

$(hp_{lim})_{lp} = K_{lp}N_s^{1.08}n_s^{.9}p^{(3.0-.07p)}$	K_{lp} = .0022 for #41 chain = .004 for all other chain number N_s- # of teeth in smaller sprocket n_s- rotational speed of the smaller sprocket p- chain pitch K_{rb} = 29 for chains # 25 and #35 = 3.4 for all other chain #4 = 17 for chains # 40-240 N_L- # of teeth in larger sprocket n_L- rotational speed of the larger sprocket	(35) [9]
$(h_{plim})_{rb} = \frac{1000K_{rb}N_s^{1.5}p^{.8}}{n_s^{1.5}}$		(36) [9]
$(hp_{lim})_s = \left(\frac{n_s p N_s}{110.84}\right)(4.413 - 2.073p - 0.0274N_L) - \left(\ln\frac{n_L}{1000}\right)(1.59\log p + 1.873)$		(37) [9]

It is important to recognize that when a designing a chain drive system, one must make sure that the system's horse power does not exceed any of the calculated horse power limits outlined above. In the sections to follow, a method used to select the chain, and sprocket as outlined by Collins, Busby and Staab in chapter 17 is presented.

6.2.1 Chain Drive Design Specifications

The first step in the process is to determine the design specification of the system. Included in the design specifications are power requirements, the input shaft speed, the output shaft speed, the allowable speed fluctuation, the shaft center distance, and the desired safety factor. The table 11 presents a summary of the design requirements for this system.

Table 11 Chain Drive Design Specifications

Power transmitted	.8 hp
Input Shaft Speed	500 rpm
Output Shaft Speed	416 rpm
Allowable Speed Fluctuation	5%
Shaft Center Distance	.127(m)
Safety Factor	2
Life Requirements	

6.2.2 Evaluating Design Horsepower Requirements

Once the system requirements have been specified, the next step is to determine the design horse power requirements. This is done by utilizing equation 31 which corresponds with equation 17-24 in Collins, Busby and Staab.

$(hp)_d = \frac{K_a(hp)_{nom}}{K_{st}}$	K_a-application factor $(hp)_{nom}$- nominal power required,(horsepower) K_{st}-Multi-strand factor	(38) [9]

The design horsepower requirement is power specification that the system should be designed for. The application factor K_a , is used to account for the shock and impact loading characteristics of the driver of the chain. In this design, the driver is an electric motor. Moreover, it is assumed that there will be uniform motion in the system and nominal amount of shock. Thus, using Table 17.2 in Collins, Busby and Staab's text the application factor of 1 is selected for the evaluation of equation 38. K_{st} represents what is known as the multi-strand factor. In general as the number of chain strands used to drive the system increases, the horse power requirements decrease. In the case of this design it is initially determined that only one chain will be used in this design. A summary of the specified quantities and the calculated value of the design horsepower requirement are given in table 12. To determine the nominal horse power required, the power transmission requirements from the table 11 is substituted into equation 31. This yielded that the nominal power requirement was .8 horsepower.

Table 12 Design Horsepower Requirement Summary

Application Factor	K_a-1	Assumed nominal amount of shock and uniform motions.
Multi-strand Factor	K_{st}-1	Only one strand is used.
$(hp)_{nom}$- nominal power required,(horsepower)	.8 hp	
Design Horse Power Requirement	$(hp)_d = .8(horsepower)$	

6.2.3 Initial Chain Selection Estimate

Once the design horsepower requirement is determined, an appropriate chain pitch was selected using the calculated value of the design horsepower. Figure 17.14 provided by Collins, Busby, and Staabs is used to determine the pitch. This graph plots the nominal power requirement vs the speed of the small sprocket in rpm on a log-log scale. Lines for different chain sizes are fit on this plot. In this design, it was determined in the motor specification that the small sprocket speed would be equivalent to the input shaft speed of 360 rpm and a total power of .8hp. When plotted on this chart it is determined that the appropriate chain size is within the regime where # 35 chains are used. Figure 7 provides an image of the chart used for this analysis is presented in the figure below.

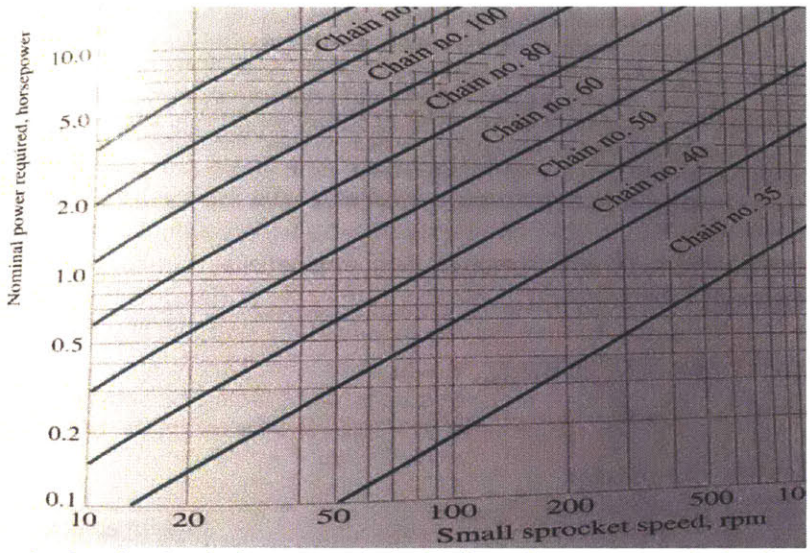

Figure 7 [3] Small Sproket Speed vs. Nominal Power Required: This figure demonstrates a plot for the appropriate sprocket speed, nominal power requirements and the appropriate chain selections for those conditions. In this design it was determined earlier that the small sprocket speed would be equivalent to the input shaft speed of 360 rpm and a total power of .8hp. when plotted on this chart it is determined that the appropriate chain size falls within the regime where number 35 chain is used.

Given the initial guess at the chain size, Table 17.6 given by Collins, Busby and Staab was consulted in order to ensure that that the minimum distance between the two shafts was conserved. After consulting the table it was determined that the center distance had to be increased to 152.4 mm in order to accommodate for the desired chain size.

6.2.4 Determination of Small and Large Sprocket Teeth count

Once the Chain size and the distance between the shafts were determined, the number of teeth of the small sprocket was selected. Once again a figure 17.13 as given by Collins, Busby, and Staab was consulted in order to get an initial estimate. This graph illustrated a relationship between the number of teeth on a sprocket and the associated fluctuations in the speed of the system. Since the desired speed fluctuation was 5% it was determined that a sprocket with 15 teeth could be best utilized for this system.

Upon determining the number of teeth for the smaller sprocket the relationship between the input shaft speed and the output shaft speed is used to determine the required tooth count for the large sprocket. Given that the input shaft speed will be 500 rpm. The desired output shaft speed is 360 rpm. In order to achieve this, larger sprocket (driven sprocket) must have 18 teeth to achieve a final speed of 416 rpm.

6.2.5 Calculating Limiting Horse Power

With the specified values outlined above, the limiting horsepower will be calculated in order to ensure that chain is designed to prevent failure. An outline of the calculated values and the necessary variable definitions are presented in table 13. Please note that equations 35,36, and 37 are employed in order to calculate the Horse Power limits.

Table 13 Summary of Horsepower Limits

Horsepower Requirement Variables	
Link Plate Horsepower Safety Factor	$K_{lp} = .004$
Number of Teeth of Large Sprocket	$N_L = 18$
Number of Teeth of Small Sprocket	$N_s = 15$
Pitch	$p = 9.5mm$
Roller and Bushing Horsepower Limit Safety Factor	$K_{rb} =$ 29 for chains # 25 and #35
Rotational Speed of Large Sprocket	$n_L = 416\,rpm$
Rotational Speed of Small Sprocket	$n_S = 500\,rpm$
Horsepower Requirement	
Galling and Wearing Horsepower Limit	$(hp_{lim})_g = 22.5064\,horsepower$
Link Plate Fatigue Horsepower Limit	$(hp_{lim})_{lp} = 1.083\,horsepower$
Roller and Bushing Fatigue Horsepower Limit	$(h_{plim})_{rb} = 68.755\,horsepower$

Note that given that the design horsepower is below all of these values, it is evident that the system will not suffer from link plate fatigue, wear or galling or roller bushing fatigue.

6.2.6 Linear Chain Speed Calculation

The equation 32 is used to determine the linear chain speed calculation is given below. The variable needed to evaluate equation 39 can be found in Table 13

$$V = \frac{pN_s n_s}{12}\ \text{ft/min} \qquad (39)\ [9]$$

$$V = 234.375\,ft/\min(\frac{1.19m}{s})$$

6.2.7 Chain Length Calculation

The length of the chain is determined using equation 40. Please refer to table 13 for the necessary variable definitions. The variable C is 16 links for this application. Note that the chain length is measured in the units of links.

$$L = \left(\frac{N_L+N_s}{2}\right) + 2C + \frac{(N_L-N_S)^2}{4\pi^2 C} \qquad (40)\ [9]$$

$$L = 48.51\ links$$

6.2.8 Pitch Diameter Calculations & Tension of the Tight Side of Chain

Prior to this point, the procedure outlined was directly taken from chapter 17 as described by Collins Busby and Staab. Specification for the pitch diameter for the sprocket and the associated tensile force was dictated using the equations outlined below. These equations can be found in the Machine Designers Reference by Jennifer Marrs.

Before the tension on the tight side can be calculated, the pitch diameter of the sprocket is determined using equation 41 [10]. A summary of the variables used in the determination of the pitch diameter and the tension in the tight side of the chain is given in table 14.

Table 14 Variable Definitions For

Pitch	$p = 9.5mm$
Pitch Diameter of Small Sprocket	$d_{psmall} = 1.80\ in\ (.0457\ m)$
Pitch Diameter of Large Sprocket	$d_{plarge} = 2.16in\ (.0549m)$
Number of Teeth on Large Sprocket	$n_{tlarge} = 18\ teeth$
Number of Teeth on Small Sprocket	$n_{tsmall} = 15\ teeth$

$$d_p = \frac{p}{\sin\frac{180}{n_t}}$$	(41) [10]

Equation 41 [10] can be used to calculate both the pitch diameter of the large and small sprockets. Note that in this equation, the variable n_t is the number of teeth on the sprocket. The calculations for these sprockets are presented in table 14.

In this book the tension in the tight side of the chain is defined as twice the value of the torque applied divided by the pitch diameter. Equation 35 and the calculated value for this application is given below. In equation 42, T represents the torque applied and d_p represents the pitch diameter. The pitch diameter used in this case is the pitch diameter for the small sprocket. Moreover the torque used to evaluate equation 35 is 25 Nm.

$$F_c = \frac{2T}{d_p}$$	(42) [10]
$F_c = 1093\ N$	

Cost of Chain Drive

Given the specifications determined above, a chain and the associated sprocket were determined that fit this design specifications. An outline of the proposed chain is outlined below.

Item	Company	Product Number	Price/unit	Quantity	Total
Sprocket(motor)	McMaster Carr	6280K118	$13.06/ sprocket	1	$13.06

Sprocket(motor)	McMaster Carr	6280K121	$14.29/ sprocket	1	$14.29
Chain	McMaster Carr	7265k2	$10.49/ft	2	$20.98
Total					$48.33

It is important to note that that the working loads of the chain is 2984 N, thus it has a safety factor of 3 and would be sufficient for the use in this design.

Chapter 7 Frame and Structure

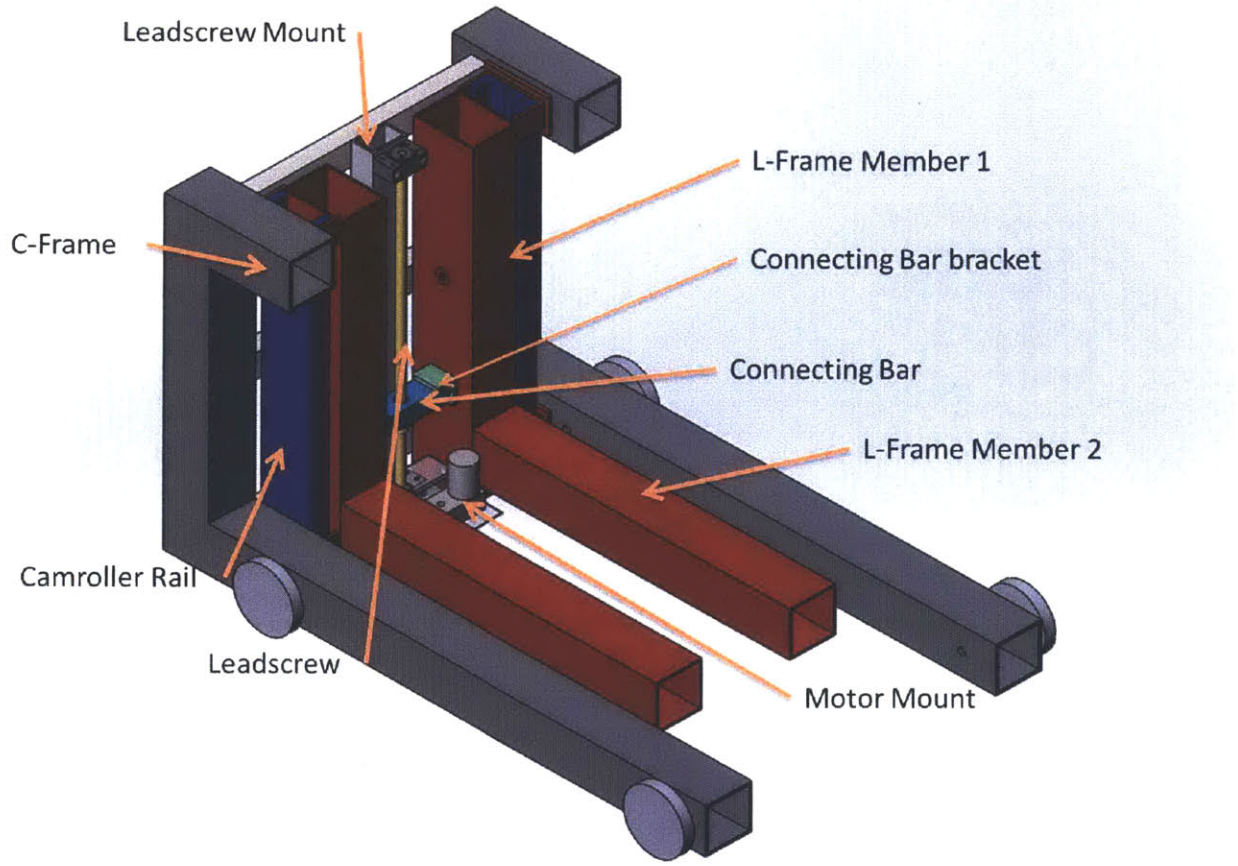

Figure 8 Frame and Structure Cad Model: This figure depicts the frame among other elements in the design. The parts that will be of particular interest in this chapter are the L-frame member which are seen as the red steel tubes. The L-frame will be the t frame upon which the platform is fixed. The second structural component that will be important in this section is the C-frame member. The C-frame provides a way to attach wheel and make the lift mobile. Moreover, through the connection to support braces in the back, the two C-frame are connected, thus making a more rigid frame for cam roller rails to attach to. In addition, this figure also depicts the Connecting Bar which will facilitate the load transfer from the leadscrew to the L-Frame. Analysis of the L-frame, C-frame and connecting Bar are found in this chapter.

7.1 Deformation of the Connecting Tube

The connecting tube is attached to the leadscrew nut in order to transfer the vertical load from the L-frame to the leadscrew. To ensure that the system is not over-constrained, the connecting tube is not fixed to the L-Frame. Rather L brackets that are fixed to L-frame member 1 and the connecting tube

pushes up against these brackets to supply support to the vertical loads. To ensure that the frame does not slip off the connecting tube an angled tab is added to both ends of the L-Bracket, thus constrains its motion. Figure 9 provides a closer view of the connection tube and connecting bracket assembly.

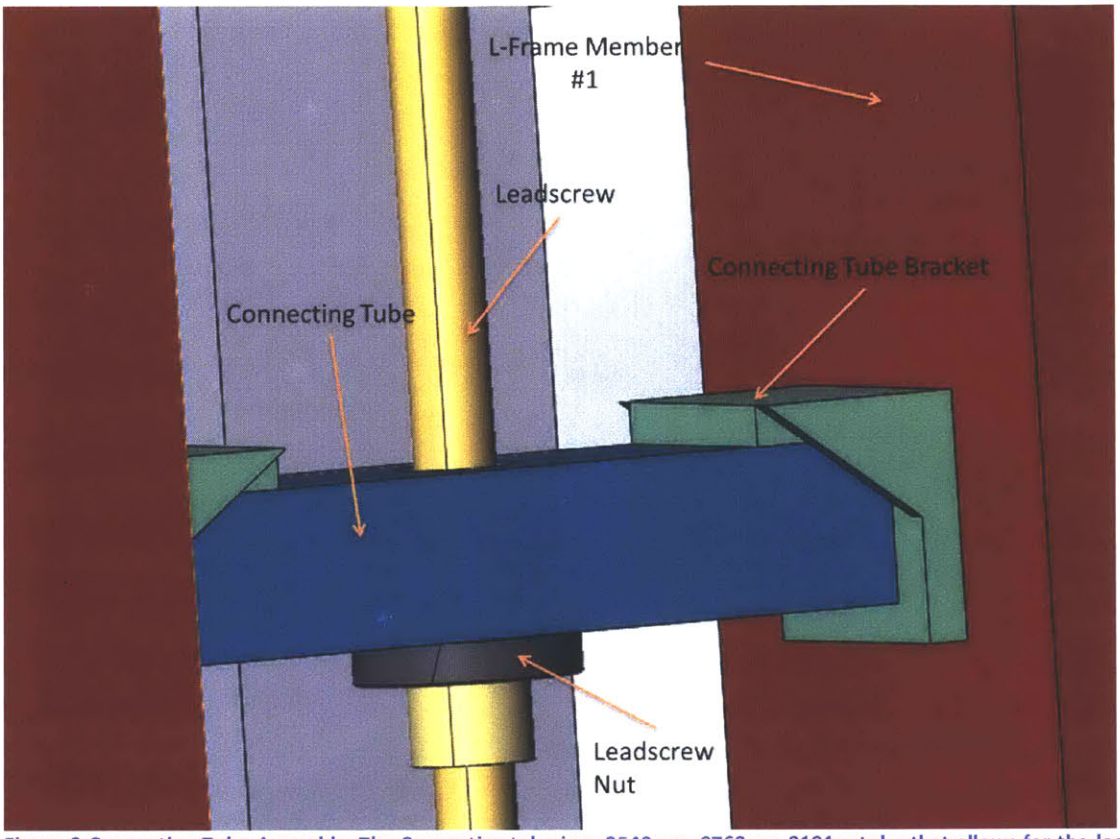

Figure 9 Connecting Tube Assembly: The Connecting tube is a .2540m x .0762mx .0191m tube that allows for the load from the L-frame member 1 to be transferred to the Leadscrew. The Connecting Bar will be attached to the lead screw nut using fastener. I order to transfer the load from the leadscrew to the L-frame member; the connecting tube brackets are introduced. The connecting tube pushes up against the connecting tube bracket as the nut moves up. As the nut pushes up against the connecting tube bracket the motion and forces will be transferred from the connecting tube bracket to the L-frame member because the connecting tube bracket will be fastened to the L-Frame member 1. It is important to recognize that the connecting tube brackets are not fastened to the connecting tube in order to avoid over constrain the system.

To begin the analysis, initial dimensions for the connecting tube are determined to be 2" (.2540m) high 3"(.0762m) wide and ¾" (.0191m) thick. In addition, the total length of the connecting tube will be 10" or(.2540m). The use of such dimensions was determined by the fact that nut on the leadscrew requires at least 3" (.0762m) width in order to properly fasten the nut to the connecting bar. The 10"(.2540m) length is a proposed distance between the two guide rails that would help facilitate vertical motion. The thickness was arbitrarily chosen and will be the parameter that is optimized. The connecting bar is modeled as a beam with two pin supports.

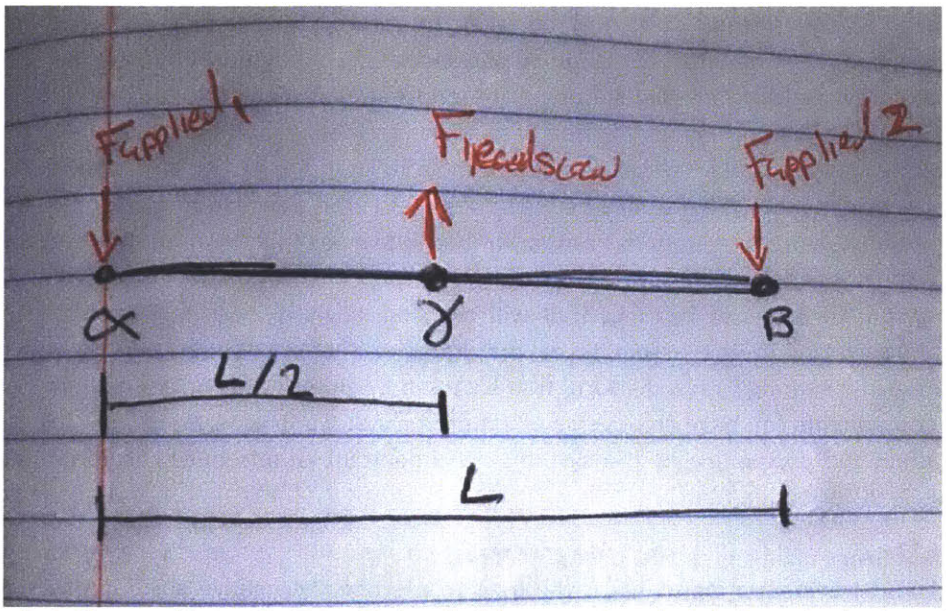

Figure 10 Free Body Diagram of Connecting Tube.: The length of the connecting tube is designated to be the variable L which is equivalent to .2540m. At the nodes α and β vertical forces are applied. These forces are equal to one another and sum up to the weight of the overall platform including the weight of the patient. At node γ the leadscrew applies a force to the connecting bar to counteract the forces applied at nodes α and β. Note also that γ is located at half the span of the connecting tube.

When the section forces and moments are evaluated for the connecting tube, it is determined that that the maximum moment with the member will be equivalent to $F_{applied} * \frac{L}{2}$. The moment is evaluated in t bending stress is evaluated in the table 15 below. The proposed dimensions of the tube are a 3" x 2" x ¼ tube. The length of the tube is .254 m and $F_{applied}$ is 4500N. The equation for bending stress is presented in equation 43 and the Necessary values need to evaluate equation 43 is presented in table 15.

Table 15 Connecting Tube Bending Stress Variables

Variable	Value
Moment	$M = 5.715 \times 10^2 Nm$
Moment of Inertia	$I = 5.398 \times 10^{-7} m^4$
Height	$y = 5.08 \times 10^{-2} m$

$\sigma = \frac{My}{I}$	(43)
$\sigma = 6.45 \times 10^7$	

Given these values, the stresses that will be experienced within this member are below the yield stress for steel. Thus, the proposed dimensions are sufficient for the design.

7.2 Analysis of Proposed L-Frame

With any linear motion system, care must be taken to ensure that jamming does not occur in the system. According *to Fundamentals of Design by Alexander Slocum* jamming can often be prevented by apply specific aspect ratios in bearing spacing. The principle that many engineers employ is that the distance between the bearings in the direction of motion should be greater than or equal to the distance between bearings perpendicular to the direction of motion. From the earlier calculations performed in section 5.1 it is evident that the distance between bearings in the direction of motion is particularly of interest when the system must support a cantilever load. The more spaced apart, they are, the less load that an individual bearing will experience. While the previous calculation provides a first order understanding on the types of bearings that will be need, analysis must be performed in order to understand how errors in the assembly of the frame can affect the loading on the structure. Misalignment of the bearings, rails, platform frame caused by either errors in assembly or deflection of mechanical components can have an adverse effect on the system. In order to be able to quantify how errors can affect the positioning of the system, it is important to introduce the formulation of the Homogenous Transformation Matrix (HTM).

7.2.1 Formulation of Homogenous Transfer Matrix

The Homogenous transformation matrix is the used to describe the relative position of a rigid body in 3D- space with respect to a given reference coordinate system. The HTM is a 4x4 matrix. The first three columns within the matrix represent the orientation of the rigid bodies coordinate frame with respect to the reference coordinate frame. The fourth column is the position vector of the system. The positon vector refers to any offsets that the rigid body coordinate system's origin has with respect tothe reference coordinate frame [11]. Equation 44 provides a general form of the HTM as presented in Alexander Sloculm's Precision Machine design book. Note that when expressing the HTM symbolically the super script refers to the reference coordinate system while N refers to the body coordinate system.

$$ {}^{R}T_{N} = \begin{bmatrix} \Theta_{ix} & \Theta_{iy} & \Theta_{iz} & P_x \\ \Theta_{jx} & \Theta_{jy} & \Theta_{jz} & P_y \\ \Theta_{kx} & \Theta_{ky} & \Theta_{kz} & P_z \\ 0 & 0 & 0 & 1 \end{bmatrix} \quad (44)\ [11] $$

In the most basic case, matrix multiplication is performed between the homogenous transformation matrix and the rigid body coordinate frame in order to obtain its positon in the reference frame. When multiple transformations take place between the reference frame and the desired rigid body (i.e. there are many links/ connections between the reference frame and the rigid body frame in question) it is important to consider the order of rotations for non-negligible angles of rotation. When angles are non-negligible, changing the order of rotation will affect the final orientation of the rigid body axes [11].

Critical to the proper formulation of the HTM is the selection of the reference frame and the rigid body frame. For this application, the reference frame is placed on the floor as denoted by the blue axis in figure 11. The x axis constructed such that the positive X direction is toward the right. The Y direction is positive in the upward direction and the z direction is pointing out of the page. The rigid body in

question is defined to be the cam roller 1. This was selected because the cam roller 1 will be the furthest of the two cam rollers. According to Abbe's principle, any angular misalignment will be greatly amplified at the position of cam roller 1 [12]. Thus, designing to minimize the deflections at this point will ensure that the deflection else were in the system are below the critical tolerances in the system. With these two major reference points chosen, the remaining coordinate systems are placed along the path to relate the two ends. One important convention that is employed in this formulation is that each coordinate frame is chosen such that they are parallel with the respective axis of the reference frame [11]. Figure 11 provides a schematic of the determined coordinate systems that will be used in this analysis.

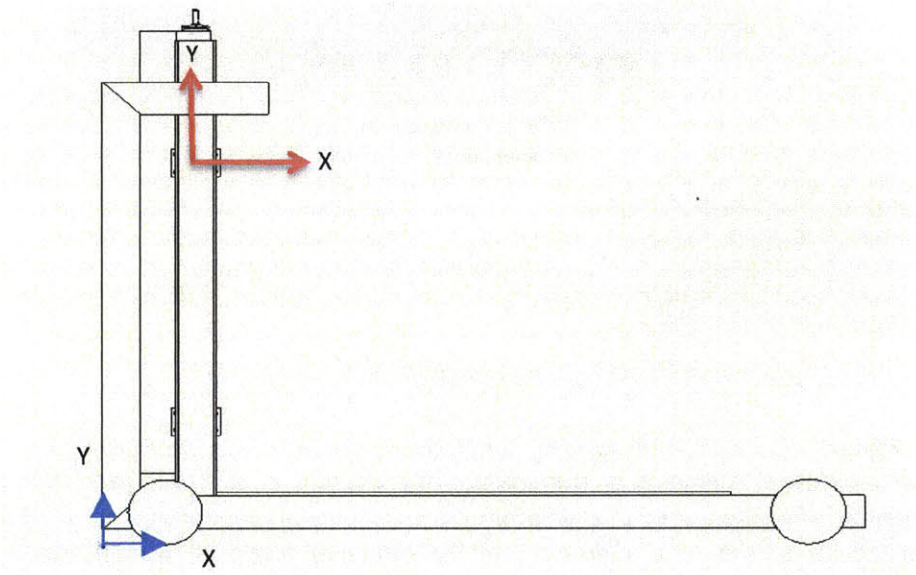

Figure 11 Reference Frame Definition of Platform Lift: This figure depicts an image of the structural frame of the platform lift excluding the platform itself and the associated ramp. The blue arrows indicate the location and the direction of the reference frame. The red arrows indicate the location and origin of the body coordinate frame of cam roller 1. The direction pointing to the right of the image is the positive X direction while the arrow pointing in the vertical direction is defined as the positive Y axis. A Positive moment is defined to be in the counterclockwise direction.

To simplify the system, the L-frame is depicted as stick figure and presented in figure 12. Node B indicates the point of connection between L-frame member 1 and L-frame member 2. Appropriate lengths were designated in order to develop the homogeneous transform matrix. Node C is chosen to be at the height at which cam roller 1 will be attached to the L-Frame member#1. The vertical distance between the Node B and C is represented by the variable b_{space}. In order to relate the system errors to the rail and cam roller surface, the position of the cam roller surface is defined in reference to the coordinate frame located at Node C.

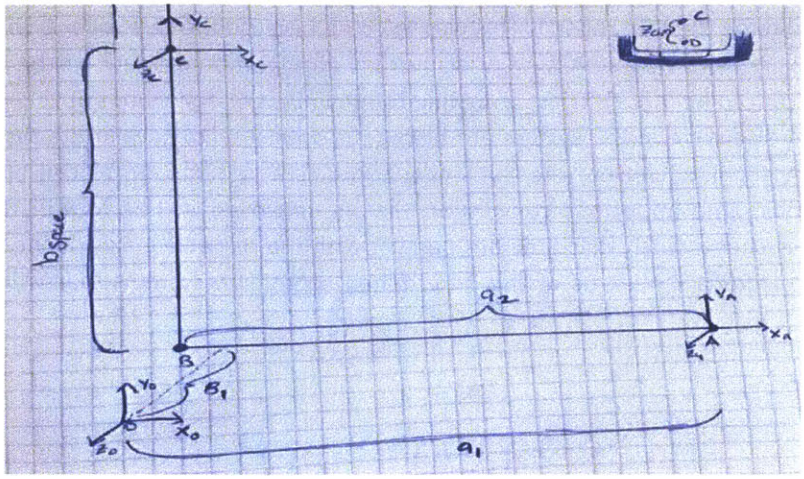

Figure 12 L –Frame Simplification: This figure demonstrates a simplified version of the L-frame. There are a total of four nodes on this system label A through D. Nodes A, B,C and D represent the tip of L-frame member 2, the connection point of L-frame members 1 and 2 , the location of the connection between L-frame member 1 and cam roller 1 and the location of center of cam roller 1 respectively. Point O represents the location of the origin of the reference frame. Note that a_1 represents the distance in the x direction from the origin of the reference frame to node a. Similarly, the distance between node A and node B in the X direction is represented by the a_2. The distance between the origin of the reference point O and node A in the z direction is represented as B_1. D_{wheel} is the offset in the y direction between the reference point O and Node A. The variable b_{space} refers to the spacing between the bearings and z_{cam} represents the offset in the z direction of the center of the cam roller to the location of node C.

7.2.1.1 Accounting for Errors In homogenous Transformation Matrix

Within each element in a structural system, there are errors that can be associated with the final positioning of subsequent elements in the system. Any element in 3D space can have a total of 6 degrees of freedom and thus a total of 6 different error components to account for. If an error matrix were constructed for an individual rigid body in the reference frame of the rigid body frame, the resulting error matrix can be written as equation 45 [11].

$E_n =$

(45) [11]

1	$-\varepsilon_z$	ε_y	δ_x
ε_z	1	ε_x	δ_y
$-\varepsilon_y$	ε_x	1	δ_z
0	0	0	1

The entries in the HTM describing the error are the following: ε_x , ε_y , ε_z describe the rotational error about the respective x, y, or z axis while the components δ_x, δ_y, δ_z represent the translational errors in the x,y,z directions of the rigid body's coordinate frame. To construct a HTM of a rigid body that accounts for error, the HTM of the rigid body in reference to its previous reference frame is multiplied by the error matrix described above. The formulation of the transformation matrix for cam roller 1 has been applied below in order to illustrate the calculations that will be used later in this analysis.

7.2.1.2 Transformation Matrix Evaluation for Node A

In this evaluation, the coordinate frame of body A, which is the second member of the L-frame is transformed to the reference frame at point O. Notice that x, y, and z offsets of node A from the reference point O are accounted for in the fourth column of the HTM ${}^{O}T_{A}$ in equation 46 [11]. Please refer to the section 7.2.1 in order to understand the meaning of each entry in this matrix. Note that in equation 46, all off diagonal terms in the first three columns are zero since the coordinate frames were defined to be parallel with one another.

${}^{O}T_{A}=$

(46) [11]

1	0	0	a_1
0	1	0	D_{wheel}
0	0	1	$-B_1$
0	0	0	1

The general error matrix for body A, would be the same as the error matrix described in equation 45 found in section 7.2.1.1. Thus, when the product of ${}^{O}T_{A}$ and E_n is performed, the homogenous transformation matrix at node A, that accounts for error in position at node A is presented in equation 47.

${}^{O}T_{AERR}= {}^{O}T_{A}\, E_n$

(47) [11]

1	$-\varepsilon_{za}$	ε_{ya}	$\delta_{xa}+a_1$
ε_{za}	1	$-\varepsilon_{xa}$	$\delta_{ya}+D_{wheel}$
$-\varepsilon_{ya}$	ε_{xs}	1	$\delta_{za}-B_1$
0	0	0	1

7.2.1.3 Transformation Matrix Evaluation for Node C

In this evaluation, the transformation matrix relating the coordinate system of node C with the coordinate system of node A must be determined. The procedure is very similar to the aforementioned procedure in section 7.2.1.2. Equation 48 expresses the HTM that relates node C to node A. Note that in the fourth column of equation 48, the offsets given are in reference to node A and not to the global reference frame at point O.

${}^{A}T_{C}=$

(48) [11]

1	0	0	$-a_2$
0	1	0	b_{space}
0	0	0	0
0	0	0	1

Note that according to the chosen sign conventions, the x position of node c relative to node A is negative. Moreover since we assume that the x-y plane of both L-frame members are within the same plane, there is no z offset between the coordinate frame of node A and node C. Accounting once again for the error of the first member of the L frame, equation 49 is produced which represents the HTM that transforms the rigid body frame at node C into the coordinate frame at node A.

$^{A}T_{CERR} = {}^{A}T_{C}\, E_{n}$ (49) [11]

1	$-\varepsilon_{zc}$	ε_{yc}	$\delta_{xc} - a_2$
ε_{zc}	1	$-\varepsilon_{xc}$	$\delta_{yc} + b_{space}$
$-\varepsilon_{yc}$	ε_{xc}	1	δ_{zc}
0	0	0	1

7.2.1.4 Calculating the Actual Position of The Cam Roller using HTM

In order to find the actual position of the cam roller based on the error in each individual structural element in the system, equation 49 is employed. This equation is the product of the HTM developed at each node of the L frame. Moreover, it is follows the conventions as specified by equation 2.2.24 [11] in Alexander Slocum's book "Precision Machine Design".

$$P_{camroller\_actual} = {}^{O}T_{AERR}\, {}^{A}T_{CERR}\, P_{camroller} \quad (49)\ [11]$$

$P_{camroller}$ refers to the position of cam roller #1 in terms of the coordinate frame at node C. It is important to note that in the multiplication of the transformation matrices $^{O}T_{AERR}$ and $^{A}T_{CERR}$ second order terms associated with the rotational and translation entries are excluded. This is a result of the assumption of small rotational and translational errors. With these assumptions established, the products of the two matrices are presented in equation 50 and the actual positon of the cam roller denoted by the $P_{camroller\_actual}$ is given by equation 51.

$^{O}T_{AERR}\, {}^{A}T_{CERR} =$ (50) [11]

1	$-(\varepsilon_{zc} + \varepsilon_{zc})$	$\varepsilon_{yc} + \varepsilon_{ya}$	$\delta_{xc} - a_2 - b_{space}\,\varepsilon_{za} + \delta_{xa} + a_1$
$\varepsilon_{za} + \varepsilon_{zc}$	1	$-(\varepsilon_{xa} + \varepsilon_{xc})$	$\delta_{yc} + b_{space} + \delta_{ya} + D_{wheel} - a_2\,\varepsilon_{za}$
$-(\varepsilon_{yc} + \varepsilon_{ya})$	$\varepsilon_{xa} + \varepsilon_{xc}$	1	$\delta_{za} + \delta_{zc} + b_{space}\,\varepsilon_{xa} + a_2\,\varepsilon_{ya} - B_1$
0	0	0	1

$P_{camroller}$ = (51)	0 0 z_{cam} 1

As stated before, this position vector is given in terms of the coordinate system located at node C. The center of the cam roller is assumed to be located at the same x and y positions as the origin of the coordinate system at node C. There is however an offset in the positive z direction for the center of the cam roller.

Equation 52 is the product of equations 50 and 51. It represents the actual position of the cam roller due to the errors in the position of the members of the L frame.

$P_{camroller\_actual}={}^{O}T_{AERR}\,{}^{A}T_{CERR}\,P_{camroller}$ (52)	$(\varepsilon_{yc}+\varepsilon_{ya})z_{cam}+\delta_{xc+}\delta_{xa}+a_1-a_2-b_{space}\,\varepsilon_{za}$
	$-(z_{cam}(\varepsilon_{xc}+\varepsilon_{xa}))+b_{space}\,\delta_{yc}+\delta_{ya}+D_{wheel}-a_2\,\varepsilon_{za}$
	$z_{cam}+a_2\,\varepsilon_{ya}+b_{space}\,\varepsilon_{xa}+\delta_{za}+\delta_{zc}-B_1$
	1

Given the actual position of the cam roller based on the assumed errors, the error in the position of cam roller 1 can be determined. This error will be defined as the difference between the difference between the cam roller and the ideal position of the cam roller. To find the ideal position of the cam roller, compute the product of equation 46 and equation 48. The ideal cam roller location is given by the position vector $P_{camroller\_ideal}$ as expressed in equation 53.The rows of the vector correspond to the x, y, and z directions of the cam roller. The fourth row of the ideal cam roller position is the scaling factor.

$P_{camroller\_ideal}$ (53)	a_1-a_2
	$D_{wheel}+b_{space}$
	$z_{cam}-B_1$
	1

The difference between equation 52 and equation 53 according to Alexander Slocum can be referred to as the error motion [11]. A general expression of the error motions for cam roller #1 is expressed in equation 54. Knowing the resulting error motions and the stiffness of the cam roller, the additional forces experienced by the cam roller applied as a result of the load applied to the system can be determined..

$P_{camroller\_error}={}^{O}T_{AERR}\,{}^{A}T_{CERR}\,P_{camroller}-P_{camroller\_ideal}$ (54) [11]	$(\varepsilon_{yc}+\varepsilon_{ya})z_{cam}+\delta_{xc+}\delta_{xa}-b_{space}\,\varepsilon_{za}$
	$-(z_{cam}(\varepsilon_{xc}+\varepsilon_{xa}))+b_{space}\,\delta_{yc}+\delta_{ya}-a_2\,\varepsilon_{za}$
	$a_2\,\varepsilon_{ya}+b_{space}\,\varepsilon_{xa}+\delta_{za}+\delta_{zc}$
	1

7.2.1.5 Sources of Error

In order to evaluate equation 46 it is important to identify the sources of error in this design. Some of the major possible sources of error in a mechanical system are geometric errors, kinematic errors, external load induced errors, machine assembly load-induced errors, thermal expansion errors, material instability errors and instrumentation errors [11]. While this is a rather extensive list of errors, it has been identified that load induced errors are among the most important to consider in this design since the loads are high. Thus, in order to obtain the errors due to the load, the stiffness method must be introduced. Stiffness of a structural member describes the force displacement relationship for a body. What the concept of stiffness thus implies is that as long as a rigid body has a finite stiffness, when it is loaded, it will also experience a deflection. This deflection can either be translational or rotational. The effects can be accumulated when in a structural frame [11].Thus, with this explanation of the stiffness; it is then evident that understanding how the load applied will cause other members of the frame to deflect will reveal how these deflections will further load other members of the frame. In the following sections, the deflection of the L-frame members will be determined in order to find the deflection of Cam roller 1. A model will be developed to generate a value for the stiffness of an individual cam roller. Using the stiffness determined for an individual cam roller, the load induced deflection will be multiplied by the determined stiffness to provide a force as a result of the deflections/ error motions in the system.

Modeling Cam roller Stiffness

The Cam roller can be viewed as a cylinder that makes contact with the flat rail surface. Employing the Alexander Slocum's analysis of line contact between bearings, it is possible to determine the deflection of a cylinder in contact with a flat surface. In order to do this, it is important to first introduce the the equivalent modulus. The equivalent modulus is given by equation 47 In this Equation E_1 and E_2 represent the elastic modulus of the of the two contacting surfaces in question respectively. η_1 and η_2 represent the values of the passion ratio for each respective material. Depending on the on the assumptions made during the analysis, one of the terms in the denominator will vanish. This will become apparent in the analysis to follow.

$$E_e=\frac{1}{\frac{1-\eta_1^2}{E_1}+\frac{1-\eta_2^2}{E_2}}$$	55 [13]

When a cylindrical surface is in contact with another surface, the area of contact is designated by a rectangle that has a width of 2b. The variable b can be evaluated for using equation 56. In this equation the half width of the contact area of the cylinder is described as a function of the applied load, the diameters of the respective elements in contact , the length of the cylinder, and the equivalent modulus as evaluated in equation 55 [13]. It is important to recognize that when evaluating the deflection on the

cylinder in contact with a flat surface,E_2 and d_2 are assumed to be infinite [13]. This makes sense because by making E_2 infinite, the model is assuming that cylinder is in contact with an infinitely stiff element and thus only the cylinder deflects. Moreover d_2 is equivalent to infinity because the radius of curvature of a flat surface is infinite.

$$b = \left(\frac{2Fd_1d_2}{\pi LE_e(d_1+d_2)}\right)^{\frac{1}{2}}$$	56 [13]

Once equations 55 and 56 are evaluated, it is possible to determine the deflection of the cylinder by employing equation 57. Equation 57 describes the deflection that the cylinder will experience when in contact with another curved element.

$$\delta_{cylinder} = \frac{2F}{\pi LE_e}\left[\log_e\left(\frac{2d_1}{b}\right) - \frac{1}{2}\right]$$	57 [13]

In order to model of the cam roller, it is important to understand the elements of the Cam roller. The cam roller specified by PBC consist of an outer ring, inner ring and cylindrical rollers that are made of harden steel. The assumption in this analysis is that the load is transferred from the outer ring to the cylindrical rollers and then to the inner ring. As a result of this assumption it follows that the outer ring, cylindrical rollers and inner ring act in mechanical series and the total deflection of the cam roller is equivalent to the sum of the deflections of each element within the roller. This implies that equations 55-57 should be evaluated for the outer ring, cylindrical roller and inner ring separately. Modeling each component of the cam roller as a spring, the deflection determined by equation 49 can be substituted into Hooke's law to solve for the stiffness of each respective element. Finally the equivalent stiffness of the cam roller was found using equation 58.

$$K_{eq,camroller} = \frac{1}{\frac{1}{K_{inner}} + \frac{1}{K_{outter}} + \frac{1}{K_{clyroller}}}$$	58
$K_{eq,camroller} = 1.712*10^8$ Nm	

The table below gives a summary of the computed values of K_{inner}, K_{outter} , $K_{clyroller}$ and the associated dimensions and values used in the computation of equations 55, 56 and 57 for each respective roller. The equivalent stiffness is presented in equation 58.

Table 16 Summary of Variables for Cam Roller Stiffness Calculation

Applied Load	$F = 4454.5N$
Diameter of Cylindrical Roller	$d_{cyroller} = .005\ m$
Diameter of Inner Ring	$d_{inner} = .060\ m$
Diameter of Outer Ring	$d_{outer} = .123\ m$

Equivalent Modulus	$E_e = 219.8GPa$
Length of Cam roller	$L = .037m$
Possion's Ratio of Steel	$\eta = .3$
Deflection Results of Cam Roller Elements	
Deflection of Cylindrical roller	$\delta_{cylroller} = 2.1410\text{^} - 6$
Deflection of Inner Ring	$\delta_{inner} = 2.169 * 10\text{^} - 5$
Deflection of Outer Ring	$\delta_{outer} = 2.294 * 10\text{^} - 6$
Stiffness Results of Cam roller Elements	
Stiffness of Cylindrical Roller	$K_{clyroller} = 2.08 * 109\ N/m$
Stiffness of the Inner Ring	$K_{inner} = 2.05 * 108\ N/m$
Stiffness of the Outer Ring	$K_{outer} = 2.08 * 109\ N/m$

With the value determined for the equivalent stiffness, this value will now be multiplied by the deflection computed in the forthcoming chapters and added to the overall load to get an idea of how deflection will additionally load the system.

7.2.1.7 Preliminary Deflection Results

The double integration method was used to determine the deflections of the members of the L-Frame as described in figure 13. The point of connection between the two members of the L frame was assumed to be a pin joint. The L-frame member 1 is isolated and a free body diagram is generated for it. From figure 13 it is evident that a moment acts on L-frame member 1. This moment is equivalent to the moment generated by the weight of the person on the platform and the weight of the platform itself. The singularity equation for L-frame member 1 was formulated and the double integration method was used to generate deflection equations for cam roller 1 at node C in figure 12. These computed deflections would be equivalent to the error motions as presented in equation 54. The figure provides an image of the model used and the designations for the moment and forces at each segment of the beam. The singularity equation that was generated for L-frame member 1 was implemented into a Matlab code that allowed for quick manipulation of the variables that significantly influenced the deflections of the cam roller. In this discussion, the singularity equation is stated and the results are discussed.

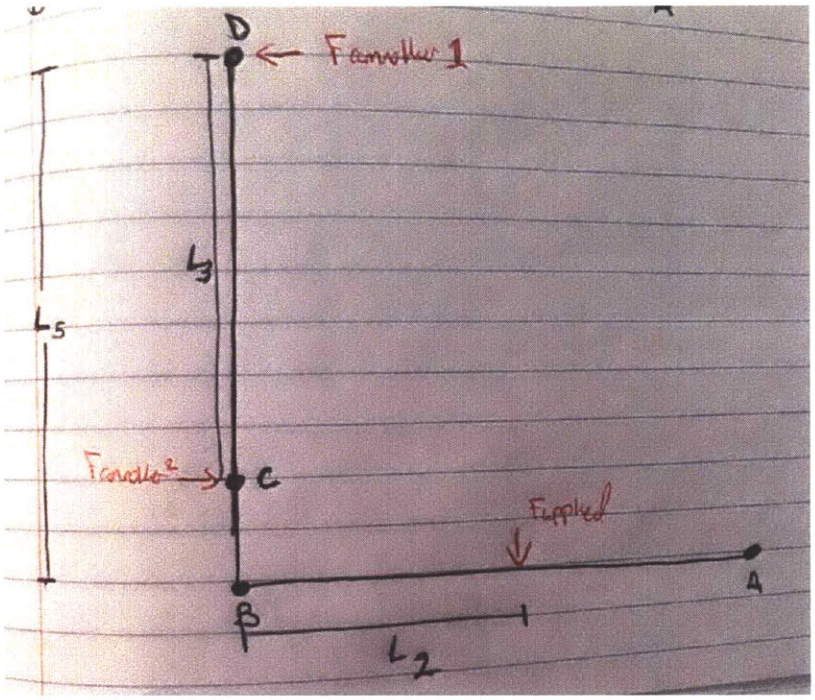

Figure 13 Initial L-Frame Design: This image depicts the initial L-frame design. Segment BD represents L-frame member 1. Segment AB represents L frame member 2 and an applied force which is equivalent to the half the load requirement of the system is applied to it at a distance L_2. It is important to recognize that node B specifies the location at which the L frame member 1 and 2 connect. The connection of the two L-frame members is facilitated by a fastener pattern. This fastener pattern will allow for node B to be able to sustain a moment. Nodes D and C represent the location of the center of the of cam roller 1 and 2 respectively. L_3 denotes the distance between the two cam rollers and L_5 is the distance from the connection point of the two L-frame members and cam roller 1. Note that the forces of the cam rollers have been directed in a manner to counteract the moment generated by the applied load on L-frame member 1.

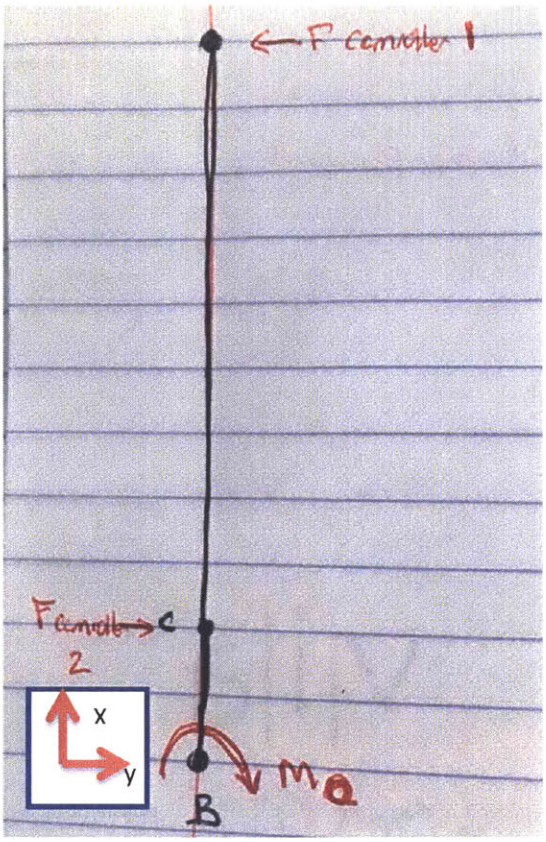

Figure 14 Free Body Diagram of L-Frame Member 1: This figure provides an image of the free body diagram of L-frame member 1. The moment M_o is equivalent to the moment generated at node B as a result of the moment generated by the applied load on L-frame member 2. The x and y Directions are as specified in this image.

The singularity equation is given by equation 59. The first term of equation 59 is defined as the component of deflection member 1 experiences as a result of the moment that member 2 exerts on it. Notice that in this equation, the moment begins to act at x=0 since the assumption is that member 2 and 1 are connected at the bottom of L-frame member one at the point defined as x=0. The second term of this equation represents the effects of the force of the cam roller 1 on the overall deflection of the beam. Notice that this force does not affect the deflection of the beam until a distance L_3 along L-frame member 1. Finally the third term of this singularity equation represents the effects of the reaction force produced by the second cam roller on the total deflection of the system. Note that the moment applied at node B is assumed to be clockwise since the applied load on member 1 would generate a clockwise rotation.

$$\varepsilon = \frac{F_{camroller}\langle x - L_3\rangle^3}{6EI} - \frac{F_{camroller}\langle x - L_5\rangle^3}{6EI} + \frac{M_o\langle x\rangle^2}{2EI} \quad (59)$$

7.2.1.6.1 Deflection Results of Frame Using the Double Integration Method

A summary of the result using the double integration method is presented in table 17.

Table 17 Deflection Results of Initial L-Frame Analysis using the Double Integration Method

Deflection/ Resultant Moment Results of Cam Roller 2		
Deflection Results (mm)	Resultant Force Corresponding to Deflection	Comments
-3.9	668kN	Deflection and force results for 3"x3"x1/4" dimensions of L-frame member 1.
-1.5	257 kN	Defection and force results for 4x4x1/4 dimensions of L-frame member 1.

The results in table 17 suggest that the current configuration as presented in figure 13 will not produce sufficiently low deflections to allow the applications of the Hevi-rail cam rollers. Thus, a new configuration must be developed in order to allow for the utilization of the Hevi-rail cam rollers.

7.2.3 New Frame Configuration

The results illustrated above indicate that in order to further reduce the deflection; the moment of inertia must be increased. However, when considering the size of this beam, it is evident that increase in the moment of inertia alone will not be sufficient to reduce the deflection of the system. If the singularity equation given by equation 59 is carefully examined, it is evident that an alternative way to reduce the deflections is to decrease the effects of the moment on the deflection. To accomplish this, one can either reduce the moment applied to the system or reduce its effect by changing where the moment is applied. The second of the two is more easily attainable since geometric restrictions prevents significant shift in the lever arm of the applied force on L-frame member 2. Thus, the location of the connection between the two members of the L-frame is shifted. A schematic is provided below for what the new configuration.

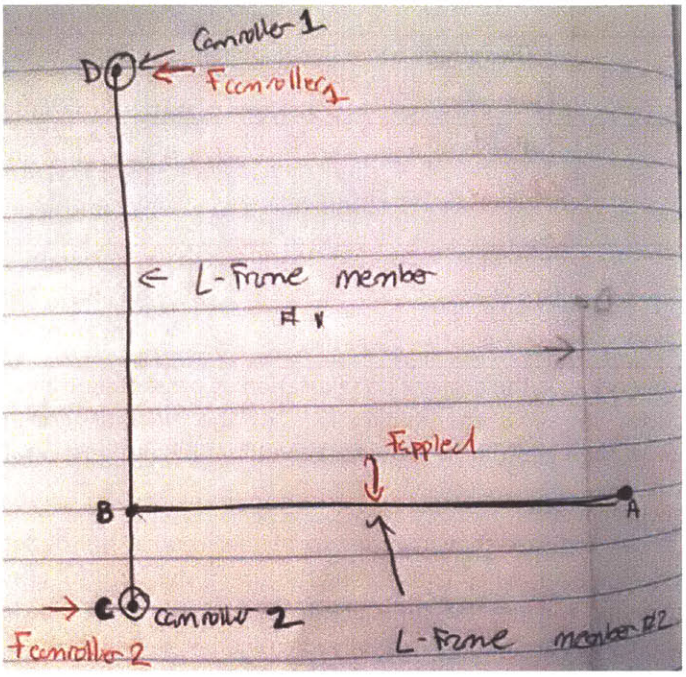

Figure 15 New L-Frame configuration: This image provides a description of the new L-frame configuration. Notice that unlike figure 13, in figure 15, node B is above node C. Thus, this reduces the effect of the moment on the displacement of cam roller 1.

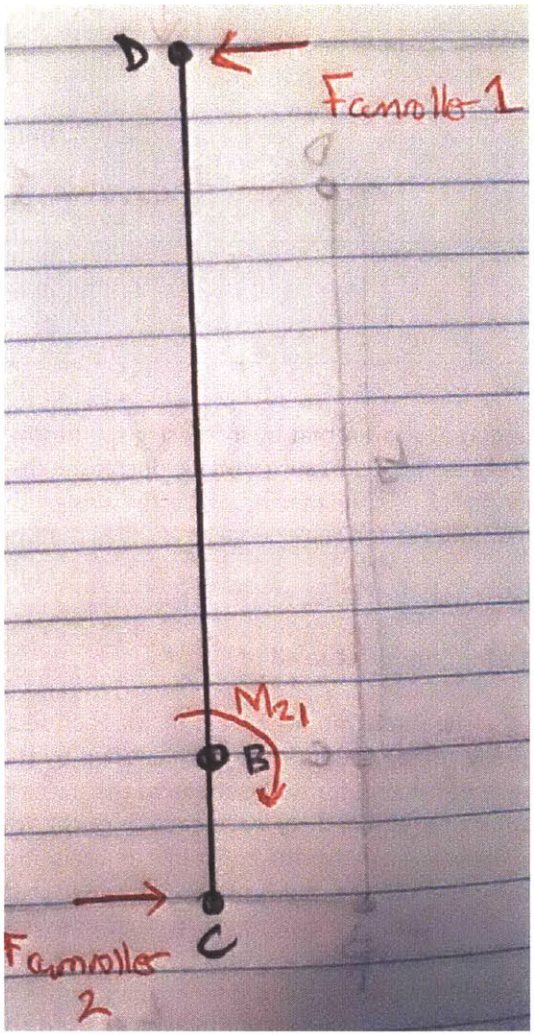

Figure 16 L-Frame Member 1(New Configuration Free Body Diagram) This figure describes the forces acting on the L- frame member 1 in this new configuration.

As in the previous section a singularity equation is generated for the new proposed configuration of the frame is given by equation 60.

$$\varepsilon = \frac{F_{camroller}\langle x\rangle^3}{6EI} - \frac{F_{camroller}\langle x - L_5\rangle^3}{6EI} + \frac{M_o\langle x - L_3\rangle^2}{2EI} \quad (60)$$

The deflection results using this new configuration are calculated at same dimensions as suggested in table 17 and it is used to motivate the new height of the connection between L-frame member 1 and L-Frame member 2.

Table 18 Deflection Results of New L-Frame Configuration using the Double Integration Method

Deflection/ Resultant Moment Results of Cam Roller 2 With New L-Frame Configuration		
Deflection Results (mm)	Resultant Force Corresponding to Deflection	Comments
-1.5	257kN	Deflection Results For 3"x3"x1/4" dimensions of L-frame member 2.
-0.58	-99.3kN	Defection Result For 4x4x1/4 dimensions of L-frame member 2.

These preliminary results have demonstrated that by increasing the height of L-frame member 2 above the height of cam roller 2 by 2 inches (.0508m) substantially decreases the deflections produced by the moment of member 2 on member 1. To further optimize the design the frame is analyzed using a combination of the virtual work methods and the double integration method.

7.3 New L-Frame Configuration: Deflection Analysis

7.3.1 Double Integration Method and Virtual Work

The first step in to determine the shear and moment diagram for each section of the frame. In the case of the L frame, there are naturally three sections that are identified by the different lengths. After the shear and moment equations are developed for each section of the frame or beam in question, one can integrate the equation of moment determined for each section of the frame or beam. The boundary conditions can then be used in order to solve for the constants of integration of the design. At this point it is important to mention that for the L-frame, the fastener pattern at node A can be best modeled as a pin joint or as a fixed joint. If modeled as a pin joint, it means that the system cannot sustain a moment in node A as specified in the diagram above. Thus, the two connection points are allowed to freely rotate about the pivot point and their rotation will not be coupled and will exhibit different slopes and rotations at the node B [14]. If the fastener pattern is modeled as fixed connection point, all members connected at that node will to rotate by the same amount [14]. Upon investigation it was determined that the intended fastener pattern will closely resemble a pin joint. However, the only caveat is that the fastener pattern will also be able to withstand a finite moment.

The double integration method involves two integrations on the moment equation. The first integral as discussed before produces the slope equation for a section of a beam. The second integral produces an equation for the deflection of the beam. In order to find the constant of integration for the displacement equation it is important to remember the assumption of node B as a pin joint. This implies that that position of this node does not change.

7.3.2 Double Integration Analysis for L-Frame Member 2

Moment Equation

To develop the moment equation, it is important to understand the force and loads acting on member 2. According to figure 16, there is a moment acting on this member that comes as a result of the

fastener pattern. Moreover, there is also a vertical reaction force at node B which is equivalent to the force applied by the platform. This applied force is equivalent to the weight of the patient and the platform.

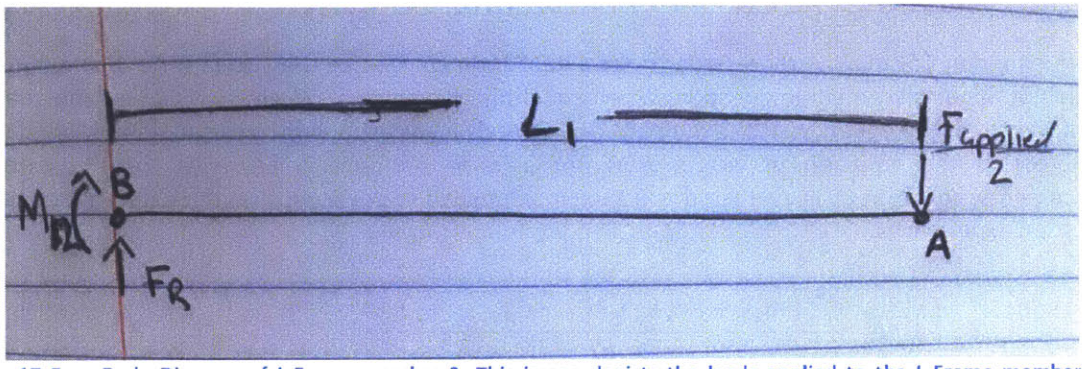

Figure 17 Free Body Diagram of L-Frame member 2: This image depicts the loads applied to the L-Frame member 2. L_1 indicates the length between the connection point at Node B and the point where the load is applied at node A. M_{12} is the moment that the fastener pattern will exhibit on the member given. Note that the connection at node B is assumed to be a pin joint, it is assumed that the deflection at the node is equal to zero.

The resulting moment equation from this analysis is given by equation 61.

$M_{section1} = M_{12} - F_{applied}x_1$	(61)
$\theta_{section1} = \frac{M_{12} * x_1 - F_{applied}{x_1}^2 + c_1}{EI}$	(62)
$\varepsilon_{section1} = \frac{M_{21}{x_1}^2 - \frac{F_{applied}{x_1}^3}{6} + c_1x_1 + c_2}{EI}$	(63)

The integrals for the moment are given in equation 59 and 60 as well. E and I refer to the elastic modulus of the specified material and the moment of inertia about the neutral axis of the beam respectively. It is important to note that c_1 and c_2 refer to the constants of integration generated in equation 62 and 63 respectively. While the assumption of zero displacement at node B (x_1=0 is available) requires c_2 to be zero, there is no way to solve for c_1 since there is no slope boundary conditions. Thus, in order to solve for c_1 another equation must be developed.

7.3.3 Virtual Work Method for L-Frame Member 2

In order to develop the additional equation needed to solve for c_1, the virtual work method is employed. Virtual work leverages the principle of energy conservation in a system. In particular applications to beams, virtual work can be used to relate the internal energy as a result of a virtual force and displacement and relate it to the external displacements of the system. This is exactly what is employed here. In this method an external virtual load is applied at L_1, which is the location where the load of the patient and the platform is applied on L-frame member 2. Section analysis is performed on the system in order to see how the virtual load *f* would affect the member. Thus, this allows for the development of the moment equations for the virtual load as stated in equation 65. Knowing the moment and recalling the relationship between the moment and the slope of a beam it is possible to use the following equation to help solve for the external deflections of the system using equation 64. In equation 64, m represents the moment within the section as a result of the resultant load. M/EI dx reflects the real deformation the element experiences.

$1 \cdot \Delta = \int_0^L \frac{mM}{EI} dx$	(64) [15]
$m_{section1} = m_{21} - fx_1$	(65)

Note in equation 65, $m_{section1}$ represents the resultant moment due to the virtual force applied in the direction of the displacement in question. When equation 64 is applied, m will be as derived in equation 65 and M will be the equation of the moment due to reals loads as described in equation 61. Equation 66 represents the equation of virtual work for L-Frame member 2. To solve for the external displacements, equation 66 is evaluated and then manipulated to get Δ which is the external deflection the system experiences.

$f \cdot \Delta = \frac{\int_0^{L_3} (m_{12} - fx_1) * (M_{12} - F_{applied} x_1)\, dx}{EI}$	(66) [15]
$\Delta = \frac{1}{f \cdot EI}\left(m_{12} M_{12} L_1 + \frac{M_{12} f {L_1}^2}{2} + \frac{m_{12} F_{applied} {L_1}^2}{4} + \frac{f F_{applied} {L_1}^3}{6}\right)$	(67)

7.3.3.1 Relating External Deflections to Deflection Equation

Following the analysis developed in the previous section, it is then assumed that the external displacement determined in equation 67 is equivalent to the equation 63 evaluated at the length L_1 as expressed in equation 68. When Equation 65 is rearranged the values of c_1 can be determined in terms of the know values, $F_{applied}$, f, m_{12}, M_{12}, L_1,E,I as stated in equation 61.

$\frac{1}{f \cdot EI}\left(m_{12} M_{12} L_1 + \frac{M_{12} f {L_1}^2}{2} + \frac{m_{12} F_{applied} {L_1}^2}{4} + \frac{f F_{applied} {L_1}^3}{6}\right) = \frac{M_{21} {L_1}^2 - \frac{F_{applied} {L_1}^3}{6} + c_1 L_1}{EI}$	(68)

Note from earlier that c_2 was found to be zero based on displacement boundary conditions at node B thus, in equation 65 zero is substituted in for c_2. Equation 65 can then be rearranged to solve for the c_1. An expression for c_1 is provided below in equation 67.

$c_1 = \frac{1}{f \cdot L_1}\left(m_{12} M_{12} L_1 - \frac{M_{12} f {L_1}^2}{2} - \frac{m_{12} F_{applied} {L_1}^2}{4} + \frac{f F_{applied} {L_1}^3}{6}\right) - \frac{\left(M_{21} {L_1}^2 - \frac{F_{applied} {L_1}^3}{6}\right)}{L_1}$	(69)

It is important for the reader to remember the rationale behind finding c_1 is to accurately determine the rotation of L frame member 2 which will help us to ultimately develop an equation for the

displacements of L-frame member 1 and thus find that deflection of the cam rollers at these points and estimate the resultant loads based on the proposed cam roller stiffness.

Referring back to equation 63 it is evident that when equation 69 is substituted for c_1 that c_1 is actually equivalent to the rotation L frame member 1 rotation at that point. Thus by substituting in all known values into equation 67, it is possible to evaluate the rotation at node B for the L-frame member 2 according to equation 68.

$$\theta_{section1}(0) = \frac{c_1}{EI_1} \quad (70)$$

7.3.4 Analysis of L-Frame Member 1 Analysis

A similar analysis can be employed for L-frame member 1. Except in this case, there are two segments. It is assumed that by continuity that both segments will have the same angular rotation at node B. Please see figure 18 for the designation of force and moment directions for the analysis of L-frame member 1.

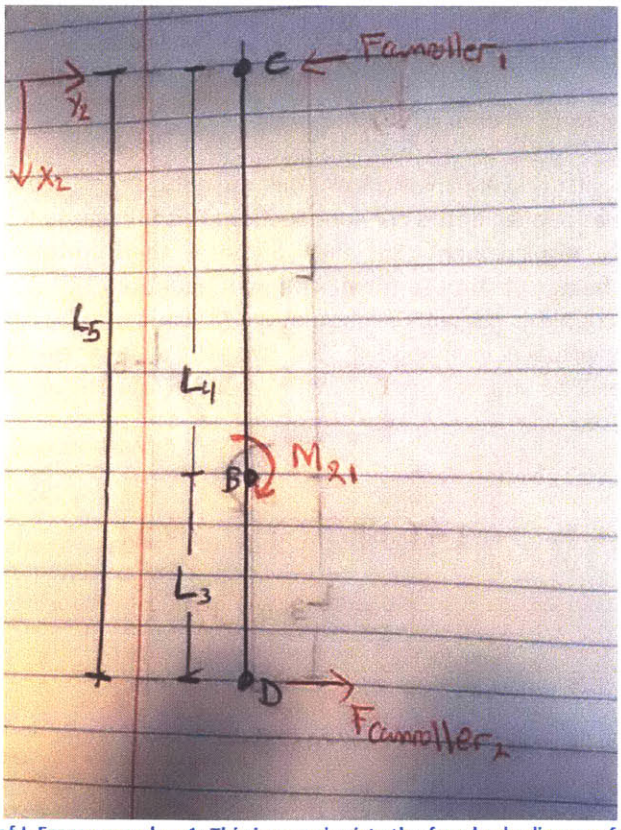

Figure 18 Free Body Diagram of L-Frame member 1: This image depicts the free body diagram for L-Frame member 2. Node C is the position along L-Frame member 2 where cam roller 1 is attached. $F_{camroller1}$ corresponds with the force applied by cam roller 1. Node D is the position where cam roller 2 is attached and $F_{camroller2}$ is the corresponding forces that cam roller 2 exerts on the L-Frame Member 2. To the left of the image the coordinate frame as designated. There are two sections of L-Frame member 2. The first section is dictated by the distance between node B and D. The second section is indicated by the segment from node B to C. M_{21} is the moment that acts on the L-Frame member 1 as a result of the cantilevered load from L-

Frame member 2. This moment is transmitted to L-Frame member 2 through the use of a fastener pattern that will be described in the section on fasteners.

7.3.4.1 Moment Equations

Note that when the moment equation for section2 is determined, it is found that the moment is equivalent to the force of the cam roller multiplied by the lever arm or the distance along the coordinate x_2. The equation of the moment in section 2 is given by equation 71. Equations 72 and 73 represent the slope and deflection of section 2 respectively.

$M_{section2} = -F_{camroller} x_2$	(71)
$\theta_{section2} = \frac{-F_{camroller} {x_2}^2 + c_3}{EI}$	(72)
$\varepsilon_{section2} = \frac{-\frac{F_{camroller} {x_2}^3}{6} + c_3 x_2 + c_4}{EI}$	(73)

Unlike in the first instance, since node B is a distance L_4 away from node C; the origin of x_2. Thus, it is not possible to retract information about c_4 so long as c_3 is unknown. Thus, the virtual work method must be employed again for L-Frame member 1.

7.3.4.2 Virtual Work Method L-frame Member 1

In the application of the virtual work method for this member a virtual moment will be applied as opposed to a virtual force as applied in the previous section. This is because the intent is to determine a rotation as opposed to a displacement. For such purposes then equation 64 is modified. m_Θ is substituted for m and Θ being substituted for Δ. The new equation relates the internal and external work as due to a virtual couple is presented in equation 74. Equation 75, demonstrates the resultant moment as a result of the virtual couple applied. The variable $f_{\text{camroller1}}$ is the force that cam roller 1 will exert on L-Frame member 2 to counter act the virtual moment applied on the system. Figure 19 has been provided for reference.

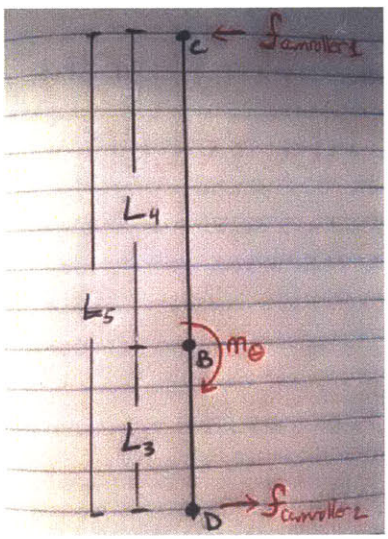

Figure 19 Free Body Diagram of L-Frame member 1 with virtual moment applied to it. In order to employ the virtual work method, a virtual moment is applied at node B. This is done in order to determine the rotation of the L-Frame member 2 at node B. The variables $f_{camroller1}$,$f_{camroller2}$ represent the forces that cam roller 1 and cam roller 2 will exert on the L-frame member 2 to counter act the virtual moment m_θ.

$$1 \cdot \theta = \int_0^L \frac{m_\theta M}{EI} dx$$	74
$$m_{section2} = -f_{camroller1} x_2$$	75

Note that in this application $m_{section2}$ is equivalent to m_θ and $M_{section2}$ is equivalent to M. By substituting equation 75 and equation 71 for m_θ and M respectively into equation 74 it is possible to generate equation 76 .

$$1\ Nm \cdot \theta = \int_0^{L_4} \frac{f_{camroller1} * F_{camroller1} x_2^{\ 2}}{EI_1} dx$$	76

Once equation 76 is evaluated, equation 77 is produced and the virtual couple is divided out. The resulting value is the angular deflection at node B for L-frame member 1.

$$\theta = \frac{f_{camroller1} * F_{camroller1} L_4^{\ 3}}{EI_1 * 1 \cdot Nm}$$	77

Equation 77 can then be equated to equation 72 and evaluated at $x_2=L_4$. This, yields equation 78 for c_3. Once c_3 is known c_4 can be determined using the displacement boundary condition at $x_2=L_4$ an equation for c_4 is given by equation 79.

$$c_3 = c_1 + \frac{f_{camroller} * F_{camroller} L_4^{\ 3}}{1 \cdot Nm} - \frac{-F_{camroller} L_4^{\ 2}}{1}$$	78
$$c_4 = -\frac{F_{applied} L_4^{\ 3}}{6 * EI_2} - \left(\frac{c_1}{EI_1} + \frac{f_{camroller} * F_{camroller} L_4^{\ 3}}{1 \cdot Nm * EI_2} - \frac{-F_{camroller} L_4^{\ 2}}{1 * EI_2} \right) L_4$$	79

This makes it possible to now evaluate the deflection of the cam roller. Note that when equation 79 is divided by EI it is possible to determine the deflection of cam roller 1 at that point. A MatLab code was used to help evaluate the aforementioned equations and determine the values of c_1, c_2, and c_3.

7.3.5 Conclusion from L-frame Deflection Analysis

While it is evident from this design that changing the height of the connection point of L-frame member 1 and 2 significantly reduced the deflections experienced by the cam roller, the utilization of this technique is limited. Recall that from the design requirements, the platforms height above the ground had to be low enough to be reasonable for patients to climb. Assuming that the cam roller at its lowest point in its travel will be in contact with the ground, the combined height from the bottom of the cam roller to the top of the platform must be equivalent to .1524m. Given that that the dimensions for L frame member 2 as outlined in the forthcoming analysis will be 0.1524m x0.1524m x 0.009525m the distance between the cam roller and location of the connection point of the two l-frame member must be 0.0254m away.

At this point in the discussion, it is important to remember that the equation 79 is dependent on L_4^3. From figure 13, it is evident that L_4 describes the distance between the connection point of the 2 L-frame members and the center location of cam roller 1. As discussed earlier in this section, shifting the connection point upward will reduce L_4 and thus reduce the deflection. However if L_4 is thought of relatively, decreasing the height of cam roller 1 relative to the connection point will also decrease L_4. To achieve this, the distance between the two cam rollers must be decreased. Thus, to further reduce the deflection of cam roller 1 the distance between the cam rollers was decreased. The results and parameters used for this optimization are presented in table 19.

Table 19 Parameters and Results on L-Frame Dimension Optimization

Design Parameter	Values	Comments
L_3	.0254m	
L_4	.5588m	Note $L_4 = L_5 - L_3$
L_5	.5842m	
w*l*t	.2032 m* .1524 m *.0127m	Dimensions of L-frame member 1
Resultant Forces and Deflections		
Cam Roller 1 Deflection	$-1.3611 * 10^4$	
Force Due to Deflection	23.4 kN	Note that the total force is found by multiplying the calculated deflection by the proposed cam roller stiffness of $1.712*10^8$ N/m
Total Cam roller Force	30.38 kN	Note that it is assumed that the cam roller would supply a force to sustain the moment equivalent of 6972 N. This value is added to force due to deflection in order to approximate the total load that the cam roller should sustain in order to select the appropriate cam roller.

From the result outlined in the table above, it is evident that the cam roller that will be used for this design is a HVB-062 offered by PBC linear. A discussion of the price of the cam roller and its associated rail length can be found chapter 5 of this document. Moreover a summary of the pricing of L-frame member 1 can be found in section 7.2.7.

An additional observation is that c_1 which is related to the rotation of L-frame member 2 has a negligible effect on the rotation of L-frame member 1. Thus, this implies is that the dimensions of L-Frame member 2 can be chosen separately from L-frame member 1. Moreover, this indicates that the assumption of joint B as a pin joint is valid since the rotation of member 2 has a negligible effect on member 1. As a result, force calculations are performed on the L frame member 2 in order to ensure that they are below the yield stress of steel. The analysis, for the stress on in L-frame member 2 is provided below.

7.3.6.1 Stress Analysis on L Frame Member 2

Recall that the equation for the moment within a section was developed in equations 61 for L frame member 2. It has been replicated below as equation 80 for convenience.

$M_{section1} = M_{12} - \frac{F_{applied} x_1}{2}$	(80)

Equation 80 indicates that the moment of the system is highest when x_1=0 which corresponds to M_{12}. Thus, using the value of M_{12} it is possible to compute the bending stress that L-Frame member 2 will experience. The equation for the bending stress is provided in equation 81 and the analysis of the bending stress is performed. It is important to mention that y in equation 80 represents the distance from the bending axis to the top of the member. A square tube with the dimension of 6" x6" x ¼" is initially specified since its coincident surfaces with L frame member 1 will make designing and mounting fastener patterns simpler. Moreover, there is torsional load acting on this member which will result in a shear stress. The torsional shear stress is evaluated in equation 82. Using the shear stress determined from the equation 82 and the bending stress evaluated from equation 81, the equivalent stress can be determined as demonstrated in equation 83. The variable definition for equations 81 and 82 are summarized in table 20.

Table 20 Summary of Variables used to Calculate Bending and Shear stresses in L-Frame Member 2

Area Moment of Inertia	$I = 1.321 * 10^{-5}\ m^4$
Distance From Bending Axis	$y = .1524\ m$
Mean Area	$A_m = 2.133 * 10^{-2} m^2$
Moment	$M = 4.073 * 10^3\ Nm$
Torque	$T_1 = 8.138 * 10^3\ Nm$
Thickness	$t = .00635m$

$\sigma_{bending} = \frac{M * y}{I}$	(81)
$\sigma_{bending} = 51.40\ MPa$	

$\tau_x = \frac{T_1}{2A_m t}$	(82) [16]
$\tau_x = 30.04\ MPa$	

Equation 82 refers to the equivalent shear stress caused as a result of the torsional load. The special variation of this equation arises from the fact that the member is both noncircular and hollow. A_m refers to the mean area. The mean area is computed by first creating a shape that is offset from the edges of the member's cross-section by half the thickness of the member. Then the area within the shape is evaluated. For this application, the shape created would be a square with a 0.14605m side length. T_1 is the torque applied to the system and this is equivalent the moment about the x axis of L-Frame member 2 and t refers to the thickness of the tube as specified above.

7.3.6.2 Equivalent Tensile Stress

$\tau_{equ} = \left[\left(\frac{\sigma_{bending}}{2}\right)^2 + (\tau_x)^2\right]$	(83)
$\tau_{equ} = 40\ MPa$	

From the equivalent tensile stress it is evident that expected stress is significantly below the maximum stress of steel thus, this tube is sufficient to use for this design. Based on the aforementioned discussion a summary of the dimensions of the L-Frame members are outlined in table 21. For member 1 the deflection of cam roller 1 is also given and the corresponding force due to the deflection is calculated.

7.3.7 L-Frame Member Selection Summary

Table 21 Summary of L-Frame Member Dimensions and Associated Forces and Deflections

L Frame Member 1	
Height	.2032 m (8in)
Width	.1524 m (6in)
Thickness	.0127 m (1/2 in)
Length	.5842 m (30in)
Deflection of Cam roller 1	$-1.3611 * 10^{-4}$ m
Total Force of Cam roller 1	30.38kN
L Frame Member 2	
Height	.1524 m (6 in)
Width	.1524 m (6 in)
Thickness	.00635 m (1/4)
Length	1.0668 m (42in)

7.4 C-Frame Structural Analysis

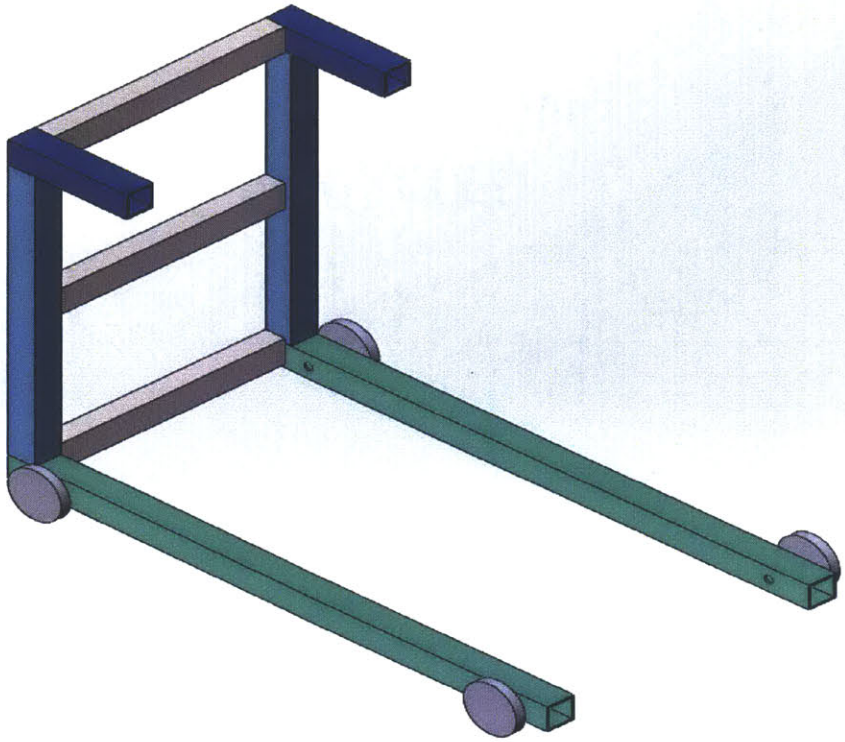

Figure 20 C Frame Diagram: This image depicts the C-Frame for the platform lift. The C-Frame is made up of three parts. The Dark blue square tube is referred to C-frame member 1. The light blue member is C-Frame member 2. C-Frame member 3 is the green member. Both C-Frame member 1 and C-Frame member 3 are attached to C-Frame member 2 using a fastener pattern. It is important to note that there are a total of two C-Frames in entire system. These two C-Frame are attached using three square tubes which also provide attachment points for the Leadscrew. The cam rollers rails which are not shown here will be attached to C-Frame Member 1 and C-frame member 3. Since the C-frames are connected, the structure is rigid and thus there is less bending in cam roller rail.

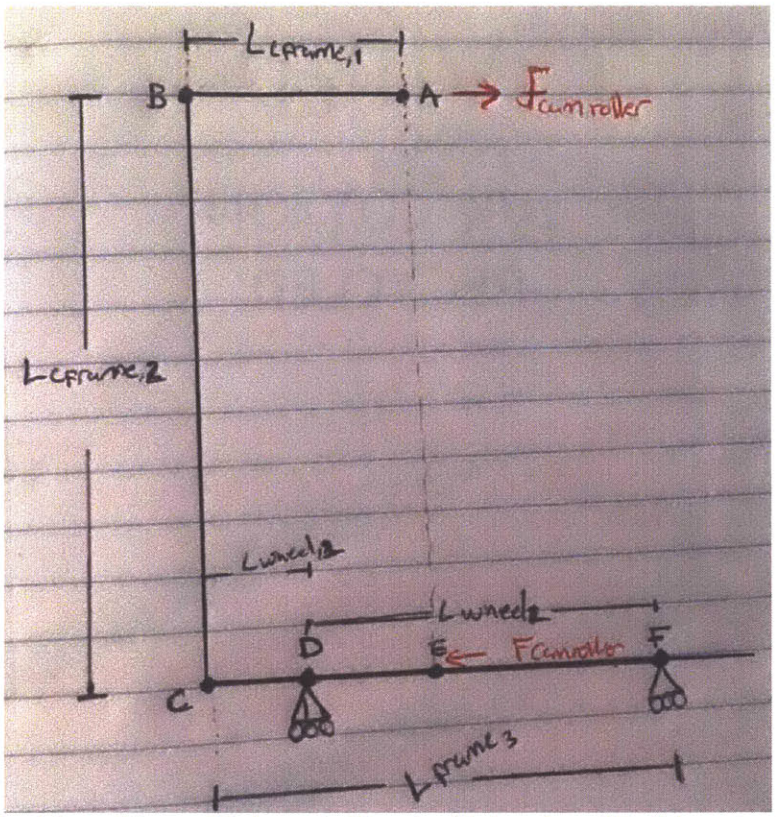

Figure 21 Simplified Hand drawn C-Frame: This image depicts a simplified versions of the C-frame in which the members of the C frame are depicted as lines. The line between node A and node B refers to C-Frame member 1. The length between the node B and C refer to C –frame member 2 and the Node between node C and F is C-Frame member 3. Nodes D and F specify the locations at which the wheels will be located on the C frame member 3. Node E specifies the point at which the cam roller rail will exert a force on C-Frame member 3. $L_{C\text{-}frame,1}$, $L_{C\text{-}frame,2}$, $L_{C\text{-}frame,3}$ represent the lengths of the respective C-frame members. $L_{wheel,1}$ specifies the distance between the back wheel and the node c where the C-frame member 2 and C-frame member 3 are connected.

Figure 20 provides a description of the C-frame and a CAD model of the C Frame. Figure 21 provides a simplified hand drawn model of the C-Frame that is used for forth coming analysis. Please refer to these figures in the following analysis.

To size the tubes for the C-Frame, it is important to identify the loads acting on the C-Frame and to make sure that the stresses do not exceed the yield stress of the specified material. A planar analysis of the C-frame is presented below. It is assumed that the force of cam roller 1 and 2 act on C-Frame member 3 and C-Frame member 1 respectively. From this analysis, it will be possible to determine the forces that the shaft of the wheels will experience and thus select the appropriate bearing and shaft dimensions for the wheel. Note that a force balance has been provided below for each member of the C-frame. To help make the analysis simpler, all the necessary variables have been specified in the table 22.

Table 22 Variable Definitions for C-Frame Analysis

Variable Definitions	
Variable	Comments
$L_{c\text{-}frame,1}$= 0.3048 m	The length of C-frame member 1
$L_{c\text{-}frame,2}$= 1.0414 m	The length of C-frame member 2
$L_{c\text{-}frame,3}$= 1.4224 m	The length of C-frame member 3
L_{wheel1}= 0.2286 m	The distance from node B to the positions of the center of the first wheel from.
L_{wheel2}= 1.2192 m	The distance between the two wheels.
$F_{camroller}$= 30.38 kN	The force that the top camroller will exert on member 1
$F_{camroler2}$= -30.38 kN	This is the force that the bottom camroller will exert on member 3.

7.4.1 Total system Force Balance

Prior to evaluating the force acting on each individual member in the C frame, a total force balance is necessary. In the analysis of this force balance, the system is defined such that the forces that the wheels exert on the system are exposed. When the sum of forces in the X, and Y directions are evaluated, it is found that the force of the cam rollers is equivalent and the forces of the wheels are equivalent as well. From the moment balance, a relationship between the forces the wheels exerts and the cam roller force is also determined. A summary of all the conclusions based on the force and moment balance of the entire system is expressed in equations 84-86

$F_{camroller,1} = -F_{camroller,2}$	Determined from force balance in the X directions.	(84)
$F_{wheel,1} = -F_{wheel,2}$	Determined from force balance in the Y direction	(85)
$F_{wheel} = F_{camroller} * \frac{L_{c-frame,2}}{L_{wheel,2}}$	Determined from moment balance	(86)

It is important to mention that in the moment balance, the force of cam roller 2 passes directly through node C and thus it is excluded in the formulation of the moment balance. With these relationships known, it is possible to find out the internal forces of each member.

7.4.2 C-Frame Member 1 Force Analysis

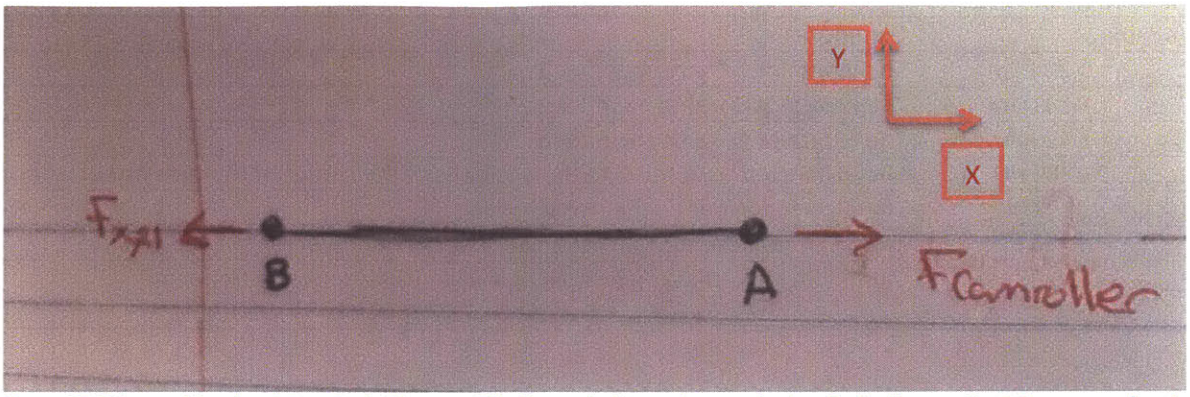

Figure 22 C-Frame Member 1 Free Body Diagram: This figure depicts an image of a free body diagram for C-Frame member 1. A force is applied at node A in the positive X direction by the cam roller rails. A force $F_{x,21}$ is applied at node B. The force represents the force in the x direction that C-Frame member 2 will impose on C-Frame member 1. The assumed direction of $F_{x,21}$ is in the negative x direction. Note that from this image there are no forces in the Y direction acting on member 1. Thus, there will be no shear forces in this member.

From figure 22, it is evident that there is only two force acting on it. A force in the positive x direction is exerted onto it by the cam roller and an internal reaction force that is pointing in the negative x direction. These two forces must be equivalent for the forces to be balanced in this member. Equation 76 gives the final result from the force balance of member 1. The Variable $F_{x,21}$ represents the horizontal force exerted on member 1 by member 2.

$F_{x,21} = F_{camroller}$	(87)
$V_1(x_1) = 0$	(88)
$M_1(x_1) = 0$	(89)

It is important to recognize that according to the diagram $F_{x,21}$ is assumed to point in the negative x direction. Also since there are no vertical forces acting on the member, the shear forces are zero and thus, the moment in this member is also zero about the z axis as stated in equation 88 and 89 respectively.

7.4.3 C-Frame Member 2 Force and Moment Analysis

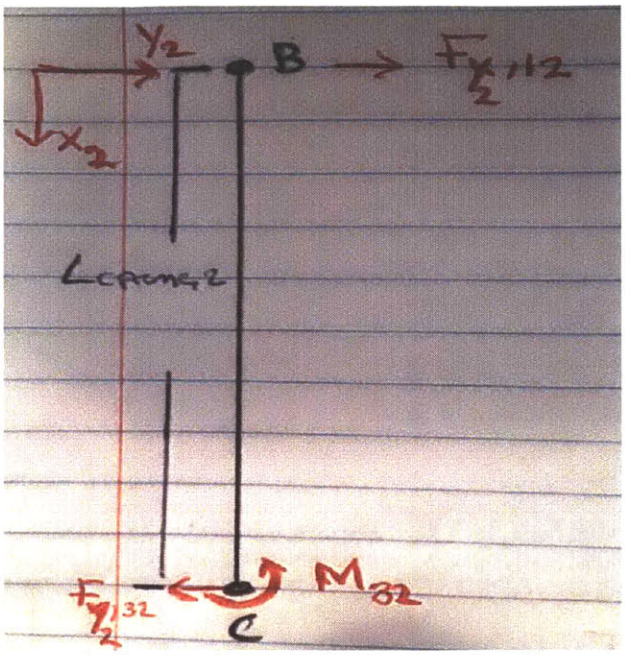

Figure 23 C-Frame Member 2 Free Body Diagram: There are two forces that act on this member $F_{y2,12}$ and $F_{y2,32}$. $F_{y2,12}$ is the force in the Y_2 direction that member 1 exerts on member 2. $F_{x,32}$ is the force in the Y_2 direction that member 3 exerts on member 2. M_{32} represents the moment that the member 3 will exert on member 2 via the fastener patterns. It is important to note that in this figure Y_2 points in the positive X direction as defined for the global frame in figure 22. This means that $F_{y2,12}$ is equivalent to $F_{x,21}$. Furthermore a force balance reveals that the $F_{y2,12}$ and $F_{y2,32}$ are equal in magnitude and act in opposite directions. Finally from the moment balance it is evident that the magnitude of the M_{32} is equivalent to the product of $F_{y2,12}$ and the length of the C Frame member 2.

According to figure 22, there are two forces acting on this member. It is important to remind the reader that the positive y direction for C-Frame member 2 is in the same direction of the positive x direction of C-Frame member 1. Thus, $F_{y2,12}$ according to Newton's third law, should be equivalent in magnitude and opposite in direction of $F_{x,21}$ as defined in figure 21. Equations 90 & 91 present a summary of the force balance and moment balance on C-Frame member 2.

$F_{y_2,12} = F_{camroller}$	(90)
$M_{32} = F_{camroller} * L_{C-Frame,2}$	(91)

Note that M_{32} is also an internal moment that will be transmitted as a result of the fastener pattern. Knowing these two values, it is possible to form Shear and moment equation and thus use the moment equation to obtain an idea of the maximum stress the member will experience. The resulting equations for shear forces and moments within the member are given by equations 92 and 93.

According to the free body diagram the shear force would be constant throughout the beam until node C is reached. Moreover the moment would grow linearly as x_2 increases. $m_{c-member2}$ is used to represent the internal moments in C-frame member 2. According to equation 83, the internal moment is largest when x_2 is largest. Thus the internal moment is largest when x_2 is equal to $L_{C\text{-}Frame,2}$

$V = F_{camroller}$	(92)
$m_{c-member2} = F_{camroller} * x_2$	(93)

7.3.4 C-Frame Member 3 Force and Moment Analysis

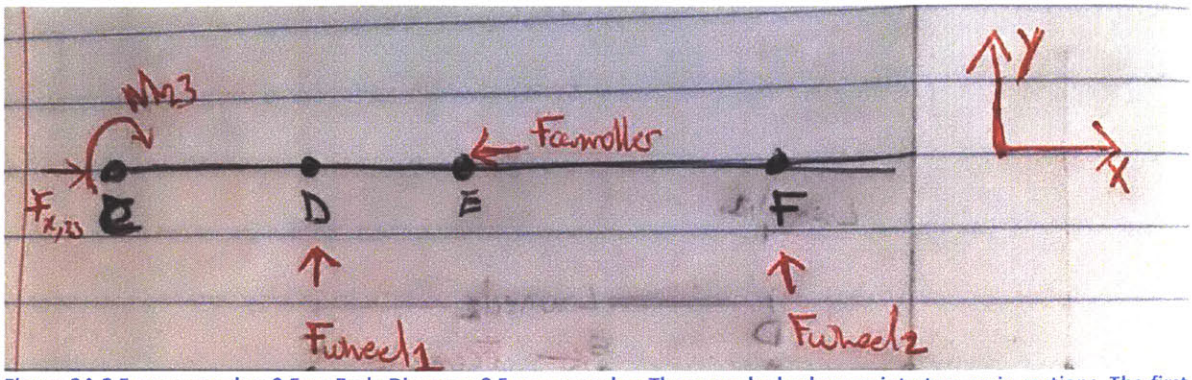

Figure 24 C-Frame member 3 Free Body Diagram: C-Frame member Three can be broken up into two main sections. The first section is designated by the point between node C and D. The second section is from node D to node F. For each section a coordinate system is determined. X_3 and Y_3 correspond with section 1 and X_4 , Y_4 correspond with the second section. Both X_3 and X_4 are collinear with the global X axis show to the right of the image. Y_3 and Y_4 are parallel with the global Y axis. The force on the wheels was previously evaluated in equation 75. M_{23} is the force that was applied at

For this member, the analysis is broken up into two segments. Segment one is the distance from the back of the C-frame-member 2 to the location of the center of the wheel 1. The length of this segment is L_{wheel1}. From the force balance of segment 1 of member 3 it is evident that there must be a moment at node B. This moment is equivalent to the product the force exerted on the back wheel and the length of segment 1. This is expressed in equation 94.

$M_{23} = F_{camroller} * L_{c-frame,2}$	(94)

In addition to the moment, the analysis suggests that the force throughout the section will be zero since there are no vertical reaction forces acting at that point.

$V_3 = 0$	(95)
$m_3 = M_{23}$	(96)

The final section of Member 3 is equal to the length between node D and node F which is equal to $L_{wheel,2}$. The shear and moment equations for this region are given by equations 97 and 98 respectively.

$V_4 = F_{wheel}$	(97)
$m_4 = M_{23} - F_{wheel}x_4$	(98)

Equation 97 assumes that the shear points in the negative y_4 direction as suggested in this diagram. Equation 98 assumes that the moment within the section is in the Counter clockwise direction thus resulting in the specified equation.

7.4.5 Evaluating the Stress in the C Frame

From the analysis it is evident that there will be two main stresses experienced. The first is bending stress and the second is stress along the axis of the member and shear stress. The member with the maximum stresses will dictate the critical dimensions.

Given that the maximum moment and shear forces will occur at the connection points of the members 2 and 3 it will be used to determine the moment of inertia for the member. The dimensions of the members will be selected such that the bending stress it experiences is below half of the yield stress of the steel which will be the material of choice. σ_y is defined as the yield stress of steel. The members will be assumed to be square tubes. Initially the members are assumed to be 4"x4"x 1/4" members to see how it compares with the stress criterion stated in equation 100. The table 23 outlines the values used and also presents equation 99 which shows the actual bending stress in the member using the bending stress equation as outlined in equation 81. Equation 92 presents the inequality that the member must satisfy in order to be permissible for this design.

Table 23 Summary of Variables for Stress Analysis of C-Frame Members

Variables for Stress Analysis of C-Frame Member	
$B = .1016\ m$	The height of the square tube cross-section
$T = .00635\ m$	The thickness of the square tube
$\sigma_y = 270\ MPa$	The yield stress of steel [17]
$M = M_{32}$	The moment at node B applied unto member 2 of C-Frame as defined in equation 80.
$\sigma_{actual} = \sigma_{bending}$	The bending stress experienced by the member
$I = 3.674 * 10^{-6}$	Proposed moment of inertia based on initial suggestion for member size.

$$\sigma_{bending} = \frac{M * y}{I}$$	(99)
$$\sigma_{actual} = \frac{27.78kN \cdot m * .1016m}{3.674 * 10^{-6}} = 768.2MPa$$	

$$\sigma_{total} = \left[(\sigma_{bending})^2 + 3\tau^2\right]^{\frac{1}{2}}$$	(100)

Equation 100 provides an equation that calculates the total stress experienced by the member where τ is the shear stress felt in the member. It is an application of the von misses stress criterion. In this case however there are no normal stresses in two directions and only shear stress is along the cross-section of the tube is non-zero. With the previously mention assumption, the resulting in its expression in equation 100. The shear stress is defined in equation 101 and evaluated underneath it. Since the shear force in member 2 is equivalent to the force exerted by cam roller 1, it is divided by the area of the cross-section of the tube to calculate the shear stress.

$$\tau = \frac{F_{camroller}}{B^2 - (B - 2T)^2}$$	(101)
$$\tau = \frac{30.38kN}{.1016^2 - (.1016 - 2 * .00635)^2} = 12.56\ MPa$$	

$\sigma_y > [(\sigma_{bending})^2 + 3\tau^2]^{\frac{1}{2}}$	(102)
$270\ MPa > 768.2\ MPa$	

From Equation 102 it is evident that the initial member guessed does not satisfy the in equality specified. Thus, the dimensions must be specified such that this condition is met. After different trials, it was determined that in order to meet the specified criteria in equation 102 a member of the dimensions of 6 x 6 x 3/8" is need for this design. Since C-frame member 2's dimension are the critical dimensions, it will be used for all the members of the C-Frame. A summary of the associated calculations is provided and the dimensions of the C-Frame are provided in table 24.

Table 24 C-Frame Member Selection Summary

C-frame Member Selection Summary	
Height of Tube	.1524m (6 in)
Thickness of Tube	.00953 m(3/8 in)
Total Length of Tube Need	3.05m (120 in)
Moment of Inertia	$2.327 * 10^{-5}\ m^4$
Actual Bending Stress	181.9 MPa

7.5 Fasteners:

While the formulations above were used to specify the dimensions of the members that should be used in this application, the stresses at the connection point are yet to be examined.

The fasteners will experience bending stresses due to the moments about the axis of the connecting beam. Moreover, it will also experience shear stresses due to the reaction forces distributed evenly on all the fasteners in the pattern. Finally, the fasteners will experience a shear stress due to torsion. Using the appropriate equations as outlined below the total shear stress that the screws will experience was calculated. The shear stress failure criterion with a safety factor of 2 was used to determine the diameter of the screw that should be used for each application. It was assumed that the fasteners screws that will be used will be made of steel.

7.5.1 Direct Shear calculation

The direct shear stress is the shear stress that the fasteners experience as a result of the reaction forces applied at a point. To properly formulate the equation for stress of the fastener pattern, it is important to remember that the entire pattern can be modeled as a pin joint found at the center of mass of the pattern. In addition, it is assumed that the forces acting directly at this point will be evenly distributed among the fasteners found in the pattern. Thus, in equation 103 $F_{applied,fastener}$ refers to the total applied force acting on the pattern. A_i represents the cross sectional area of each bolt found in the fastener pattern. For the simplicity of this calculation, it is assumed that all the screws have the same cross sectional area A_b.

$\tau_{direct} = \frac{F_{applied,fastener}}{\sum_1^4 A_i}$	(103) [18]
$\tau_{direct} = \frac{4500\ N}{4 * A_b}$	(104)

Equation 104 substitutes all the known values into equation 103. In this application $F_{applied,fastener}$ is equivalent to the 4500N which is half of the total weight of the platform. Note that A_b remains unknown

thus the formulation of this analysis will be used to solve for the cross-sectional area of the bolts in the pattern and thus find the associated radius for this bolt.

7.5.2 Torsional Shear calculation

At the center of the fastener pattern, it is possible to experience torsion as a result of the moments in the plane of the fastener pattern. In order to calculate the shear stress as a result of torsion, the center of mass of the fastener pattern is located. Unlike the direct shear stress, the torsional shear stress is dependent on the distance away from the center of mass. Thus, in an asymmetric pattern, each bolt in the pattern will experience a different amount of torsional shear stress. Given the symmetry of this pattern, all the fasteners are equidistant from the center of the fastener pattern which is located at the geometric center of the fastener pattern. As a result, the torsional shear stress calculated below is representative of the torsional shear stress experienced by each bolt.

In order to calculate the torsional shear stress, equation 105 is employed. In equation 105, T refers to the torsion, r_i refers to the distance from the center of the bolt to the center of the fastener pattern and $J_{inertia}$ refers to the total area moment of inertia of the fastener pattern which is given by equation 107. Equation 96 refers expresses r_i in Cartesian coordinates.

$$\tau_{torsional.i} = \frac{T * r_i}{J_{inertia}}$$	(105) [18]
$$\tau_{torsional.i} = \frac{T * ({x_i}^2 + {y_i}^2)}{J_{inertia}}$$	(106) [18]

$J_{inertia}$ can also be rewritten in Cartesian coordinates as seen in equation 108. The total magnitude can be found for each bolt in the pattern and then the total area moment of inertia is calculated. Likewise a similar formulation can be achieved for the torsional shear stress.

$$J_{inertia} = \sum_{i=1}^{4} A_i * r_i$$	(107) [18]
$$J_{inertia} = \sum_{i=1}^{4} A_i * ({x_i}^2 + {y_i}^2)$$	(108) [18]

7.5.3 Bending stresses:

The bending stress on the fastener pattern is determined by the moments that cause the fasteners to bend. In the case of this design the pitch moment is responsible for the bending. Using equation 109, the force generated by this moment on an individual bolt can be calculated. The evaluated force is divided by the area of the bolt in order to determine the bending stress. The equation for the bending stress is expressed in equation 110. The variable 'I_j' refers to the total area moment of inertia. However, unlike $J_{inertia}$, it is not in reference to the center of the pattern. Rather, since the screw is bending, the reference distance will be dependent on the dimensions of the two clamped members. Thus, y in this equation 109 and 110 is determined by the vertical distance from the designated pivot point. This idea will become more apparent in section 7.5 when the bending stress for the fastener pattern between the two L-Frame members is evaluated.

$F_i = \frac{M_{pitch} * y}{I_j} * A_i$	(109) [18]
$\sigma_{bending} = \frac{M_{pitch} * y}{I_j}$	(110) [18]

Given the symmetric nature of this bolt pattern, both the direct shear and torsional shear are evenly distributed on all bolts. However, due to the dependency of the vertical distance from the pivot point for the bending stresses, the bending stress is not uniformly distributed for the all fasteners since they are located at different vertical distances. Thus, it makes the most sense to only evaluate the bending stress for the screws furthest from the pivot point. The bending stress of the furthest fastener is identified as critical parameter of the fastener design and selection since it would exhibit the most bending stress. Thus, the area obtained from this critical fastener will be the designated area for all the fasteners in the fastener pattern.

7.5.4 Equivalent Stress and Failure Criterion:

In this section the values for the bending stress, shear stress and torsional stress are used to calculate the equivalent shear stress on the critical bolt. Using a safety factor of two, the failure criterion for the critical bolt is evaluated.

$\frac{\tau}{2} > \left[{\sigma_{bending}}^2 + {\tau_{direct}}^2 + {\tau_{torsional}}^2\right]^{\frac{1}{2}}$	(1011) [18]

If the critical bolt is assumed to be made of steel, then the area of the bolt can be determined by manipulating equation 112. Since the fasteners have circular cross-sections the diameter of the fastener can be determined by using the equation for the area of a circle.

$\frac{\tau}{2} > \left[\left(\frac{M_{pitch} * y}{I_j}\right)^2 + \left(\frac{4500\ N}{4 * A_b}\right)^2 + \left(\frac{T * ({x_i}^2 + {y_i}^2)}{J_{inertia}}\right)^2\right]^{\frac{1}{2}}$	(112) [18]

With all the equations thus explained one can now evaluate the screw patterns using the equations described above.

7.6 Calculations for Fasteners Connecting the Two L-frame member

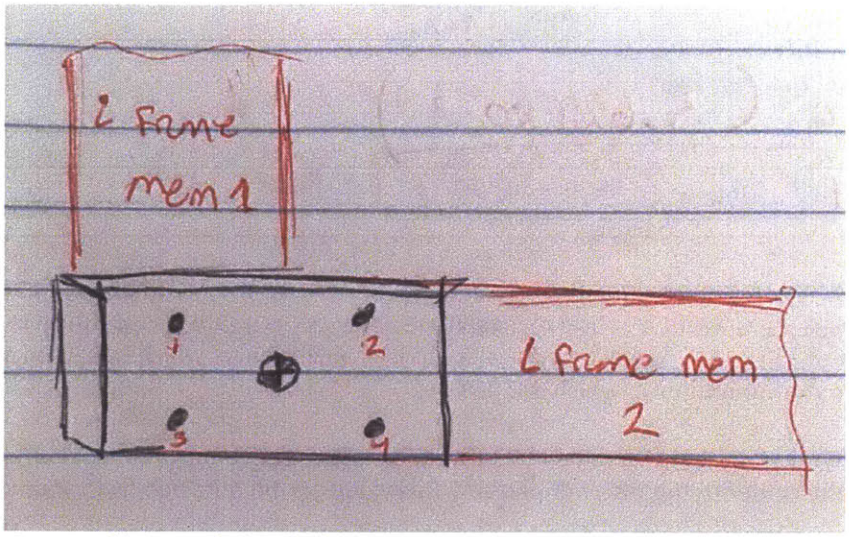

Figure 25 Fastener Pattern: This image depicts the fastener pattern that will be used to connect the two members of the L-Frame. Fastener 1 and three will be secured unto L frame member 1 and fasteners 2 and 4 will be secured unto L-frame member 2. The center of the fastener pattern corresponds with node B in figure 11. Thus the force and moments that were evaluated at node B will act at the center of this pattern.

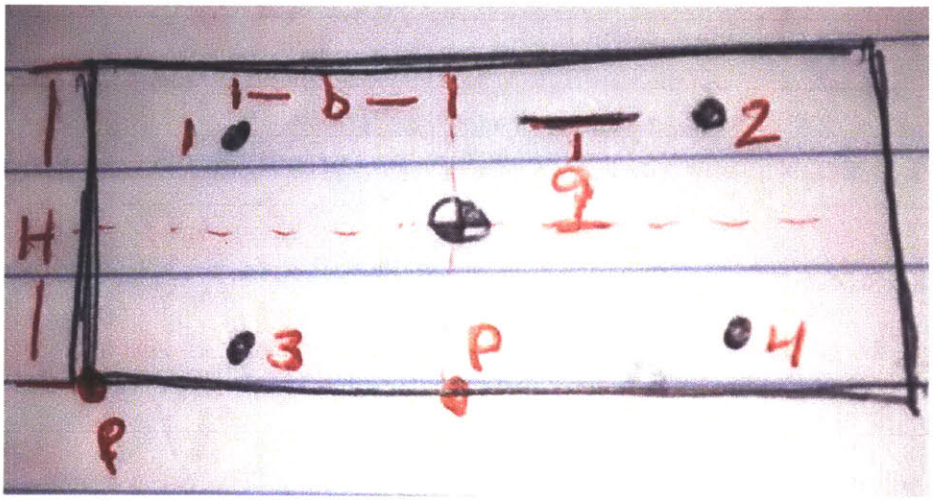

Figure 26 Zoomed View of L-Frame Fastener Pattern This image represents a closer view of the fastener pattern. The locations of the fasteners are number from 1-4 starting in the top left hand point and moving clockwise. The fastener pattern is symmetric that each fastener is equally spaced from the center of the fastener pattern. Moreover the variable a and b represent the fasteners' respective y and x distances from the center. The Initial proposals for the dimensions of a and b are .0381m and .0508m respectively. The variable H represents the height of the clamp plate that will be used to connect the two members together. This variable will become particularly important in the evaluation of the bending stress on this fastener pattern. Point P is designated along the bottom edge of the clamp fastener pattern and will be used in the analysis of the bending stress on the fastener pattern.

7.6.1 Direct Shear:

$\tau_{direct} = \frac{4500\ N}{4 * A_b}$	(113) [18]

7.6.2 Torsional Shear Stress:

$J_{inertia} = A_b * (x_1{}^2 + y_1{}^2 + x_2{}^2 + y_2{}^2 + x_3{}^2 + y_3{}^2 + x_4{}^2 + y_4{}^2)$	(114) [18]
$J_{inertia} = 4 * A_b * [0.051^2 + 0.038^2] * m^2$	(115)
$J_{inertia} = 1.62 * 10^{-2} m^2 * A_b$	(116)

Note that equation 114 can be simplified to equation 115 due to the fact that the fastener pattern is symmetric. Thus, x_1, x_2, x_3, x_4 are identical in magnitude and y_1, y_2, y_3, y_4 are also identical in magnitude. As suggested in figure 26 x_1, x_2, x_3, x_4 will be equivalent to the dimension 'b' which is .0508m and y_1, y_2, y_3, y_4 are equivalent to the dimension 'a' which is 0.0381m.

It is important to mention that the value 4073 Nm in equation 117 comes from evaluating the moment experienced at the center of the fastener pattern. This value can be obtained by evaluating equation 80 at x_1=0 .

$\tau_{torsional.i} = \frac{4073N * m * (0.051^2 + 0.038^2)^{\frac{1}{2}} * m^2}{J_{inertia}}$	(117) [18]
$\tau_{torsional.i} = \frac{4073N * m * (0.051^2 + 0.038^2) * m^2}{1.62 * 10^{-2} m^2 * A_b}$	(118) [18]

To find the total shear stress use equation 119.

$\tau_a = [\tau_{direct}{}^2 + \tau_{torsional}{}^2]^{\frac{1}{2}}$	(119)
$\tau_a = \frac{16.029kN}{A_b}$	(120)

7.6.3 Bending Stress

Assuming that the bending will take place about the designated point P as depicted in figure 26, the total area moment of inertia can be represented using equation 121 where r_k represents the distance from the pivot point and the center of the bolt.

$I_j = \sum_{i=1}^{4} A_k * y_k{}^2$	(121) [18]

The coefficient of 2 is placed in front of the two terms as expressed in equation 122 is because bolt 1 and 2 and bolt 3 and 4 are each at the same respective distance away from the point. If H is assumed to be .0762m and the pattern is symmetric about the center, it means that the vertical distance from point P to bolts 3 and 4 is .0195m and the distance from point P to bolts 1 and 2 is .0572m.

$I_j = A_b * [2 * 0.0195^2 + 2 * 0.0572^2] * m^2$	(122)

Now that the total area moment of inertia is known, the bending stress for bolts 1 and 2 can be evaluated using equation 123. It is important to remember that M_{pitch} in this analysis is equivalent to the total weight of the system multiplied by a total distance of .9144m away. This is assumed to be the worst case scenario for this design.

$\sigma_{bending1.2} = \frac{M_{pitch} * y_k}{I_j}$	(123) [18]
$\sigma_{bending1,2} = \frac{8147Nm * 0.0572m}{7.30 * 10^{-3}m^2 * A_b}$	(124)
$\sigma_{bending1,2} = \frac{63.836kN}{A_b}$	(125)

A similar formulation can be conducted for the bending stress of bolts 3 and 4 as well. The calculations for these are expressed below.

$\sigma_{bending3,4} = \frac{8147Nm * 0.0253m}{7.30 * 10^{-3}m^2 * A_b}$	(126)
$\sigma_{bending3,4} = \frac{28.23kN}{A_b}$	(127)

7.6.4Critical Stress/ Failure Criterion:

Only the calculations for bolt 1 and 2 are considered because they will produce the most critical stress. All other bolts will experience stresses that are less than that of these two bolts.

$\frac{\sigma_{yield}}{4} > \left[\left(\frac{\sigma_{bending1.2}}{2}\right)^2 + {\tau_a}^2\right]^{\frac{1}{2}}$	(128) [18]

Assuming that σ_{yield}= 270 MPa [17] and substituting the expressions for $\sigma_{bending1.2}$ and τ_a ,equation 118 was used to solve for A_b. By rearranging the equation of the area of a circle, the solution obtained for A_b is used to solve for the radius of the screw.

$\frac{\sigma_{yield}}{4} > \left[\left(\frac{63836N}{2 * A_b}\right)^2 + \left(\frac{16092N}{A_b}\right)^2\right]^{\frac{1}{2}}$	(129)
$67.5\ MPa = \frac{[1.277 * 10^9]^{\frac{1}{2}}}{A_b}$	(130)
$A_b = \frac{[1.277 * 10^9]^{\frac{1}{2}}}{67.5MPa}$	(131)
$A_b = 5.294 * 10^{-4}m^2$	(132)
$r_{screw} > \left[\frac{A_b}{\pi}\right]^{\frac{1}{2}}$	(133)

$r_{screw} > 1.298 * 10^{-2} m$	(134)

From the equation 134 it is evident that the fastener that will be able to be used for the fastener pattern connecting L frame member 1 and L frame member 2 is a fastener with a radius that is at least 1.298 $*10^{-3}$ m. The fractional screw sizes that closely fits this requirement is the 9/16 screw.

The table 25 summarizes the necessary information for the L-Frame Fastener pattern.

Table 25 Summary of L-Frame Fastener Pattern Details

Summary of L-Frame Fastener Pattern Details	
$a = .0381m$	The vertical distance between the center of fastener pattern and the bolts. Please refer to figure 20
$b = .0508m$	The horizontal distance between the center of fastener pattern and the bolts. Please refer to figure 20
$r_{screw} > 1.298 * 10^{-2} m$	The specified bolt radius based on analysis.

7.7 Calculations for Fasteners Connections for C-Frame

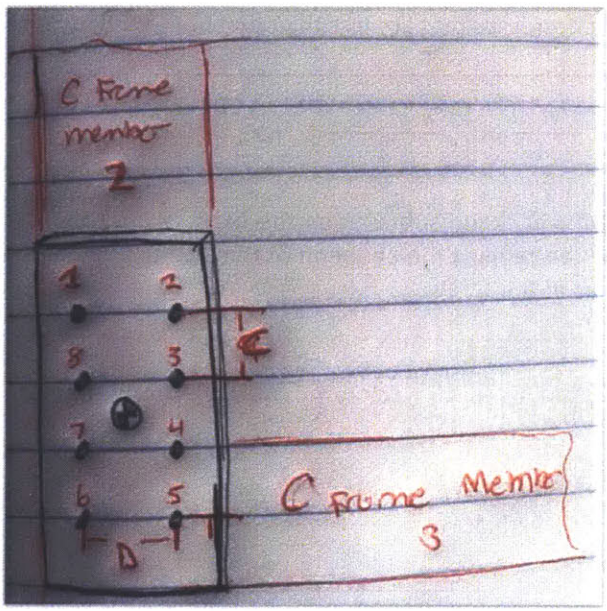

Figure 27 C-Frame Fastener Pattern Schematic This figure depicts the fastener pattern that will be used to connect C-Frame member 2 and C-frame member 3. The center of this fastener pattern is equivalent to node C. Thus the force and moment that act on mode C in figure 23 will be expressed at the center of this fastener pattern. The variable C represents the vertical distance between screws and dimension D represents the horizontal distance between the fasteners in the pattern. The proposed values of C and D are .0381 m and .1016 m respectively. Unlike the fastener pattern for the L-Frame, there is no reason to specify a second pivot point in addition of the fastener pattern's center. This is because there will be no bending on these fasteners. Thus, only torsional and direct hear stresses will be evaluated for this fastener pattern.

7.7.1 Direct Shear:

$\tau_{direct} = \frac{30.38\,kN}{8 * A_b}$	(135) [18]

In figure 23 it is important to recognize that the force F_{y32} is equivalent to the force that the cam roller will exert. Moreover, this force will be evenly divided by 8 since there are a total of 8 fasteners in this design.

7.7.2 Torsional Shear Stress:

$J_{inertia} = 2A_b * ((x_1{}^2 + y_1{}^2) + (x_3{}^2 + y_3{}^2) + (x_4{}^2 + y_4{}^2) + (x_5{}^2 + y_5{}^2))$	(166) [18]
$J_{inertia} = 4 * A_b * [(.00585 + .0029)] * m^2$	(137)
$J_{inertia} = 3.5 * 10^{-2} m^2 * A_b$	(138)

Due to the geometry of the fastener pattern all the x values for each individual bolt are equal. By symmetry the y values for fasteners 3,8,7,4 are equivalent. By symmetry the y values for fasteners 1,2,6,5 are equivalent. Thus, x_1, x_2, x_3, x_4, x_5, x_6, x_7, x_8 are identical in magnitude and y_3, y_4, y_7, y_8 are also identical in magnitude. In addition, y_1, y_2, y_5, y_6 are also identical in magnitude. As specified in figure 27 all the x distances will be equivalent to the dimension D which is .0508m and y_1, y_2, y_3, y_4 are equivalent to the dimensions of at which is 0.0381m which is C.

$\tau_{torsional.i} = \frac{27.78kN * m * (0.051^2 + 0.057^2)^{\frac{1}{2}} * m^2}{J_{inertia}}$	(139)
$\tau_{torsional.i} = \frac{27.78kN * m * (0.051^2 + 0.057^2) * m^2}{3.5 * 10^{-2} m^2 * A_b}$	(140)

To find the total shear stress use equation 127.

$\tau_a = [\tau_{direct}{}^2 + \tau_{torsional}{}^2]^{\frac{1}{2}}$	(141)
$\tau_a = \frac{64.50kN}{A_b}$	(142)

7.7.3 Critical Stress/ Failure Criterion:

Only the calculations for bolt 1 and 2 are considered because they will produce the most critical stress. All other bolts will experience stresses that are less than that of these two bolts.

$\frac{\sigma_{yield}}{2} > \left[\left(\frac{\sigma_{bending1.2}}{2}\right)^2 + \tau_a{}^2\right]^{\frac{1}{2}}$	(143)

Assuming that σ_{yield}= 270 MPa [17], and substituting the expressions for $\sigma_{bending1.2}$ and τ_a, equation 143 was used to solve for A_b. It is important to recognize that according to figure there are no bending stresses applied on this fastener pattern. Thus equation 143 can be rewritten as equations 144. Equation 144 is evaluated below it.

$\frac{\sigma_{yield}}{4} > [{\tau_a}^2]^{\frac{1}{2}}$	(144)
$\frac{\sigma_{yield}}{4} > \frac{64.50kN}{A_b}$	

Then rearranging the equation of the area of a circle, equation 144 is used to solve for the radius of the screw.

$\frac{\sigma_{yield}}{4} > \left[\left(\frac{64.50kN}{A_b}\right)^2\right]^{\frac{1}{2}}$	(145)
$67.5\ MPa = \frac{[4.161 * 10^9 N^2]^{\frac{1}{2}}}{A_b}$	(146)
$A_b = \frac{[4.161 * 10^9 N^2]^{\frac{1}{2}}}{67.5\ MPa}$	(147)
$A_b = 9.556 * 10^{-4} m^2$	(148)
$r_{screw} > \left[\frac{A_b}{\pi}\right]^{\frac{1}{2}}$	(149)
$r_{screw} > 1.744 * 10^{-2} m$	(150)

From the equation 150 it is evident that the associate fastener that will be able to be used for the fastener pattern connecting the members of the C-frame together must have a radius larger than $1.744*10^{-2}$ m. The closest fastener that can be used in this design is a ¾ " screw.

The table 26 summarizes the necessary information for the C-Frame Fastener pattern.

Table 26 Summary of L-Frame Fastener Pattern Details

Summary of L-Frame Fastener Pattern Details	
$C = .0381m$	The vertical distance between the center of fastener pattern and the bolts. Please refer to figure 27
$D = .1016m$	The horizontal distance between the center of fastener pattern and the bolts. Please refer to figure 27
$r_{screw} = .0174m$	The specified bolt radius based on analysis.

Chapter 8 Platform Material Selection

To determine the necessary material for the platform solid works finite element analysis was performed with the constraints that will be described in figures 28-31. The design propose would fasten the platform unto the . The initial proposal is to fix the platform at four different locations: two on each L frame. To achieve this L brackets would be used to fasten the system to the L- frame.

It is important to recognize in that in the analysis of the Platform, the platform only has to sustain a total of 570lbs (2535.5N). This is because the platform is responsible to hold the weight of the patient and not

the weight of the whole system. Only the leadscrew must be able to support the full 2000lbs (8909N) because it must be able to support both the weight of the patient and system structure itself that includes the L-frame, connecting bar, and the cam rollers. The weight of the person on the platform was modeled as two loads acting on a small areas to approximate a point loads. The reasoning for using two square areas is that assuming a patient is in a wheel chair, the load will be distributed between the two wheels. Using the assumed load and geometric constraints, is possible to find the amount of displacement experienced. It the FEA model set, it is important to propose a material for the platform. Table 27 provides the material properties for ABS, AISI 1018 Steel, Aluminum and Poly Carbonate.

Table 27 Material Properties Table for Platform Material Selection

Material	Density	Yield Strength
Polycarbonate	1020-1430 kg/m^3	51.0-138 MPa
ABS	1000-3500 kg/m^3	28.0-93.1 MPa
Aluminum	2700 kg/m^3	276 MPa
AISI 1018 Steel	7872 kg/m^3	370 MPa

Steel was dismissed from this design since the use of steel plates would significantly increase the weight of the overall design for a given dimension. As seen in the table 27 Steel is nearly 6 times denser than polycarbonate and some abs materials. Upon further investigation aluminum was chosen. Aluminum was particularly chosen because while observing other platform lifts in use, Aluminum was the material of choice. Moreover, Aluminum's yield strength is the same order of magnitude of steel yet is only a fraction of the density of steel. Thus, aluminum reduces the total system weight while maintaining high strength.

Initially it was assumed that the thickness of the plate was 1/4". With such a thickness, the deflection experienced when a 570lb (2335N) force was applied near the center of the platform was approximately 14mm at the points where the loads are applied. From such a design, it is evident that the most deflection happens at the locations of the applied load. The results as presented in figure 27 and figure 28 suggest that in order to reduce the stress experienced as well as the deflections, supports should be provided beneath the platform. Thus, it was decided that three steel tubes with the dimensions of 3 x 3 x ¼ will be spaced evenly underneath the platform. These tubes will be fixed to the L-frame member 2 using fasteners. They will also be attached to the platform with fasteners as well. Figure 29 and 30 demonstrate the deflection and stress concentrations of the platform once it is supported underneath by the tubes.

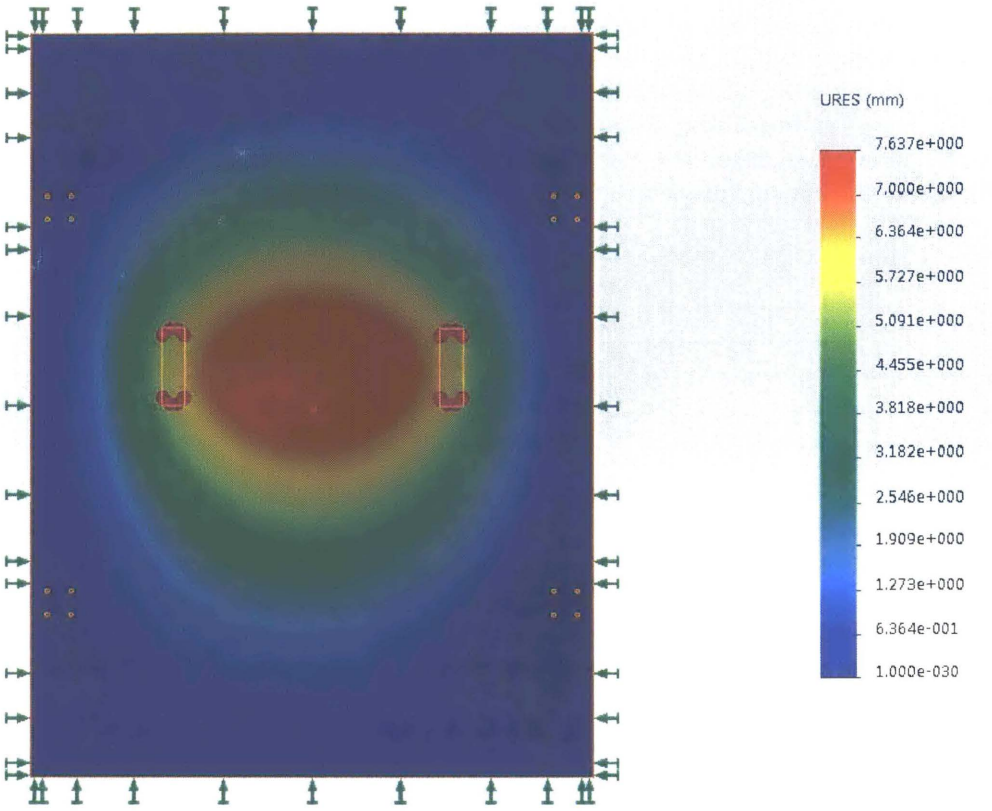

Figure 28 Deflection Result of Platform without Supports: This figure demonstrates the deflections result when a 6.35mm Aluminum plate is loaded with 2540N of force. The plate is all four sides to approximate a simply supported plate. Moreover, the pink arrows indicate the locations where the load is applied. From this image, it is evident that without supports beneath the platform, the resulting displacements are large.

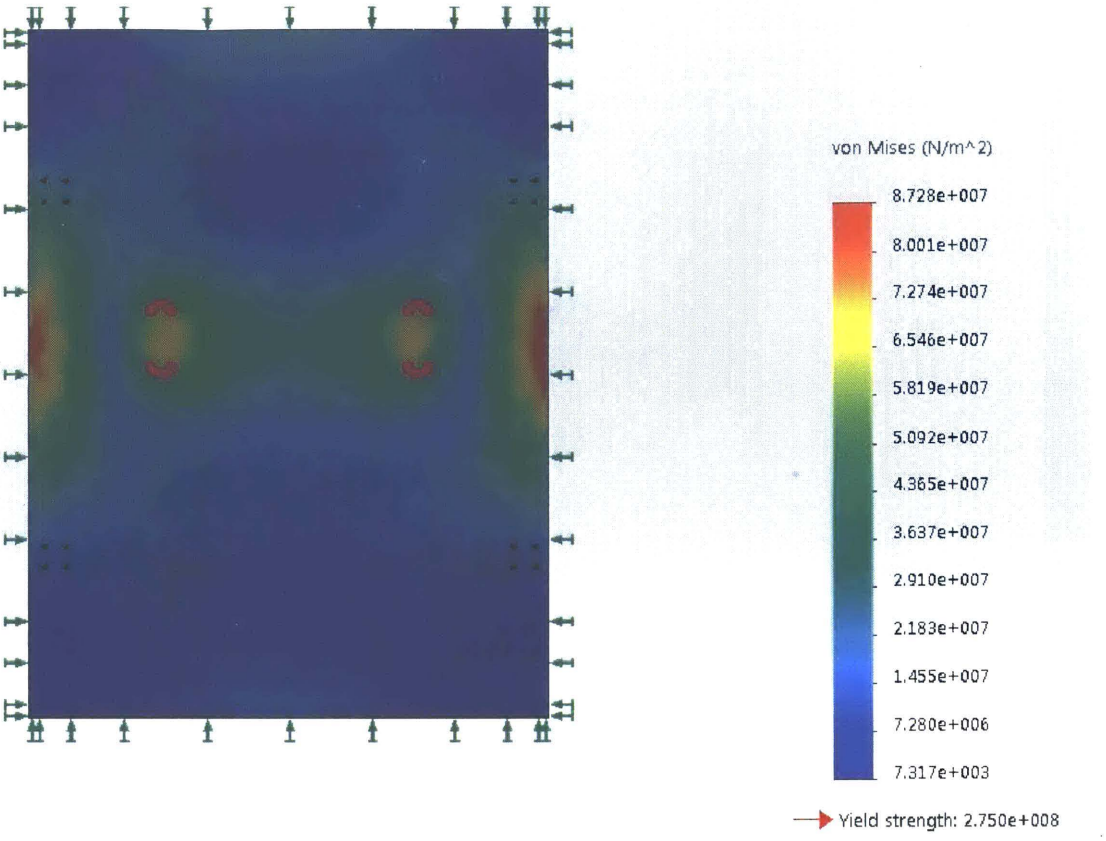

Figure 29 Stress Concentration Results for Platform without Supports this figure depicts the stress concentration in the platform without support. The geometry is fixed such that to replicate the loading of a simply supported plate and the load locations are indicated by the pink arrows. The maximum stresses that the plate experiences is 87.28 MPa. This stress is below the yield stress of Aluminum. While the stresses are low, figure 28 demonstrates that the deflections in this loading condition are high. Thus, in the forthcoming figures steel tube will be placed underneath the platform to help reduce the deflections.

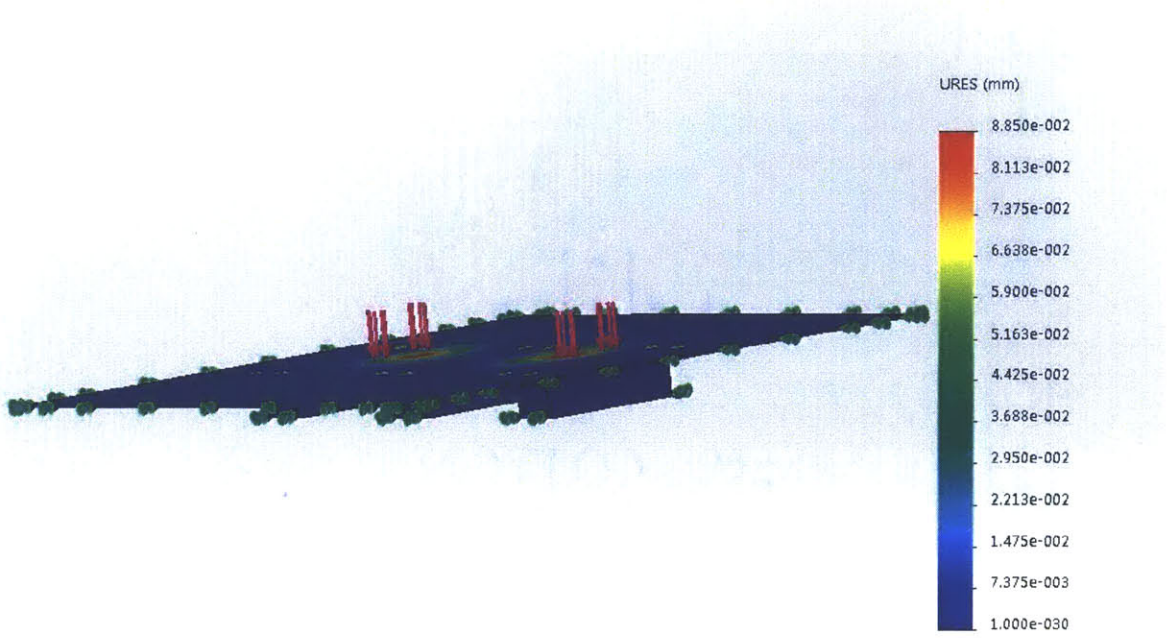

Figure 30 Deflection Results for Platform with Supports: This figure demonstrates the deflections experienced by the platform when supported by steel tubes. The plate is oriented at an angle to reveal the loading conditions in this analysis. In this case, the ends of the tubes are fixed. This is because in the design the tubes will be attached to the L-frame members and thus, it will be essentially fixed. From the plot on the side it is evident that due to the addition of these tubes, the deflection of the member was decreased to .0885 mm. Thus, the tubes at the given dimensions significantly reduce the deflections that the platform experiences.

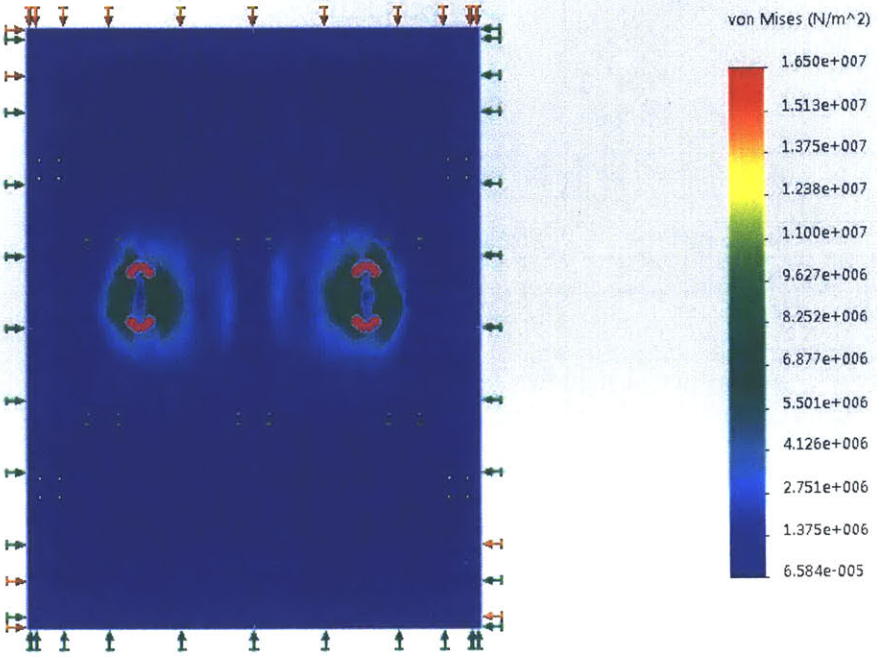

Figure 31 Stress Results for Platform with Supports: this figure demonstrates that with the addition of the steel tubes, the stress within the system decreases substantially as well. Given that the yield strength of aluminum 275 MPa the maximum stress of 16.5 MPa is well below the yields stress of aluminum and is no need to worry about over stressing the plate.

The total price associated with the design of the platform is presented in Table 28. This includes the price for the safety rails that must be added to the system for safety as speficified in chapter 1.

Table 28 Total Material Cost of Platform

Item	Company	Part number	Price	Quantity	Total
Aluminum Plate 48" x 36"	DiscountSteel.com	05037	$135	1	$135
Safety Rails	McMaster	3355T27	$323.09	2	$646.18
3"x4"x1/4" steel tube 6ft (platform support)	McMaster	6527K624	$103.36	1	$77.44
Total					$858.32

8. 2 Cost Of Structural Frame & Platform

Table 29 Total Cost of Structural Frame and Platform

Item	Company	Part number	Price	Quantity	Total
C-Frame & L-Frame member 2	Tuner Steel		$640	2- 6 x6 x 3/8 rectangular Tube 1-6 x 6 x1/4	$640
L-Frame member 1	DiscountSteel.com	10312	$260	2	$260
Fasteners	McMaster	92865A356	6.85	8	$54.80
Connecting Plates	McMaster	47065T264	12.00	6	$72.00
4 x4x1/4 steel tube(leadscrew Mounts)	McMaster	6527K524	38.72	1	$77.44
Aluminum Plate 48" x 36"	DiscountSteel.com	05037	$135	1	$135
Safety Rails	McMaster	3355T27	$323.09	2	$646.18
3"x4"x1/4" steel tube 6ft (platform support)	McMaster	6527K624	$103.36	1	$77.44
Total					$1963

Chapter 9 Total System Summary

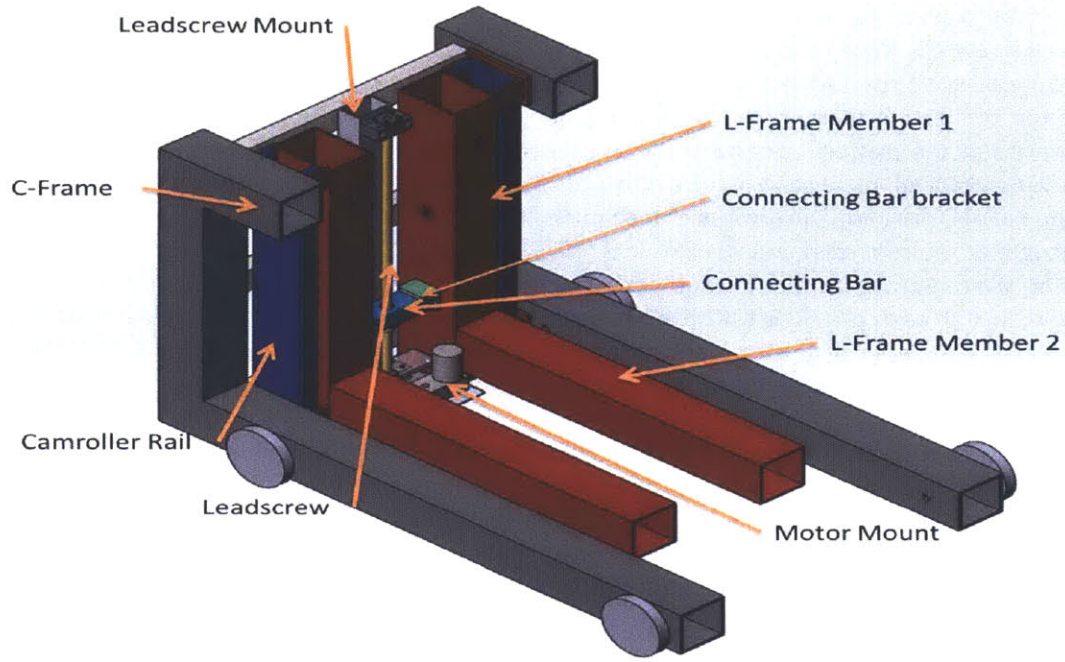

Figure 32 Frame of Platform Lift

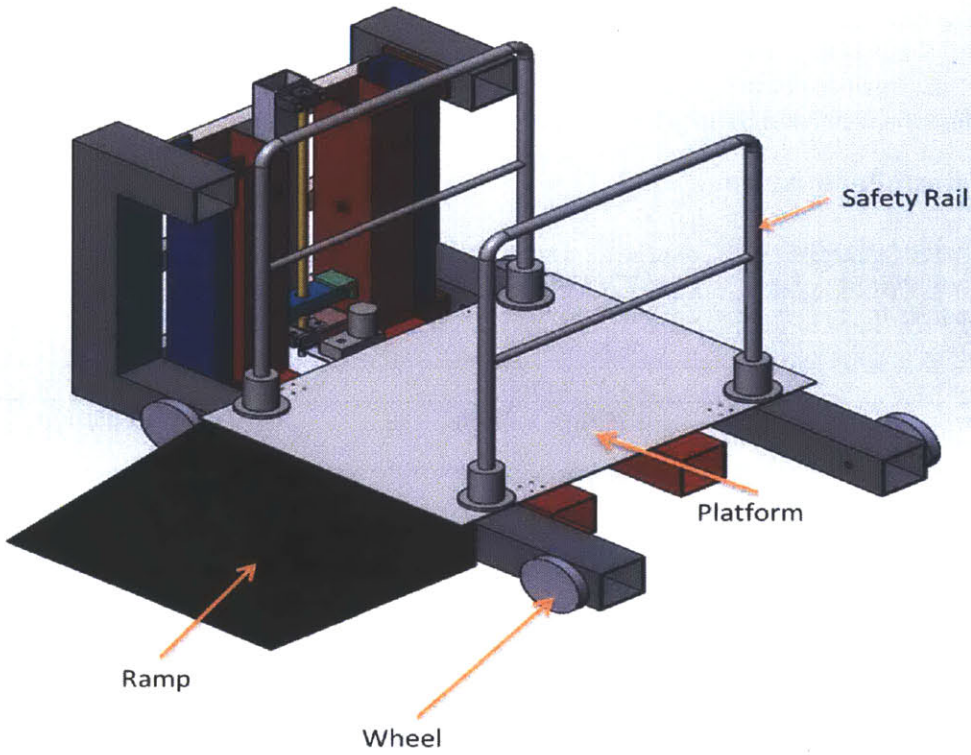

Figure 33 Overall System Design This figure provides an overall description of the design. Coupled with figure 32 one is able to understand the total design.

Figure 32 mainly depicts the mainly the structural and actuation components of this design. The force transfer between the L-Frame Structure which is mounted to the platform as seen in figure 33 is facilitated by the connecting tube and the connecting tube bracket. The connecting tube is mounted unto the lead screw nut. When the leadscrew rotates as a result of actuation from the motor, it causes the connecting tube to rise. Since the connecting tube bracket is attached to the L-Frame and rest directly on the connecting tube, and motion is transferred to the L-frame and the loads experienced from the weight of the platform can be easily transferred to the leadscrew. To help the platform to maintain a vertical travel and also resist the moments generated by the load of the combined patient and platform weight, the Hevi-Rail cam roller technology from PBC linear is used. These cam rollers ride along the length of the cam roller rail which is identified in figure 32. The total length of the Cam roller rail is 1.016m. The reasoning for such a length is that in order to sustain a moment, there must be a total of two cam rollers on each rail. The distance between the cam rollers determine the radial forces that the cam roller will experience thus to provide for the travel desired, enough rail length is need to accommodate for both the travel length and the distance between the cam rollers.

The cam rollers stated earlier are connected to L-Frame member 1 which has the dimensions of 8 x6 x ½" and is a total of .9144 m long. The L-frame member 1 is attached to L-Frame member 2 via a fastener pattern outlined in section 7.5. This fastener pattern allows for the load transfer from L-frame member 2 to L-Frame member 1. To support the cam roller rails mentioned earlier in this description, the cam roller rails are attached to the C-Frame. The C-frame not only provides support for the L-frame but it also provides points of attachment for the wheels that will be fitted for this system. The dimensions of the C frame members were determined to be 6x6x 3/8" according to the analysis in section 7.3.5. Since the platform rests on C -Frame member 3 at its lowest point in the travel, the dimensions of the C-Frame limits how low the platform can reach the ground. As a result, a ramp is needed to raise .1778m (7 in) to help patients mount the Sky Walker. Safety Rails are placed on the platform. These rails comply with ADA regulations and thus satisfy the safety requirement for this design. The remainder of this chapter will discuss the system performance and cost. The conclusion will briefly describe recommendations for the future a possible method to reduce cost.

9.1 System Performance

Table 30 System Performance Chart

Design Parameters	System Requirements	Proposed System Performance
Load Capacity	8909 N	8909N
Linear Travel	.4572 m	.4572
Linear Speed	>0.0381 m/s	.0440 m/s
Platform Size	0.762m x 1.219m	.9144m x 1.2192m
Vertical Height to mount the Platform	<.1524m	.1788
Total Platform Weight	4454N	4633N
Safety Rail	yes	yes

Below is a discussion on system performance. The proposed design consist of major elements such as the leadscrew, the motor, the L-frame, the connecting Bar, the C-Frame and the platform. Each of these elements was selected based on one of the design specifications supplied above. In the coming sections

this document will discuss how the selection of the different parts affected by the final system requirements.

9.1.1 Load Capacity

The final load capacity of the system is dictated by components such as the leadscrew, the platform, the L-Frame members and the C-Frame member. Although the current leadscrew selected for this design is capable of holding a total of 20kN, the other aspects of the platform lift were designed to withstand loads and moments related to an 8.9 kN prescribed load capacity. This is reflected in the selection of the L-frame member and C-Frame members. Thus, the total load capacity of the system is 8.9kN.

9.1.2 Linear Travel

The linear travel is dictated by a variety of components such as the leadscrew length, and the distance between the cam rollers as well as the size of the cam rollers and the height of the connecting bar bracket. From the discussion of the L-frame selection, it was determined that the distance between cam roller 1 and cam roller 2 should be .5588m. Assuming that the cam roller touches the ground when the platform is at its lowest point, the accompanying rail would have to be longer than the distance between the cam rollers in order to achieve the desired travel. Thus, by setting the length of the cam roller rails as to 1.016m for this design, it is ensured that the system will have the desired travel.

9.1.3 Linear Speed

The final speed of the lift was determined by the motor selected. In this design the motor selected has to spins at 500 rpm in order to supply the necessary torque of 23.7 Nm. When the chain drive was analyzed in section 6.2 it was determined that with the current chain and sprocket selection, the leadscrew will spin at a rate of 416 rpm. This corresponds to a lifting rate of 0.0440m/s which is higher than the desired 0.0381m/s.

9.1.4 Vertical Height of the Platform Mount

The vertical height to mount the platform is highly dependent on the C-Frame dimension. According to figure 32, it is evident that the platform will rest on top of the C-frame member 3. Since C-Frame member 3 has a height of.1524m, a wheel with a diameter greater than .1524m is needed in order to make the lift mobile. Thus, in this design the diameter of the wheel is .2032m. Assuming that the center of the wheel is aligned with the mid-section of C-frame member 3, the height from the floor to the top of C-frame member 3 is .1788m. Since the dimensions of C-frame member 3 are dependent on the load requirements of the system, the only way to decrease the height of the C-frame member 3 is to decrease the load requirement. For now however, a ramp is added to the system to allow for patients to roll up unto the platform.

9.1.5 Total Platform Weight

The intended platform weight was supposed to be 4454.5 N which corresponds to 1000lbs. The weight is supposed to be the combined weight of the patient, their wheel chair and the materials for the platform. Table 31 outlines the weight of the current design.

Table 31 Platform Weight Distribution

Patient & Wheel Chair Combined	2539 N (570lbs.)
L-Frame Member 1 (total)	1122 N (252 lbs.)
L-Frame Member 2 (total)	774 N (173.8 lbs.)
Platform	198 N (44.39 lbs.)
Steel Tubes	176 N (26.4lbs.)
Total	4753 N (1067 lbs.)

From table 31 it is evident that the amount of the total weight of the platform is slightly above the specified weight of the platform. There are two main aspects that contribute to this. The first is the material selected for the platform. To reduce the deflection in the L-Frame, steel was chosen as the material for the L-frame. Coupled with the large dimensions of the L-frame member, this increased the total weight of the system which resulted in the system being overweight. Given that the dimensions of the members are highly dependent on the load capacity, decreasing the load capacity is linked to decreasing the total system weight.

9.2 Total System Cost

Table 32 Total System Cost

Component	Company	Price (per unit)	Number of Units	Total
Leadscrew	Nook Industries	$1176	1	$1176
Motor	Ampflow	$289	1	$279
Motor Controller	Amp Flow	$450	1	$450
Sprocket& Chain Drive	McMaster-Carr	$48.33	1	$48.33
Linear Guide system	PBC Linear	$1269	1	$1269
Structural Frame Components &Platform	McMaster	$894.74	(see section for itemized cost)	$1963
Total				$5195.3

Conclusion

It is important that while the current design meets the necessary speed and load criteria, the price is beyond the budget allotted. At scale, the prices would only drop by a small percent and thus does not make it a feasible design. As an exercise, one parameter is chosen to be altered in order to see its effects on this design. A particular focus is placed on structural component since it has the highest price in the price summary in section 9.2. Components within the structure include the plate and the L-Frame.

In the discussion below, an attempt is made to reduce the cost based on reducing load requirements. The initial assumption was that the combined weight of the patient and their accompanying wheelchair would weigh a total of 565lbs which included safety factor of 1.5. In addition it was assumed that the combined weight of the system and the weight of the structure would be 1000lb. On this value an additional safety factor of 2 was multiplied. With these initial assumptions, one can concluded that the total load capacity is approximately 3.5 time larger than the combined load of the patient and accompanying wheel chair. Thus, the load capacity is redefined and the safety factor is based on the current information of the system.

The newly defined load requirement is as followed. It is assumed that the total weight of the patient with their wheelchair would total 377lbs. From the current design it is evident that the platform without the patient is equivalent to 496.59lbs. This is approximately 1046lbs. A safety factor of 1.5 will be placed on the entire system. Thus the new system load requirement would be approximately 1600lbs or 7130N. This new value is used to evaluate the deflections and forces that cam roller 1 would experience as a result of this load new load requirements. Initially the dimensions as specified in Chapter 7 for L-frame

member 1 and 2 are kept the same to allow for a comparison between the changes in the safety factor. A summary of the system dimensions are provided in table 34.

Table 33 Summary Force and Deflection Results Due to Modified Load Capacity

Design Parameters	Original Load Capacity (8909N)	Modified Load Capacity (7130 N)	Comments
L-Frame Member 1			
Cam roller 1 Deflection Under (Current Dimension)	$-1.3611 * 10^{-4}$ m	$-4.6989 * 10^{-5}$ m	The current Dimensions L-Frame member 1 IS 8" x 6"x1/2"
Force Due to Deflection	23.33 kN	19.16 kN	
Total Cam Roller Force	30.27	24.74	
Cam roller 1 Deflection Under (Modified Dimensions)	$-1.8126 * 10^{-4}$	$-1.4507 * 10^{-4}$	The modified Dimensions L-Frame member 1 IS 8" x 4"x1/2"
Force Due to Deflection	31.03 kN	24.8 kN	
Total Cam Roller Force	38.00 kN	30.41 kN	
Cost of member with current Dimensions			$258
Cost of member with modified dimensions			$253
L-Frame Member 2			
Total equivalent Stress(current dimensions)	40 MPa	30 MPa	The current dimensions L-Frame member 1 is 6" x 6"x 1/4
Total equivalent stress modified Dimensions)	95.43 MPa	72.35 MPa	The modified dimensions L-Frame member 1 IS 4" x 4"x1/4"
Cost of member with current Dimensions			$150
Cost of member with modified dimensions			$100

What this table reveals is that if Load requirements were reduced to for this system, it would be possible to reduce the dimensions of L-frame 1 from 8" x6" x ½" to 8" x 4" x ½". Likewise it is possible to decrease L-Frame member 2 to from 6" x 6"x ¼" tube to a 4" x 4" x ¼" tube. Although they result in higher stresses, they resultant stress remain within the allowable range of the parts and materials selected. When the price of the new L-frame is assessed, it is determined that the new price for the L-Frame combined would be $350. Compared to the current price of $410 this is not much of a reduction. Thus, from this exercise it is evident that a simple load reduction does not change the price of the structural member substantially.

Given the current cost of the machine, the recommendation of the author is to not build the design. With its current dimensions the platform would only be necessary to transport the patient an additional .2749m once the patient mounts the platform. For such a lift to cost $5195 suggest that the design in a region that is beyond feasibility. Possible alternatives to this design would be to simply provide a ramp. Although it will require an extra foot in length, a ramp is does not require actuation. Patients can be either be wheeled onto the Skywalker via the ramp or they can wheel themselves onto the Skywalker. An alternative possibility is to employ the use of pallet jacks. These have the load ratings desired for the application of lifting people. While this is a potential design consideration, designers should recognize that these devices are not meant to lift humans. Thus, the design utilizing such devices would have to take safety into strong consideration.

Appendix A

Q&A

Q: Isn't the friction coefficient between bronze and steel .3.

A: Initially I was using a text reference that assumed that the coefficient of friction was .06 for lubricated contact. The coefficient of friction is ~ .3 when the screw is not lubricated. However, since I intend to lubricate the leadscrew, the value of the static friction will be about .16 according to the engineering tool box. I verified these values with some of the companies selected for the quotes. For example, Joyce typically uses a value of .15 for the static friction and .12 for the dynamic friction for their lead screw assemblies.

While I agree that the value used for my calculation is off; the amount of toque required to raise the load as prescribed by the selected manufacturers is within the limits of the motor selected. Thus, neither the selection of the leadscrew or the motor is affected by this mistake. I have however, changed my calculations to reflect the information I found. I am now using .16 as the coefficient of friction.

When these changes were applied to the calculation, I found that the torque required to raise the load would be 25.748 Nm which is within the range of the values suggested by the manufactures. To lower the load from rest, it would now require 7.245 Nm. Because the value of the torque need to lower the load is positive, it means that this system is not back drivable. I hope this helps to answer your question. Please let me know if you have any further questions.

The Coefficient of friction for the Thompson Linear Screw ranges from .2 to .3.

Q2: Mounting of motors & Motor controls

The following answer was based on the idea that the motor would drive the lead screw by using a gear as the transmission system. Later in the design however, the transmission system was changed to a chain drive. The design of the Motor mount however, continues to remain relevant for this design.

The amp flow motor will be mounted on the tube that supports the lead screw end supports. From the manufacturer specifications the motors have been supplied with 4 mounting bolts that are a ¼-20 in dimensions. Theses bolts are long enough to support a mounting plate of 3/8 thickness. When making the mount for the motor, the major aspects to consider is that the motor is mounted in such a way that the gear mate between the gear on the leadscrew and the gear on the motor will remain intact regardless of the motion. Moreover, the mount should not deflect sufficiently enough that the face width of the two motors will lose contact with one another. That that then means in the design of this

motor mount in terms of specification is that the mount cannot deflect more than 1 in as a result of the weight of the motor. The other determining attribute in maintaining gear mates comes as a result of the dimensions of the motor and the mounting surface. To further understand this point, an image of the current motor is provided below.

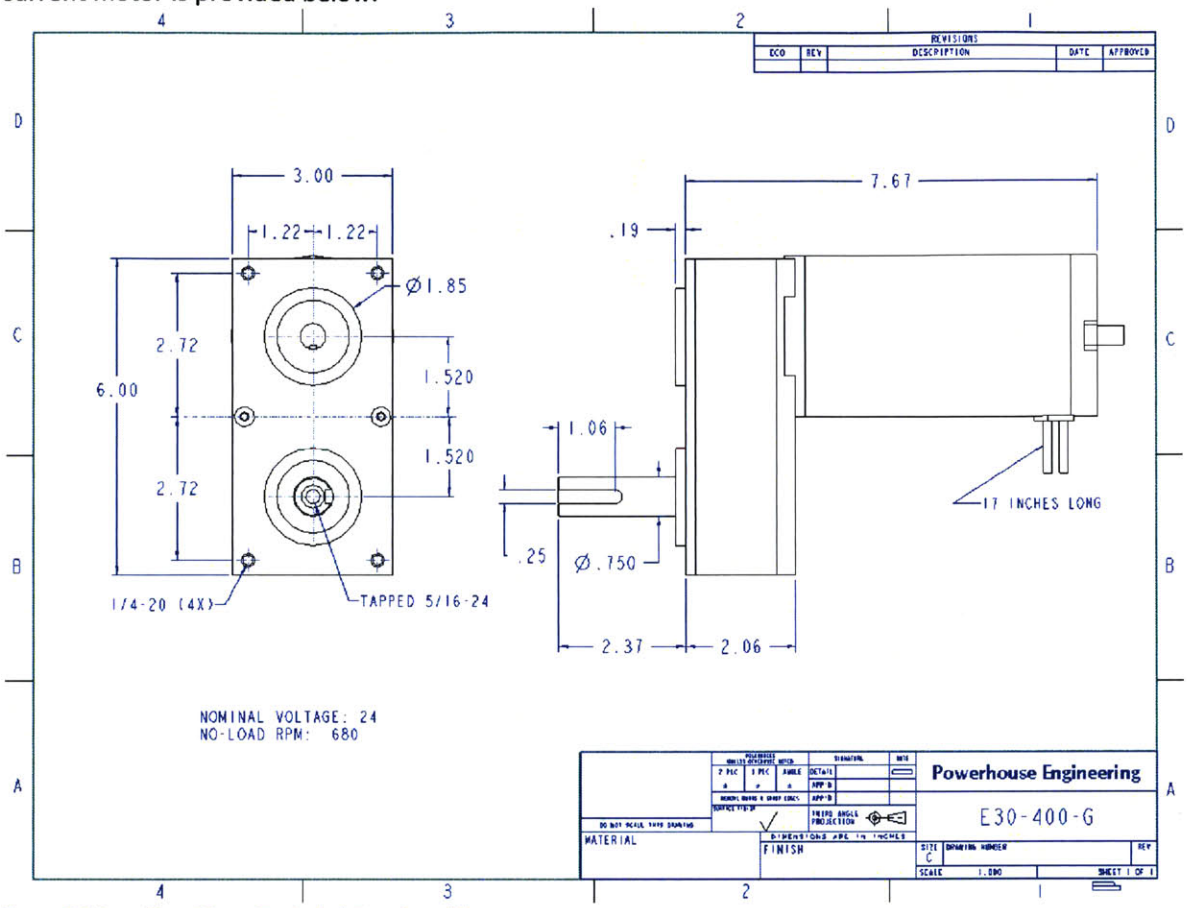

Figure 34 Amp flow Motor Technical Drawings [4]

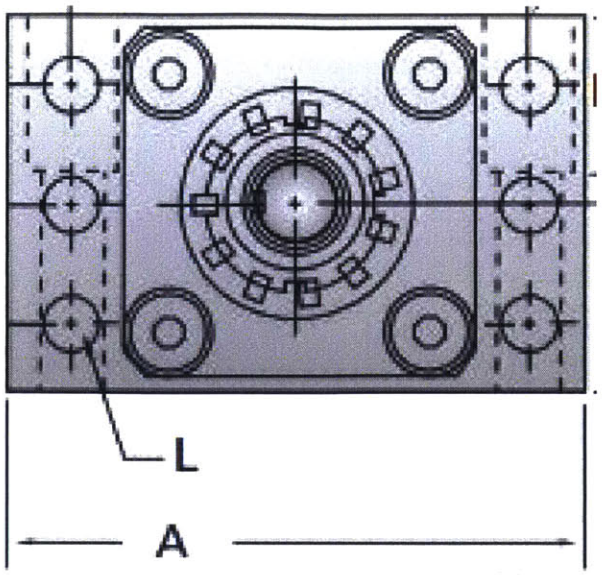

Figure 35 Leadscrew End Support Schematic [5]

We find from figure 34 that the width of the motor reduction base plate is 3". The center of the shaft mount is located at the center of the width. Moreover, from the image on the right, we find that the extended shaft from the leadscrew end support will also be at the center of the end support. The width denoted by A in figure 35 is 4.5in wide and thus, the distance between the two centers is a total of 3.75in apart. To account for the bracket that will be used to mount the motor to the tube, it is then assumed that the distance between the two centers 4 in. Using the same gear on both ends we have that unlike previously determined, the gears will have to be 4in in diameter to allow for proper matting with the given dimensions.

Thus, the chain and sprocket was used to drive the system as opposed to gear mate. Please refer to section 6.2 for the selection of the chain drive.

To fix this problem however we will place a flat pate above the end support. Then also we will orient width end of the gear reduction is facing the leadscrew. To figure out the thickness of the plate, we take a look at the deflection of the plate and find the thickness to prevent the two plates from losing a contact with the chain.

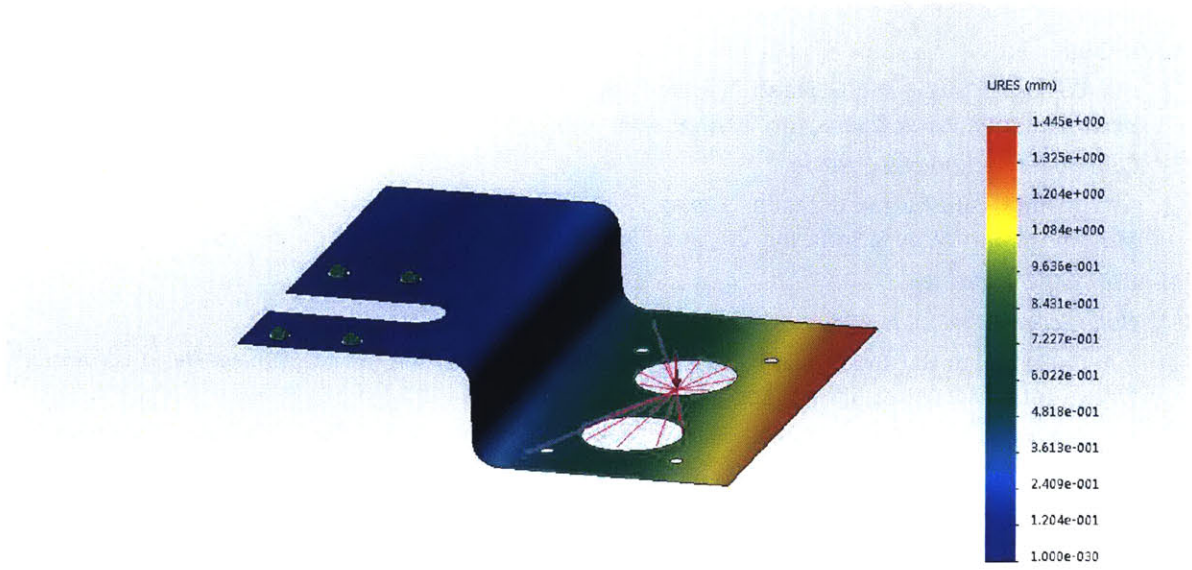

Figure 36 FEA Analysis of Motor Mount: This image demonstrates that the deflection in this system is only 1 mm when loaded with the weight of the Ampflow motor.

From the FEA given below, we find that there will be little deflection. This ensures that it will not disengage with the face width. This mount should fit into the design because the L shape frame ensures that there is no interference between the plate and the platform. The thickness of this plate is 3.175mm.

Q3: Can you tell me the mechanical power you need to apply at the platform to achieve your design goal (linear), and the mechanical power you need to apply at the output shaft of the motor (rotational) to drive the screw? What is the total efficiency of the transmission from rotational input to linear output of the transmission. Based on this number, are you more, or less, confident that your specification makes sense?

To raise the platform linearly with the net weight of 8909N a total of .4572 m in 10 seconds according to the current is equivalent to 407.3 W of power. The Torque required to raise the load with the given leadscrew selection is 24.687Nm and the angular velocity is 43.56 rads/s. The angular velocity is determined by converting the current system performance of 416 RPM to the radians. When these two terms are multiplied we get 931W. The efficiency would be the linear output, divided by the rotational input power. This yield an efficiency of 37.8% I am confident in my specifications because in this system, the most mechanical inefficiency is generated by the leadscrew. The friction in the system causes much of the energy inputted to be lost. Generally the efficiency of a leadscrew is about 33% thus, this value indicates that the specifications we chose are correct.

Works Cited

[1] J. A. Collins, H. Busby and G. Staab, "Figure 12.9," in *Mechanical Design of Machine Elements and Machines*, John Wiley &Sons, Inc, 2010, p. 474.

[2] *Cam Roller Technology Catalog.*

[3] J. A. Collins, H. Busby and G. Staab, "Figure 17.14," in *Mechanical Design of Machine Elements and Machines*, John Wiley & Sons, Inc, 2010, p. 775.

[4] *E30-400-G Drawings.*

[5] *Nook Screw Catalog,* p. 208.

[6] J. A. Collins, H. Busby and G. Staab, "Elastic Instability and Buckling," in *Mechanical Design of Machine Elements and Machines*, John Wiley and Sons, 2010, p. 38.

[7] J. A. Collins, H. Busby and G. Staab, "Power Screw Assemblies," in *Mechanical Design of Machine Elements and Machines*, John Wiley& Sons, 2010, pp. 462-485.

[8] J. A. Collins, H. R. Busby and G. H. Staab, "Gears and System of Gears," in *Mechanical Design of Machine Elements and Machines*, John Wiley & Sons Inc, 2010, pp. 624-647.

[9] J. A. Collins, H. Busby and G. Staab, "Belts, Chain, Wire Rope, and Flexible Shafts," in *Mechanical Design of Machine Elements and Machines*, John Wiley & Sons, 2010, pp. 746-798.

[10] J. Marrs, "Table 11-59: Chain Equations," in *Machine Designers Reference*, 2012, p. 638.

[11] A. H. Slocum, "Chapter 2 Principles of Accuracy, Repeatability, and Resolution," in *Precision Machine Design*, 1992, pp. 58-107.

[12] A. Slocum, "Fundamental Principles," in *Fundamentals of Design*, 2008.

[13] A. H. Slocum, "Contact Between Curved Surfaces," in *Precision Machine Design*, 1992, pp. 228-236.

[14] R. C. Hibbler, "Deflection Diagrams and the Elastic Curve," in *Structural Analysis*, Upper Saddle River, Prentice Hall, 2002, pp. 269-271.

[15] R. C. Hibbeler, "Method of Virtual Work: Beams and Frames," in *Structural Analysis*, Upper Saddle River, Prentice Hall, 2002, pp. 310-320.

[16] R. C. Hibbeler, "Torsion," in *Mechanics of Materials*, Prentice Hall, 2014, p. 230.

[17] "MatWeb," [Online]. Available: http://matweb.com/search/DataSheet.aspx?MatGUID=273b2b0b975b46c7bba978f48e062d47&ckck=1. [Accessed 13 January 2016].

[18] J. A. Collins, H. Busby and G. Staab, "Threaded Fasteners," in *Mechanical Design of Machne Elements and Machines*, John Wiely &Sons, 2010, pp. 509-512.

[19] R. C. Hibbeler, "Plane Frame Analysis Using the Stiffness Method," in *Structural Analysis*, Upper Saddle River, Prentice Hall, 2002, pp. 533-553.

[20] R. C. Hibbeler, "Torsion," in *Mechanics of Materials*, Prentice Hall, 2014, p. 230.